Characterization of Active Fiber Composite Actuators for Helicopter Rotor Blade Applications

by

Viresh K. Wickramasinghe

B.S., Aeronautical Engineering
United States Air Force Academy (1997)

Submitted to the Department of Aeronautics and Astronautics
in partial fulfillment of the requirements for the degree of

Master of Science

at the

MASSACHUSETTS INSTITUTE OF TECHNOLOGY

June 2001

Signature of Author .....
Department of Aeronautics and Astronautics
09 March 2001

Certified by .....
Nesbitt W. Hagood IV
Associate Professor of Aeronautics and Astronautics
Thesis Supervisor

Accepted by .....
Wallace E. Vander Velde
Professor of Aeronautics and Astronautics
Chair, Department Graduate Committee

Characterization of Active Fiber Composite Actuators for Helicopter Rotor Blade Applications

by

Viresh K. Wickramasinghe

Submitted to the Department of Aeronautics and Astronautics
on 09 March 2001, in partial fulfillment of the
requirements for the degree of
Master of Science

Abstract

Significant structural vibration and noise are two notable and undesirable characteristics of helicopter flight. A high degree of vibration results in structural fatigue, passenger fatigue, and high acoustic signature. Active material actuators are presently being employed for integral twist actuation of rotor blades in order to perform vibration reduction in helicopters.

The primary objective of this thesis is to develop a standard methodology to characterize the Active Fiber Composite (AFC) actuator material system for the Boeing Active Material Rotor (AMR) blade application. AFCs consist of peizoceramic fibers embedded in an expoxy matrix. The actuators are integrated directly into the blade spar laminate as active plies in order to perform structural control for vibration reduction. Thus, extensive material characterization is necessary to evaluate the AFC material properties as structural actuators as well as structural components of the blade. Numerous tests are designed to extract the important mechanical, electrical and electromechanical properties under simulated blade operating conditions. The tests include stress-strain tests, free strain tests, performance under tensile load tests, electrical fatigue tests, and mechanical fatigue tests.

The characterized AFC actuator material system consisted of 0.01" diameter PZT-5A fibers, dry film matrix, and silver ink interdigitated electrodes on Kapton substrate. The actuator material system exhibited highly non-linear stress versus strain behavior and a "knee" in the stress-strain locus is observed at $\sim 2500\mu\varepsilon$, indicating the onset of catastrophic damage in the actuator. The initial longitudinal and transverse modulus are 39.1GPa and 14.5GPa, respectively. The actuator material system showed high robustness qualities in mechanical fatigue under nominal loads. The optimized voltage cycle selected for the AMR blade operation is 3000Vpp with 0Vdc and the average actuator free strain at this level is $\sim 1200\mu\varepsilon$. Electrical fatigue caused microscopic burns in actuators and may lead to potential long-term reliability issues.

The results of the AFC material characterization tests facilitated the design and operation of the Boeing AMR blade. Furthermore, the testing process developed in this thesis facilitates the characterization of similar actuator material systems for future applications.

Thesis Supervisor: Nesbitt W. Hagood IV
Title: Associate Professor of Aeronautics and Astronautics

Acknowledgements

It is with heartfelt gratitude that I dedicate this thesis to everyone who have played a role in its successful completion. There are many people who deserve my utmost gratitude for their effort in support of my studies at MIT. Special thanks goes to my advisor, Professor Nesbitt Hagood, for his continued support and for providing me with a challenging but rewarding opportunity. I would like to thank everyone in AMSL and SSL who provided invaluable input and support throughout the good and the bad times. Many thanks goes to my family and my friends for their continuous support and encouragement. Specially, I would like to thank my wife Dinu for sticking by my side through all the ups and downs in my life. I couldn't have done it alone!

Funding for this research was provided by the Defense Advanced Research Projects Agency, under contract MDAA72-98-3-0001, and was monitored by Ephrahim Garcia of the DARPA Defense Sciences Office.

Contents

List of Figures

List of Tables

Chapter 1

Introduction

A relatively new structural actuator system based on piezoceramic fibers, called Active Fiber Composites (AFC), has been in development at MIT for the past decade. Boeing Helicopters and NASA-Langley has been collaborating with MIT to integrate AFC actuators into helicopter rotor blades in order to provide integral twist actuation for vibration control [Rodgers, 1998; Derham, 1996; Schmidt, 2000b; Shin, 1999; Cesnik, 1999]. AFC actuators are directly embedded into the skin of the composite blade spar in order to enable active deformation of the stiff blade structure. An AFC embedded active blade was developed and tested at MIT by John Rodgers in a collaborative effort with Boeing in 1998. A similar set of blades were build and tested under the NASA-Langley program [Wilbur, 2000; Shin, 2000]. Both Boeing and NASA programs have demonstrated the feasibility of embedding AFCs for integral twist actuation of rotor blades. The next generation of active rotor blades using the latest AFC material system is underway at MIT with the collaboration of Boeing [Schmidt, 2000b].

This thesis will focus on characterization of the latest generation of AFC actuator material system. Extensive material characterization is necessary to evaluate the properties of AFCs as structural actuators as well as structural components of the blade. AFC material properties important to the rotor blade application are identified and comprehensive characterization tests are developed to extract the necessary properties under simulated blade operating conditions. The results of AFC actuator material characterization are used in the blade design, analysis of the blade performance, determination of operational limits and also to recommend changes necessary for future AFC actuator systems.

1.1 Motivation

Significant structural vibration and high internal and external noise are two notable and undesirable characteristics of helicopter flight. There are number of unsteady aerodynamic disturbance sources in the rotor blade operating environment which causes rotor vibration and noise [Miller, 1964; Johnson, 1980; Lemnios, 1972]. These include atmospheric disturbances, retreating blade stall, blade/vortex interaction, and blade fuselage interaction, as well as blade and rotor instabilities due to ground/air resonances [Ham, 1987]. The resulting vibration is transferred through the rotor hub to the helicopter cabin and to the rest of the structure [Lemnios, 1976]. The high degree of vibration in helicopters results in structural fatigue, passenger fatigue, and high acoustic signature [Arcidiacona, 1961]. Structural fatigue leads to reduced operational life of expensive helicopter structural components. The noise and vibration also leads to poor ride quality for passengers and also contributes to pilot fatigue. Furthermore, high noise signature contributes to noise pollution of the environment and increases the detectability in military applications.

In this project, an Individual Blade Control (IBC) concept is pursued through the use of Active Fiber Composite (AFC) actuators in order to reduce rotor vibration. AFCs are manufactured with piezoceramic fibers and the actuators are embedded directly into the blade structure along the span of the blade to be used as a distributed structural actuator system to deform the relatively stiff structure. The structural actuation capabilities of the AFCs are used to alter the shape of the blade to take advantage of the energy in the fluid flow over the blade. These blade mounted actuators are used in a feedback control loop to vary the blade angle-of-attack to produce loads necessary to cancel the vibratory loads in the rotor system. Such integrally actuated rotor blades which performs IBC can be effectively employed to reduce helicopter vibration and noise [Chen, 1994]. Beyond the vibration and noise benefits, actively twisted rotor blades may increase the helicopter payload and cruise speed [Derham, 1996].

Under the Phase I of the Boeing Rotorcraft program, a prototype integrally actuated rotor blade using AFC actuators was developed and tested at MIT [Rodgers, 1998]. It demonstrated the viability of embedding AFCs to be used as structural actuators. The AFC actuators demonstrated the capability of providing distributed controllable twist actuation in the blade. The actuators were relatively easily integrated directly into the composite laminate structure as

active plies in the blade spar. The active plies are oriented at $\pm 45^{\circ}$ angle to the blade span in order to induce shear stresses resulting in a twisting deformation of the blade. The advantages to using AFC actuators in rotor blades are its capability to offer large bandwidth response as well as low impact to current manufacturing and the rotor blade operating standards. Since the AFC actuators are directly embedded in the composite skin of the blade spar, the actuator material system must withstand the demanding rotor environment and meet all the requirements of blade's structural materials. Furthermore, the AFC material system must be an efficient actuator system that demonstrates long term operationability, reliability and performance under high loading conditions.

Only a few AFC material characterization studies have been conducted in the past. Bent conducted the initial characterizations of the material system during the early stages of the AFC development [Bent, 1997]. Under the Phase I of the Boeing Rotorcraft program, Rodgers conducted characterization studies on the AFC material system used in the prototype integral blade [Rodgers, 1996; Rodgers, 1998]. Pizzochero conducted theoretical and experimental studies on residual actuation and stiffness properties on an earlier generation of AFC material system [Pizzochero, 1997]. More recently, Wickramasinghe conducted preliminary electromechanical characterization of a secondary AFC actuator material system considered for Phase II of the Boeing Rotorcraft program [Wickramasinghe, 2000]

The development of the next generation of AFC embedded Active Material Rotor (AMR) blade is underway under at MIT under the Phase II of the Boeing Rotorcraft program. The objective of the current program is to manufacture a set of 1/6-scale (60" Radius), Mach-scale advanced CH-47D rotor blades integrating AFC actuators for forward flight tests. The actuators used in these blades are comprised of the latest composition of AFC actuator material system which is not characterized for high electromechanical loading conditions that exists in the blade application. Therefore, the focus of this thesis is to characterize the new AFC actuator material system selected to be embedded in the AMR blade. The uniqueness of the characterization requirements stem not only from the AFC's actuation capability but also from the fact that they are used in the rotor blade application as hybrid laminates. The actuator material characterization process involves the identification of the important mechanical and electrical properties of the material system as well as electromechanical operational limits.

Various mechanical, electrical and combined electromechanical tests are developed in order to extract actuator properties and limits under simulated electromechanical load conditions. A comprehensive test matrix and a testing procedure is outlined for each characterization test. Further, the tests are designed to provide an in-depth understanding of the AFC behavior at high strain and fatigue environment exists in the rotor blade application.

1.2 Background

During the past few decades, many methods have been studied extensively to improve helicopter vibration and noise because it is a great concern for manufacturers, pilots, passengers and operators. A variety of passive vibration absorbers and isolators have been applied in helicopters to reduce structural vibration and noise. Passive control devices provide a moderate reduction in vibration with a low risk of instability and less complexity, compared to active devices [Landgrebe, 1984]. Passive devices are used in many operational helicopters by tuning them to filter out specific vibrational frequencies. Most are used in the helicopter cabin, but a few studies have investigated the use of passive devices on the rotor blades themselves [Bielawa, 1992; Chopra, 1981]. Pendulum absorbers can be mounted at the root of the blade to create a node at a given frequency. Reduction of approximately 50% in vibratory loads have been achieved with such systems [Amer, 1974]. Isolation systems can also be implemented between the fuselage and the drive unit and the rotor [Braun, 1984]. These systems alter the dynamics of the vehicle to create a point of zero vibration at a given frequency [Desjardins, 1978]. However, such methods impart undesirable weight penalties as well as insufficient vibration reduction. One of the main disadvantages of using passive dampers to reduce vibration in helicopters is that passive devices are generally tuned to a specific frequency. Since helicopter vibration usually occurs over a wider spectrum of frequencies, including many harmonics of the primary rotor vibration, passive vibration isolation or passive damping can only have a limited success [Millot, 1992]. Therefore more complex actively controlled rotor blades are currently being investigated as a means of reducing vibration and noise in helicopter flight. A significant reduction in the vibration and noise levels would improve pilot effectiveness, enhance passenger comfort, and also reduce helicopter operation and maintenance costs.

1.2.1 Active Rotor Control

Active rotor control concept has been investigated as a means to reduce the noise and vibration in helicopters. Due to the random nature of the rotor dynamics in flight, the active feedback control using active devices would lead to greater performance benefits in comparison to passive control [Payne, 1958]. Two general methods have been developed to implement active rotor control: Higher Harmonic Control (HHC) and Individual Blade Control (IBC).

In HHC, the whole rotor system comprising all of the blades are treated as the source of vibration and the feedback control inputs are applied to the whole system. In contrast, IBC treats each rotor blade as a source of vibration and independent feedback control input is applied to each of the rotor blades [Kretz, 1976]. Many experimental studies have been conducted to demonstrate the benefits of active blade concept using HHC and IBC. One of the earliest studies in HHC was performed by Kaman with Controllable Twist Rotor where a training edge servo-flap was used for controlling the dynamic behavior of the rotor system [Lemnois, 1976]. Full-scale wind tunnel tests of this rotor by Lemnios and McCloud showed that a mechanically controlled servo-flap in combination with a torsionally soft rotor blade could be used to redistribute the lift on the rotor disk through HHC [Lemnois, 1976; McCloud, 1978]. HHC using swashplate control of blade pitch was applied by Shaw in a comprehensive wind tunnel study of a 1/6 Mach-scale CH-47D rotor [Shaw, 1985]. Nguyen and Chopra performed an analytical study of the same rotor and confirmed these results [Nguyen, 1992]. Many other researchers have also investigated HHC using blade mounted actuators [Millot, 1992; Jacklin, 1994; Kube, 1989]

It is important to note that HHC results in a rigid-body pitch actuation of the blades to reduce rotor vibration and noise. However, there are many advantages of placing actuators closer to the blade tip [Garcia, 1994]. These advantages include better vibration control, higher noise reduction, more degrees of freedom, and lower maintenance [Prechtl, 2000]. Furthermore, the blade mounted actuators would not be considered a flight critical system and thus a failure of actuators would not lead to safety of flight issues. Advantages of mounting the actuators directly on the blades has lead to the in-depth study of various actuator types that could be used to implement the IBC concept. The IBC actuators are designed to control the pitch of each blade independently. Therefore, actuators must provide sufficient authority to apply the

desired control while meeting inertial and geometric constraints of the rotor blade. Carpenter and Paulnock first used blade mounted actuation with a trailing edge servo-flap driven by a hub mounted pitch link system [Carpenter, 1950]. Since then, numerous other rotor blade mounted actuation concepts have been proposed and implemented. A few very good surveys of these techniques have been presented [Straub, 1993; Strehlow, 1993; Friedmann, 1998].

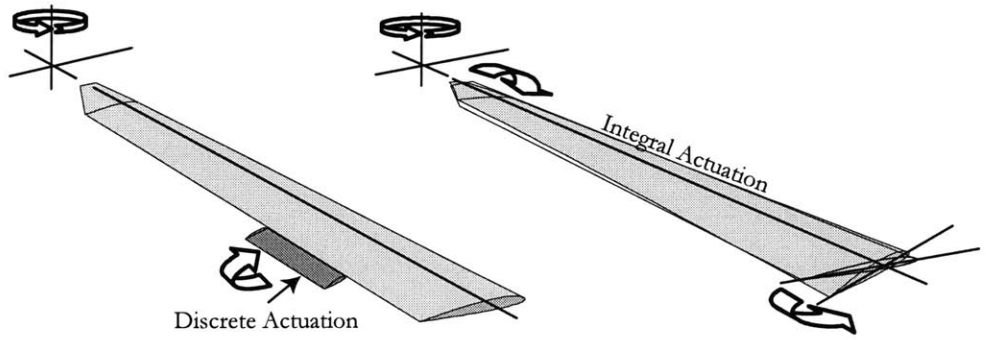

Figure 1-1: Integral and discrete actuation concepts for rotor blade application

1.2.2 Active Material Actuators

Active material actuators have become a viable option to implement IBC to reduce rotor vibration and noise [Spangler 1990]. In early 90s, Spangler and Hall designed a trailing edge flap actuator using a piezoelectric bimorph cantilevered from the blade spar. The use of active materials for blade mounted actuation in IBC provides two additional advantages over hydraulic or pneumatic systems. First, the high bandwidth characteristics of the active material improves closed-loop control performance. Second, active materials are powered electrically and electrical actuation is preferred over hydraulic or pneumatic actuation because standard slipring and wiring techniques could be employed. It simplifies the implementation of the actuator system while reducing manufacturing and maintenance costs. Thus, active material actuators have helped to overcome the size, weight, and complexity problems that have limited the incorporation of hydraulic actuators into helicopter blades [Straub, 1996]. A number of concepts have been proposed for using active material actuators in rotor control. Two fundamentally different actuation concepts have emerged. These are termed discrete actuator and integral actuator rotor blade concepts. Discrete and integral actuation concepts are illustrated in Figure 1-1.

The discrete actuator concept employes an actuator embedded in the rotor blade structure to control a trailing edge servo-flap, located near the blade tip [Friedman, 1998]. The actuator is typically powered by a high bandwidth active material. High frequency deflections of the servo-flap leads to linear blade pitch variations inducing aerodynamic lift and moment forces, which result in changes in rotor hub reactions [Lemnios, 1976; McCloud, 1978]. The challenge in the discrete actuator concept has been the development of an effective discrete actuator to adequately perform the servo-flap control. Spangler and Hall first proposed trailing edge servo-flap actuation using a piezoelectric bender actuator [Spangler, 1990]. Many other researchers have implemented bimorph "bender" concepts and demonstrated their capabilities in hover and wind tunnel testing [Walz 1994, Fulton 1998; Ben-Zeev, 1996]. More recently, a discretely actuated rotor blade was developed at MIT by Prechtl and Hall, in conjunction with Boeing Helicopters [Prechtl, 2000]. This actuation scheme was based on a "X-Frame" piezoelectric stack actuator with a displacement amplification mechanism to drive a trailing edge flap [Hall, 1996]. The blade showed success in vibration reduction studies, virtually eliminating vibration at several rotor harmonics simultaneously [Prechtl, 2000b].

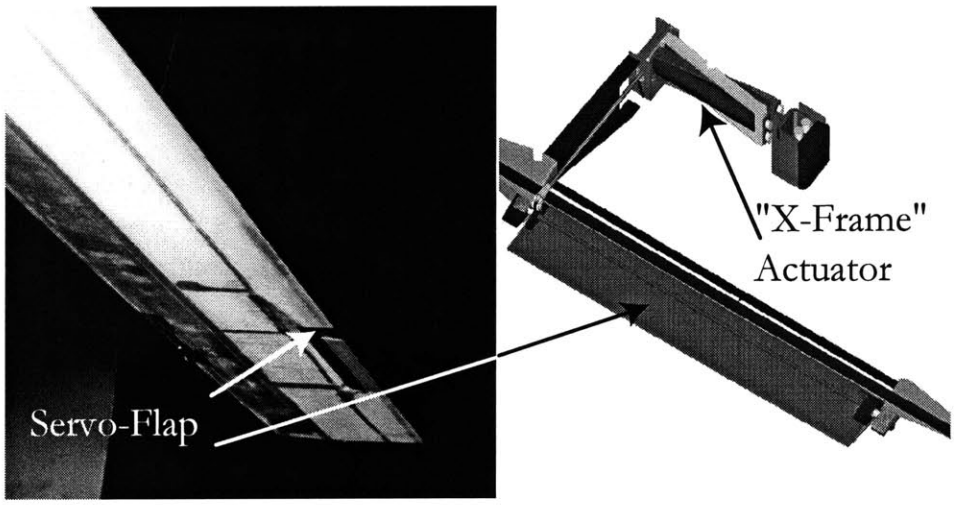

Figure 1-2: MIT/Boeing discrete blade with the "X-Frame" actuator [Prechtl, 2000]

A full scale discrete actuator dubbed as "Double X-Frame" is being incorporated into an MD-900 rotor blade by Boeing Helicopters, Mesa [Straub, 2000]. This blade incorporates a piezo stack actuator for high frequency actuation.

1.2.3 Integral Actuation Concept

In the integral actuator concept, the actuator system is either bonded or embedded in the blade skin or integrated directly into the blade structure in order to obtain a smooth continuous deformation in the blade as illustrated in Figure 1-1. A number of theoretical studied have been performed to estimate the degree of twist required to achieve rotor vibration and noise reduction [Waltz, 1994]. Since the active material actuators can be embedded directly into the structure without any external components, this concept has a clear aerodynamic advantage over the discrete actuation concept. The structural actuators are designed to generate actuation force at $\pm 45^{\circ}$ orientations to induce torsional moment on the stiff blade structure. Typically, the actuators are distributed over the entire span of the blade, resulting in an effective torsional moment near the blade tip. Research of this type of active rotor blade actuation has been performed at the University of Maryland by Chen and Chopra by embedding piezoceramic actuators [Chen, 1994]. This early attempt showed very limited authority but illustrated the feasibility of the general concept. More recently, two projects are ongoing at MIT in order to develop the integrally actuated rotor blades using piezoelectric actuators known as Active Fiber Composites (AFCs). The AFC actuator concept and details of the actuator material system is discussed in more detail in Chapter 2. Employment of AFC actuators for integrally actuated rotor blade is pursued by Hagood in collaboration with Boeing Helicopters and Cesnik/Hagood collaborating with NASA Langley. Both MIT integrally actuated rotor blade efforts are based on embedding AFC actuators in the composite structure of the blade.

In 1998, a 1/6-scale, 60.6" radius, Mach scaled CH-47D integrally actuated rotor blade was built by John Rodgers at MIT in collaboration with Boeing Helicopters [Rodgers, 1998]. This blade was manufactured under the Phase I of the Boeing Rotorcraft program and it incorporated AFC actuators embedded in the blade spar laminate along the span of the blade. This prototype blade proved the concept of integrating AFC actuators for integral actuation and the blade was tested in the MIT hover test facility. The MIT/Boeing blade showed a $0.8^{\circ}/m$ twist rate at half of the design voltage with 69% of the actuators working. There were many actuator failures that occurred before and during testing. A full failure history has been published [Rodgers, 1998]. Further investigations into the actuator failure and manufacturing difficulties were conducted order to improve the performance and manufacturability of future blades [Schmidt,

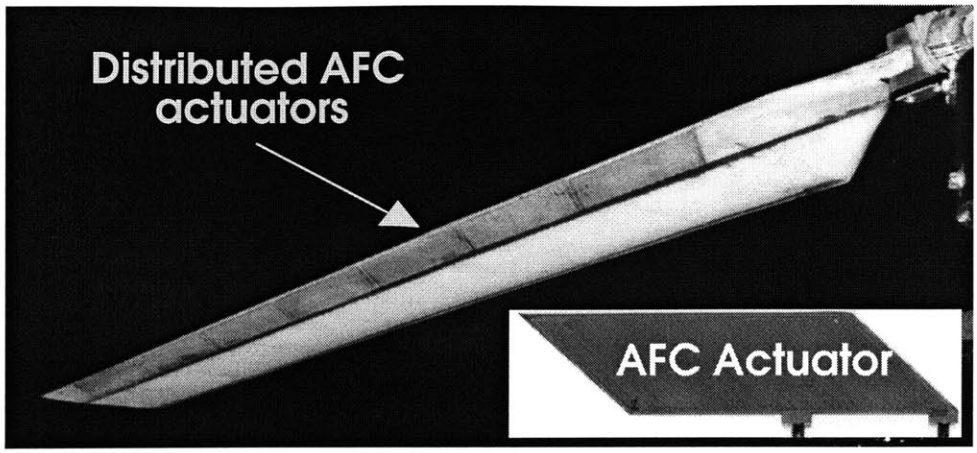

Figure 1-3: MIT/Boeing integral blade incorporated with AFC actuators [Rodgers, 1998]

2000a]. Many improvements to the blade manufacturing process and the AFC actuator material system were suggested [Schmidt, 2000b]. Under the Phase II of the Boeing Rotorcraft program, a set of 5 advanced CH-47D 1/6-scale, Mach scaled blades are built by Boeing Helicopters for hover and forward flight tests. These advanced CH-47D blades incorporate a modified AFC actuator material system and the blades are manufactured according to an improved blade designed and manufacturing procedure [Schmidt, 2000b].

In 1999, Sanjoon Shin at MIT built an integrally actuated blade using AFC actuators with the collaboration of NASA-Langley [Shin, 1999]. This was a Froude scaled blade based on NACA-0012 airfoil with a chord length of 4.24" and a rotor radius of 55" [Cesnik, 1999]. The prototype MIT/NASA blade was tested in hover at the NASA-Langley wind tunnel and it showed moderately successful results [Wilbur, 2000]. Another set of blades similar to the prototype blade were also built by NASA for further testing. These MIT/NASA blades were tested in hover and they have produced expected results [Shin, 2000b].

1.3 Objectives

The objective of this thesis is to characterize the latest generation of AFC actuator material system to be embedded into the composite structure of the Active Material Rotor (AMR) blade manufactured under the Phase II of the Boeing Rotorcraft program. The AMR is a 1/6-scale,

Mach scaled advanced CH-47D blade employing integrated AFC actuators for active twist. A set of 5 blades are manufactured by Boeing Helicopters to conducted hover and forward flight wind tunnel tests. Since the AFCs represent a relatively new and unique type of material system, it is necessary to extensively modify the existing test procedures, where they existed, and develop new testing procedure to characterize all of the relevant physical, mechanical, electrical and coupled electromechanical properties required for structural application development. The uniqueness of the characterization requirements stem not only from the AFC's actuation capability but also from the fact that they are used in the rotor blade application as hybrid laminates, incorporated as active layers among the passive composite structure. Therefore, extensive material characterization is necessary to evaluate the properties of AFCs as structural actuators and as structural components that can withstand the demanding blade operating environment. Important material properties for the rotor blade application must be identified and comprehensive characterization testing methodology must be developed to evaluate the relevant material properties and limits under simulated blade conditions.

Important AFC actuator material properties can be grouped into three broad categories based on how they are used in distinct phases of the blade development and operation process.

1. Physical and mechanical properties required for the basic blade design and to predict blade properties.

2. Electrical and actuation properties for the determination of system-level actuation capabilities and performance.

3. Mechanical and electrical strength and durability properties needed to determine the blade operating envelope and verify the safety of operation.

In addition to determining these properties, a key result of this work is to make recommendations for future AFC actuator development and to improve material characterization testing methodology for similar applications.

Basic physical, mechanical properties of the actuator material system are required from the initial conceptual design to the final analysis of the active blade performance. The most important of these basic properties are the AFC thickness, density, elastic modulus and Poisson's ratios for both the longitudinal and the transverse directions. These properties are used to determine the physical and mechanical properties of the overall blade, which can be compared

to similar properties of other passive and active blades or used as input into aeroelastic codes to predicted blade loads. The estimated loads are used to predicted stresses and strains in the passive composites and thus perform a preliminary structural analysis.

The electrical and actuation properties are key to determining the blade performance as an active structure for vibration control. For the preliminary design purposes, the key actuation properties include the nominal operating voltage cycle of the actuators and the corresponding induced strain under both free strain and elastic constraint conditions. Detailed design of both the blade and the overall system requires more extensive characterization. It includes the determination of voltage limits based on arcing and depoling, knowledge of actuator heating effects based on current and power consumption, understanding actuation correction factors due to elastic constraint conditions, analysis of actuator performance based on voltage, frequency and applied mechanical loads.

The strength and durability properties of the AFC are required to determine the blade operating envelope and verify safety of operation. On the highest level, the blade structure is designed such that loss or degradation of actuator properties would not, under any circumstances, pose a safety of flight issue. From a structural design standpoint the most important mechanical properties are the static strength and the fatigue strength. Due to the fact that AFCs are used in a hybrid laminated configuration, the testing focuses on stiffness retention capability of the actuator rather than the overall strength of the AFC. The stiffness properties are determined for bare actuators, simple hybrid laminates containing both actuators and passive plies, and complex hybrid laminates representative of the intended laminate configuration. The simple hybrid laminate actuator specimens must be produced to provide the same level of elastic constraint on the AFC as the blade structure. The representative laminates specimens must be constructed to represent the composite structure of the blade spar laminate. The static testing is conducted to failure, while fatigue testing represents loads that would be seen on the model rotor blade in the forward flight condition during the wind tunnel tests. The electrical fatigue tests are also included to evaluate the long-term reliability, performance and safety of the actuator material system. Although the later factors may not enter into the safety of flight issue, they are useful in setting limits on the blade tests as well as support for the eventual application of the AFC actuator system for human flight vehicles.

1.4 Approach

The approach used in AFC material characterization for the rotor blade application is a modified version of the building block methodology used in the design and testing of traditional composite structures. The building block approach begins with tests at the simplest level and gradually expanding the testing to include more complex and complete structures. During the whole process the test data is analyzed, fed into the design process and modifications are made to the material system to obtain the required properties and behavior. The building block approach used in the integrally actuated rotor blade project is illustrated in the Figure 1-4.

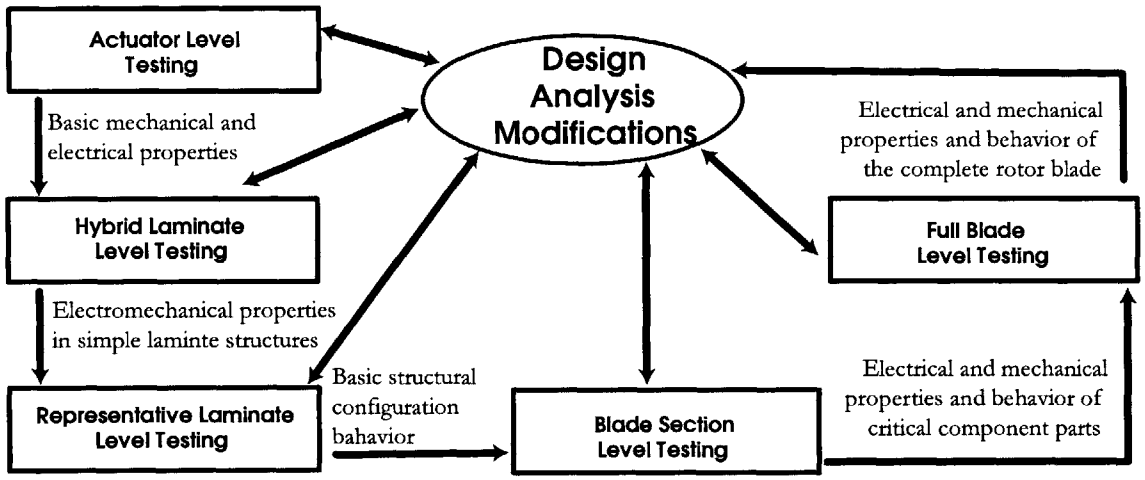

Figure 1-4: Building block approach used for AFC actuator characterization process

The first three segments of the building block approach illustrated in Figure 1-4, namely, bare actuator level testing, hybrid laminate level testing, and representative laminate level testing, are discussed in the thesis. The details of the last two segments of the building block approach, namely, blade section testing and complete blade testing, are discussed in detail in Schmidt's thesis [Schmidt, 2000b].

Numerous tests are designed in order to achieve all of the objectives discussed in Section 1.3. AFC test articles are designed specifically for each test to simplify the extraction of the required material properties. A comprehensive test matrix is developed for each test in order to completely understand the behavior of the actuator in different configurations and

test conditions. Detailed testing procedures are developed for each test to standardize the testing methodology in order to obtain repeatable results during the current testing process and future AFC characterization efforts. The following tests are conducted on the AFC actuator material system in order to understand the material behavior and extract the important material properties required for the AMR blade development.

- Stress-strain tests: To extract elastic modulus and Poisson's ratios for both the longitudinal and the transverse directions as a function of the mechanical strain on the actuator.
- Free strain performance tests: To understand the variation in the longitudinal and the transverse actuator performance due to voltage, frequency, and elastic constraint levels.
- Performance tests under tensile loads: To determine the actuator performance degradation and the performance recovery due to tensile loading conditions.
- Electrical fatigue tests: To evaluate the durability and performance of the actuator system due to repeated actuation.
- Mechanical fatigue tests: To quality the actuator system as a structural component and evaluate the actuator induced strain performance under mechanical fatigue conditions.

The objectives of the test, details of the test specimen, complete test matrix, step-by-step test procedure and test results for each of the above tests are provided in the following chapters. The results of the AFC material characterization tests are analyzed and conclusions are made in order to facilitate the design and operation of the AMR blade. Finally, recommendations for the actuator material system modifications are made in order to facilitate improvements to actuator system for future applications.

1.5 Summary of Document

Chapter 2 introduces the AFC actuator concept and provides a historical background in the actuator material system progression. Details of the AFC material system selected for the current AMR blade project is presented with a discussion of advantages and disadvantage of the selected material system. The design and preparation of various AFC material characterization

test articles are discussed. A simple rule of mixtures model is introduced to evaluate the fiber direction stiffness properties of the actuator. This model is used to estimate the AFC longitudinal modulus and the constraint effects due to passive materials on the longitudinal actuation performance.

Chapter 3 presents the details of stress-strain tests designed to extract multidirectional elastic modulus and Poisson's ratios from the AFC actuator material system. The tests are conducted in accordance to the ASTM D3039 standard, the standard test method for tensile properties of polymer matrix composite materials. A comprehensive test matrix is developed to evaluate stress-strain behavior of the AFC actuator system under various configurations and test conditions. Details of the test setup is provided and a step-by-step testing procedure is outlined to perform the stress-strain tests efficiently while minimizing experimental errors. Important test results are identified and the relevance of the results are discussed in context of the AMR blade development.

Chapter 4 explains the free strain performance tests that are conducted to measure the actuator induced strain output due to electrical excitation. The free strain performance is used as the primary performance metric of the AFC actuator. The actuator performance is measured for a range of peak-to-peak voltages (Vpp), DC bias voltages (Vdc) and frequencies as well as unlaminated and E-Glass laminated actuators to understand the non-linear variation in the actuator strain output. A customized test setup is developed and a detailed testing procedure is outlined. Important free strain actuator properties are extract from test results and the optimum voltage cycle to be used in the AMR blade operation is determined.

Chapter 5 outlines the process of testing the AFC actuator performance under static tensile loads. It is important to evaluate the actuator robustness and performance under high tensile strain conditions because the AFCs embedded in the AMR blade are expected operate under high tensile loads. A test matrix is developed to evaluate the actuator performance during and after loading up to three maximum tensile load levels, namely, $2000\mu\varepsilon$, $4000\mu\varepsilon$, and $6000\mu\varepsilon$. Details of the test setup and the step-by-step testing procedure is outline. The results are discussed to identify the extend of total accumulated damage, residual actuation, performance recovery, and the rate of degradation in the performance. The test results are analyzed in order to verify the capabilities of AFC actuators to operate under high tensile load conditions.

Chapter 6 discusses the electrical fatigue tests conducted on actuators to simulated the repeated actuation of AFCs during the blade operation. The tests are conducted under two mechanical loading conditions. The first part of the chapter presents the details of tests conducted under free strain condition. In the free strain condition, the AFCs are electrically fatigued up to 20 million cycles without any external mechanical load applied to the actuator. The second part of the chapter presents the details of electrical fatigue tests conducted under tensile loading condition. In the tensile load condition, the actuators are electrically fatigued up to 10 million cycles while a constant tensile load is applied to the actuator. The test results are discussed to evaluate the durability issues of the actuator material system and the long-term operational reliability of the AMR blade.

Chapter 7 presents the mechanical fatigue tests conducted on the AFC material system to simulate the repeated mechanical loading on actuators during the AMR blade operation. The tests are conducted using two types of AFC test specimens, namely, E-Glass laminated actuators and representative laminate coupons. The first part of the chapter details the test setup, testing procedure, and the test results from the mechanical fatigue tests conducted on laminated actuators. The laminated actuators are tested up to 10 million mechanical cycles under two load levels: the nominal fatigue cycle of $1000\mu\varepsilon \pm 900\mu\varepsilon$ and the extended fatigue cycle of $15000\mu\varepsilon \pm 1350\mu\varepsilon$. The test results are used to evaluate the fatigue strength of the AFC actuator material system under simulated rotor blade conditions. The latter part of the chapter discusses mechanical fatigue tests conducted on the representative laminate coupons. The test coupons are constructed to represent the composite structure of the blade spar laminate. The test setup and the testing procedure used for the representative laminate mechanical fatigue tests are not discussed in this thesis because the tests are conducted at Boeing Helicopters, Philadelphia. The results from the representative laminate tests are discussed to evaluate the mechanical fatigue strength of the hybrid laminate in the AMR blade spar.

Chapter 8 concludes the thesis by summarizing the contributions and conclusions of the work. Recommendations for future actuator material characterization tests for similar applications are provided along with recommendations to improve the AFC material properties and performance.

Chapter 2

Active Fiber Composite Actuator

Active Fiber Composites (AFCs) have been in development for the past decade for structural actuation applications. AFC actuators are fundamental to the integrally actuated AMR blade in which the actuators are integrated into the composite structure. Embedded actuators induce stresses required for twist actuation of the stiff blade structure. Thus the AFC material system is required to fill dual roles in the AMR blade application. As an actuator, it must be capable of providing required actuation authority to perform structural control while withstanding the demanding rotor environment. Furthermore, it must meet all requirements of a structural component in order to maintain the structural integrity of the blade. Therefore, the material system in the AFC actuator must be selected to satisfy both the structural and the actuation requirements of the AMR blade application. The versatility of the AFC has enabled wider applicability than other conventional structural actuators due to its greater performance, high strength, conformability and ease of integration. This chapter provides a description of the AFC actuator concept, details of the actuator material system, preparation of various actuator tests articles and a simple model to estimate AFC stiffness properties in the fiber direction.

2.1 AFC Concept

The primary material used in the AFC actuator system is piezoceramic fibers. Continuous and aligned piezoceramic fibers are used to provide the in-plane actuation due to its inherent coupling between the electrical and the mechanical behavior. Mechanical displacement of

piezoceramic material causes a charge flow through the material, generating electrical energy. Similarly, an application of an electric field causes a mechanical deformation in the piezoceramic material. Extensive information on piezoceramic have been published, and therefore details are not discussed in this thesis [Bent, 1997; Ghandi, 1998; Jaffe, 1971; Buchanan, 1986].

At present, most piezoceramic actuators are based on piezoceramic wafers, either as single wafer actuators or as wafer stack actuators. In contrast, the AFC actuators consist of piezoceramic fibers embedded in a polymer matrix as seen in Figure 2-1. Brittle ceramic fibers with very high stiffness provide the actuation authority. However, piezoceramic fibers tend to crack at relatively low strains due to its brittle nature. The strength and toughness properties of the AFC is significantly improved due to the polymer matrix that surrounds the fibers. Matrix material provides a path for an efficient load transfer mechanism around fiber cracks. Thus, the matrix reinforces the fibers, allowing the actuator to withstand higher strains than individual fibers. Further, the matrix helps to prevent a crack on a fiber from propagating to adjacent fibers, inhibiting catastrophic damage in AFC actuator at high strains. This presents an improvement over actuators based on ceramic wafers, which are prone to macroscopic and catastrophic damage resulting from cracks in the ceramic [Jones, 1999].

The piezoceramic fibers in the epoxy matrix are sandwiched between two layers of polyimid film which has a conductive pattern in the inner surface for applying the driving electrical field. The electrical field is applied to the fibers using an interdigitated electrode pattern. The interdigitated electrode pattern is an efficient method to orient the electric field along the fiber, thus enabling the use of primary piezoceramic effect. Excitation of the actuator using an electrical field causes an in-plane mechanical deformation in the direction of the fibers with a small deformation perpendicular to the fibers.

One of the primary advantages of the AFC actuator system is the anisotropic actuation due to its inherent unidirectional fiber structure [Bent, 1997]. Anisotropic actuation enables to induce shear stresses necessary to directly twist the blade structure. Further, the anisotropic performance of the actuator is enhanced due to the use of the primary piezoceramic effect. The electric field alternates in successive electrode fingers of opposing polarity as shows in Figure 2-1. The net effect is a significant positive strain in each of the segments with an applied electrical field in the fiber direction.

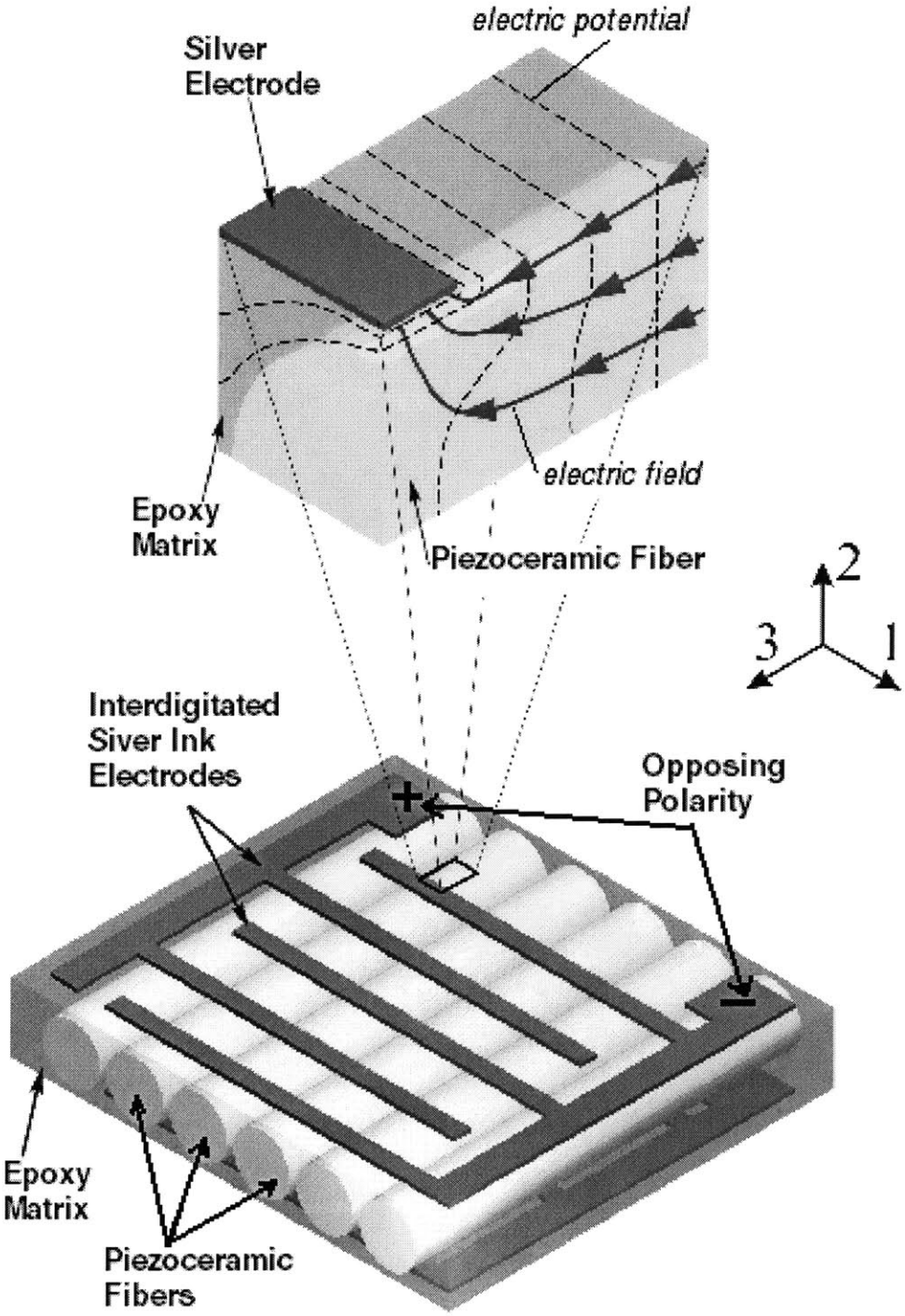

Figure 2-1: Macro and micro view of the AFC actuator concept

Another major advantage of the AFC actuator system is the conformability due to its inherent composite structure [Rodgers, 1998]. In contrast, conventional electroceramics are brittle and they must be specifically designed and fabricated to match the required curvature of an application. The AFC actuators can be bonded or embedded within a non-planer structure, for example, the rotor blade, due to its ability to conform. The structural integrity of the actuator is also significantly greater since the composite construction allows the load sharing between the fibers through the matrix. When embedded in a structure, the structure itself provides a load sharing paths around the cracks in ceramic fibers, enhancing the integrity of the active structure. The distributed actuation system using a number of AFC actuators increases the robustness of the system. This robustness is due to the redundancy of the system where a failure of a single or few actuators does not catastrophically affect the integrity of the entire active structure or the performance of the system.

The main disadvantages of AFCs as structural actuators are the high cost and the high driving voltages required for operation [Janos, 2000]. The cost is expected to decrease with the commercialization of AFCs. High volume production and large scale manufacturing techniques would help reduce the cost in the future. The required voltage is also expected to decrease as advances are made in AFC related technology, such as, improvements in piezoceramic fiber quality and actuator manufacturing techniques.

2.2 Material System Development

The AFC actuator concept originated form the work of Bent and Hagood of the Active Material and Structures Laboratory at the Massachusetts Institute of Technology in early 1990s. At present, the AFC actuator systems are commercially available through Continuum Control Corporation[1]. AFCs have been under steady development over the past decade and the actuator constituent material system has progressed over time. The actuator system has become more reliable and manufacturability has been improved [Strock, 1999]. The cost of the actuator system has also decreased while the performance of the actuators have improved steadily.

[1] Continuum Control Corporation, Billerica, MA, Ph: 978-670-4910.

2.2.1 Fibers

At the early stages of the AFC actuator technology, a variety of piezoceramic fiber compositions were studied extensively to optimize the actuator performance, manufacturability, structural integrity and reliability. The piezoceramic fibers consisted of PZT (Lead Zirconate Titanate) and variations of the PZT composition, such as, PZT-5A, PZT-5H, PZT-4S, and PZT-8M, were studied [Bent, 1997]. PZT is a ferroelectric ceramic material with piezoelectric properties which enable behavior that converts electrical energy to mechanical energy and vice-versa. Behavior of PZT material is non-linear and hysteric. Both circular and rectangular fiber geometries were also studied to optimize the actuator performance [Bent, 1997]. Circular PZT-5H fibers were selected initially and the fiber composition was changed to PZT-5A due to depole stress considerations [Bent, 1997]. The diameter of PZT-5A fibers selected originally was 0.005". At the end of 1999, 0.01" diameter fibers were introduced as a possible alternative to the 0.005" fibers. Larger diameter fibers improved the manufacturability and scalability of the AFC actuator system for large scale applications. The advantages and disadvantages of the 0.005" versus 0.01" diameter fibers are discussed in Section 2.3.

2.2.2 Matrix

The actuator martrix material has also evolved over time. The original matrix material selected for the AFC actuator system was wet thermoset matrix comprised of EPON^{TM} Resin 9405 with EPI-CURE^{TM} 9470 curing agent[2]. At present, Continuum Control Corporation is using a dry film resin matrix material. The dry film resin system has enabled the use of hybrid lamination approach to be used in the AFC manufacturing process [Pizzochero, 2000]. Better handling qualities of the new dry resin system has simplified the manufacturing process, cutting down the manufacturing time drastically. The dry film has improved the reliability of the actuator and lead to an increased yield in manufacturing because it provides less opportunities to trap air bubbles inside the matrix, thus increasing the dielectric breakdown strength of the actuator. It has also enhanced the high volume AFC production capability.

[2] Shell Chemicals, Houston, TX, Ph: 800-872-7435.

2.2.3 Electrodes

At the beginning of the AFC actuator development process, the interdigitated electrodes were made out of copper on top of 0.0005" Kapton substrate. Labor intensive copper etching technique was used to produce copper-Kapton electrodes [Rodgers, 1998]. The thickness of the Kapton substrate was increased to 0.001" in order to overcome handling difficulties. Due to the high cost and manufacturing difficulties, the copper-Kapton electrodes were abandoned in favor of cheap screen printed electrode system. At present, the electrodes are screen printed onto a 0.001" Kapton substrate using silver based conductive ink. These electrodes are manufactured in large volumes at a relatively low cost [Pizzochero, 2000]. Further, the silver ink electrodes are more malleable, thus conforming better to the shape of the fibers, providing a better contact between the electrodes and the fibers. This increases the performance of the actuator by introducing more of the electrical field into piezoceramic fibers.

The AFC actuator material system continues to evolve even at present to further enhance its actuation and structural qualities while simplifying the manufacturing process and reducing the unit cost.

2.3 Selected AFC Material System

The AFC actuator material system selected for the current AMR blade application consists of PZT-5A circular fibers embedded in a polymer matrix material. At the beginning of the actuator material selection process 0.005" diameter fibers were selected. In 1999, 0.01" fibers were introduced as an alternative to the 0.005" fibers.

2.3.1 Advantages

Larger diameter 0.01" fiber actuators provided many advantages for the AMR blade application. Larger fibers are easy to handle, improving the actuator manufacturability and reducing labor cost. Also, the driving factor for higher actuation authority is the volume of active material, therefore, a given actuation authority can be achieved from a quarter as many 0.010" fibers as from 0.005" fibers. Furthermore, straighter 0.010" fibers helps to achieve higher fiber line fractions than with 0.005" fiber. Fiber line fractions as high as 90% are achievable with the

0.01" fibers since the fibers can be packed more closely together due to increased straightness, further increasing the actuation authority [Pizzocchero, 2000]. The fiber line fractions up to only 80% are achieved in 0.005" diameter fiber AFCs due to increased wavy nature of the fibers. A lower number of fibers required to produce a given actuation authority also leads to cost savings as well. The cost of piezoceramic material used in an actuator depends on the number of fibers and not on the volume of bulk material. Therefore AFCs with lower number of fibers are less expensive. Furthermore, larger fibers increases the potential to scale up the use of the actuator material system from a 1/6-scale blade to a full-scale AFC based rotor blade [Weems, 2000].

2.3.2 Disadvantages

The AFCs with larger diameter fibers have a few disadvantages as well. The higher cross-sectional area in the 0.01" fibers increases the probability of having defects in the ceramic material. The increased probability of defects in larger fibers decreases the fiber strength and leads to fiber cracking at lower strains. To compound the problem of fiber cracking, the higher attainable fiber line fractions in 0.01" fiber actuators limit the amount of epoxy matrix surrounding the fibers as seen in Figure 2-2. This results in a lower matrix volume fraction in 0.01" fiber AFCs and compromises the load transfer path around cracked fibers. Therefore, a crack on a single fiber creates a stress concentration that may facilitate the propagation of the crack to the adjacent fibers, causing macroscopic damage to the composite [Jones, 1999].

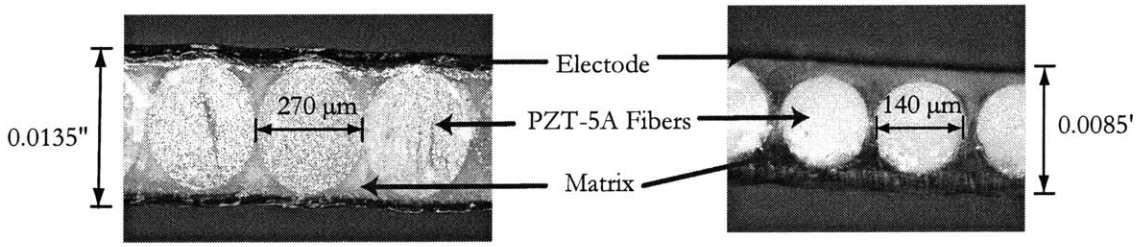

Figure 2-2: Cross-section pictures of 0.01" and 0.005" diameter fiber AFCs

2.3.3 Characterized Material Systems

The actuator material characterization is primarily conducted on an actuator material system consists of 0.01" diameter PZT-5A fiber embeded in a dry film matrix. The fibers are manufactured by CeraNova Corporation[3] using an in-house extrusion process. The electrodes are screen printed with silver ink on 0.001" Kapton substrate. Copper pads are incorporated onto the silver electrode tabs to simplify high voltage wire connections. The total thickness of the actuators made out of 0.01" fibers is ~0.0135" and the nominal fiber line fraction is ~90%.

The secondary AFC actuator material system that is characterized include 0.005" diameter PZT-5A circular fiber with Shell Epon[4] wet resin matrix system. The interdigitated electrodes are screen-printed using silver ink on 0.001" Kapton substrate. The total thickness of the AFC actuators made out of 0.005" fibers is ~0.0085" and the nominal fiber line fraction is ~80%.

The summary of the primary and the secondary AFC material systems are shown in Table 2.1. Both 0.01" and 0.005" AFC actuator systems are manufactured by Continuum Control Corporation[5], contracted vendor for the AMR blade actuators.

Material Specifications	**Secondary material system**	**Primary material system**
piezoceramic fiber type	PZT-5A	PZT-5A
Fiber diameter	140 μm	270 μm
Fiber line fraction	~80 %	~90 %
Matrix material	Shell Epon wet resin	Dry film resin
Electrode substrate	0.001" Kapton	0.001" Kapton
Electrode material	silver ink	silver ink
Electrode tab	silver ink	copper pads
Total thickness	0.0085"	0.0135"

Table 2.1: Characterized AFC actuator material system specifications

The manufacturer is responsible for poling the AFC actuators. Poling process is required for piezoceramic based actuators in order to enhance the electromechanical qualities that leads to higher induced strain output. The poling is performed in air at 100°F with a constant DC voltage of 4000V. The actuators are allowed to warm up to the poling temperature and then the voltage is applied and held for 20 minutes.

[3] CeraNova Corporation, Franklin, MA, Ph: 508-520-7600.
[4] EPON™ 9405 with EPI-CURE™ 9470, Shell Chemicals, Houston, TX, Ph: 800-872-7435.
[5] Continuum Control Corporation, Billerica, MA, Ph: 978-670-4910.

2.4 AFC Test Article Design

Different types of AFC tests articles are utilized for characterization tests in order to optimize their ability to extract the required material property from a given test while simplifying the experimentation process and the data analysis. The high cost of the actuator material is also considered when designing the material characterization test articles. Active test articles are used to evaluate the actuator performance under various test conditions and configurations. If the actuator induced strain output is not measured during the test, passive test articles are used. Furthermore, some of the test are conducted on actuators laminated with passive E-Glass plies in order to simulate the hybrid use of the AFC actuator. As discussed in Section 1.3, the AFC actuators are used in the AMR blade application as hybrid laminates.

2.4.1 Narrow Test Coupons

A narrow AFC test coupon is designed specifically for actuator material characterization in accordance to the ASTM testing standard for tensile properties of polymer matrix composite materials [ASTM, D3039]. However, the ideal test coupon could not be designed due to limitations in the AFC actuator material components. Therefore, the narrow test coupon is designed to maximize the conformity to the above standard. The length of the actuator coupon is limited by the maximum length available in piezoceramic fibers. At the time of this project, the maximum length of fibers available from the manufacturer is approximately 6" [Pizzochero, 2000]. The Figure 2-3 shows the dimensions and a picture of the narrow AFC test coupon.

The overall length of the narrow test coupon is 6.5" and the active length is limited to 3.95". The active length is defined as the distance between the last electrode finger at each end of the electrode pattern. The electrode tabs are located on both ends of the actuator and they are used to supply the voltage necessary for actuation. The end areas of the test coupon is also used to bond the loading tabs when the actuator is used for mechanical testing.

The screen printed silver ink electrodes fingers are 0.007" wide and they are 0.045" apart. The electrode railings are 0.045" wide and they connect all of the appropriate electrode fingers to the correct electrode tab. A detailed drawing of the electrode is shown in Figure 2-4.

As illustrated in Figure 2-4, the interdigitated electrode pattern creates an active width in

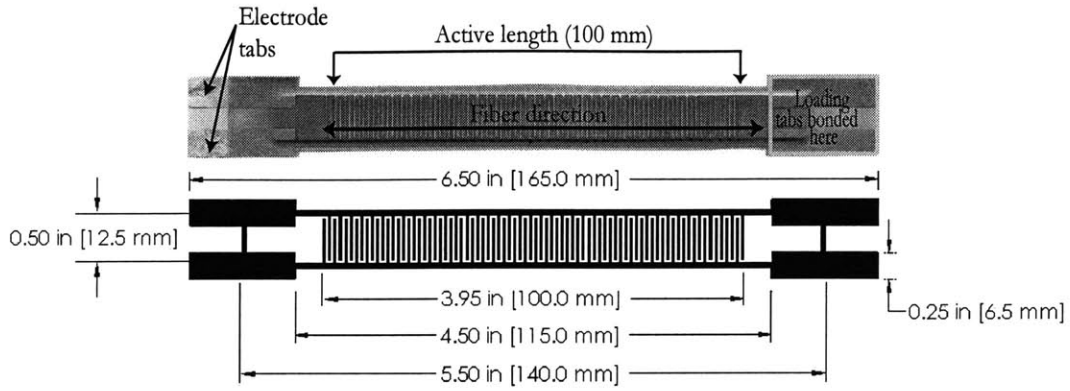

Figure 2-3: Dimentional drawing and a picture of a narrow AFC test coupon

the middle of the actuator and an inactive width on each side. The active width is defined as the area where both the positive and the negative electrodes are side by side of each other to provide an effective electrical field for the fibers. The inactive width has only one of the electrodes present, positive or negative, thus the fibers in the inactive width does not actuate.

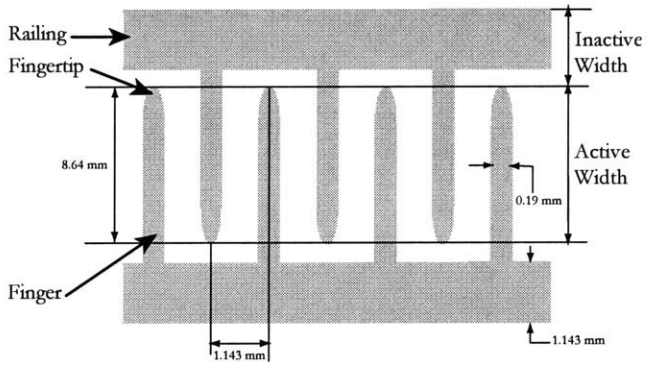

Figure 2-4: Detailed drawing of the interdigitated electrode pattern

The active width of the narrow test coupon is selected to represent the behavior of the AFC actuators incorporated in the AMR blade with the minimum number of piezoceramic fibers. This is to reduce the cost of each tests article because the major cost item is the fibers. Therefore, the active width of the narrow test coupon is limited to 0.34" and it holds 30 fibers of 0.001" in diameter or 54 fibers of 0.005" in diameter. The piezoceramic fibers that lie within

the active width provide the actuation authority. All of the materials in the inactive area act as a constraint to the actuator, providing a clamping effect on the actuation. It is important to note that piezoceramic fibers in the inactive width introduce a large clamping effect due to high stiffness of the ceramic. It results in lower induced strain performance in the actuator. Such clamping effect due to high number of fibers in the inactive area resulted in lower than expected induced strain performance on early generation of 0.005" fibers AFC coupons. At present, the improvements in the manufacturing techniques enable to contain all the piezoceramic fibers within the active area, resulting in higher induced strain performance.

2.4.2 Wide Actuators

The wide (2.0" x 5.75") AFC actuator type shown in Figure 2-5 is used to obtain the transverse actuation measurements. This type of wide actuators are manufactured by Continuum Control Corporation as a standard product. The narrow test coupons discussed Section 2.4.1 can not be used to measure the transverse actuation due to the limited active width. Furthermore, the narrow test coupons can not be mounted properly on the AFC testing rig discussed in Section 4.3 to obtain the transverse performance.

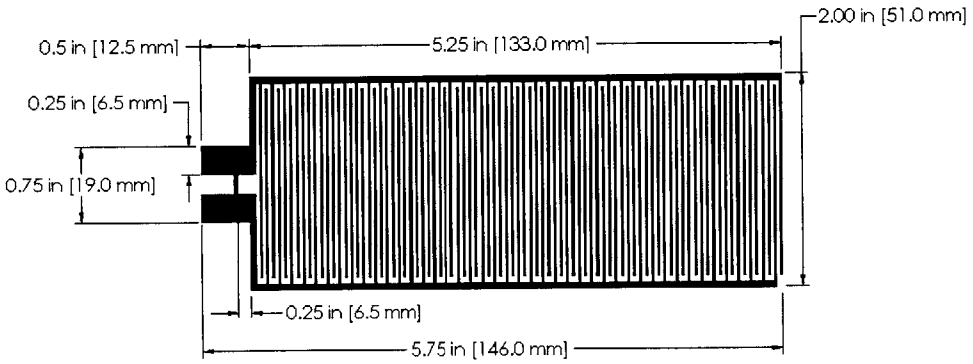

Figure 2-5: Dimentional drawing of a wide AFC actuator

2.4.3 Passive Test Articles

The passive test articles are used for characterization tests designed to evaluate only the mechanical properties of the material system, such as the stress-strain tests. The wide passive

articles are cut from wide actuators discussed in Section 2.4.2. The 1.0" wide longitudinal and the transverse modulus test articles are cut as shown in Figure 2-6. These passive articles can not be actuated due to the lack of proper electrodes. A benefit in the passive test articles is that the cut out pieces have a coherent cross-sectional area due to elimination of the edge regions, such as the inactive width.

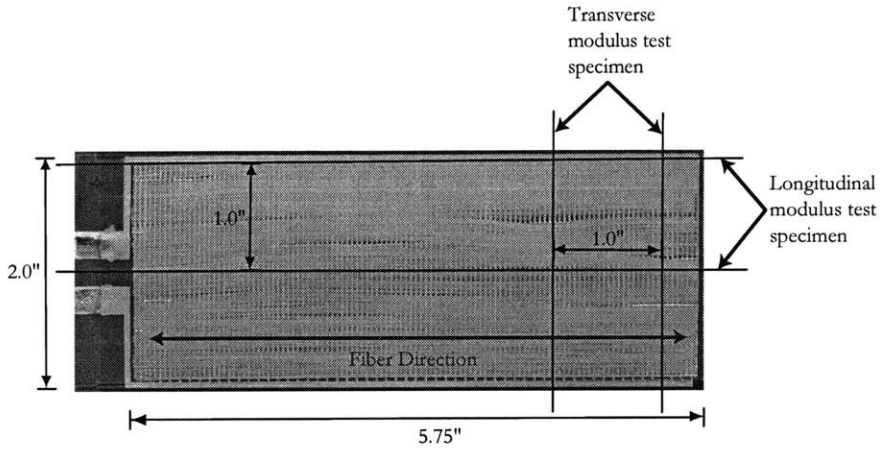

Figure 2-6: Extraction of passive test articles from a wide actuator

2.5 Test Article Preparation Process

Many of the test articles needed prior preparation before undergoing various characterization tests. The preparation process include E-Glass lamination, high voltage wiring, strain gage application and loading tab bonding.

2.5.1 Lamination Procedure

The actuator specimens are laminated with E-Glass[6] in order construct simple hybrid laminates and the lamination introduces passive elastic constraint to the actuator. The test matrix of each characterization test described in latter chapters requires the actuator specimens to be

[6]Hexcel E120-155 prepreg cloth, Pleasanton, CA, Ph: 925-847-9500.

symmetrically laminated with one or two plies of E-Glass.

The cure plates used for the lamination process are made out of steel and they are wrapped in a Guaranteed Non-Porous Teflon[7] (GNPT) sheet. Covering the steel plates from GNPT prevents the plates from bonding to the laminate during the cure. The lamination process begins by cutting the E-Glass to the required dimension and the ply orientation. The E-Glass used for lamination is 0.0045" thick E120-style prepreg cloth. The surface of the AFC specimens are cleaned with acetone and methanol to ensure proper bonding. The E-Glass strips are placed on both surfaces of the AFC and the hybrid laminate is placed on the bottom cure plate. A strip of GNPT is cut to the test article dimensions and placed on top of the hybrid lay-up. The Figure 2-7 shows the details of the E-Glass lamination process.

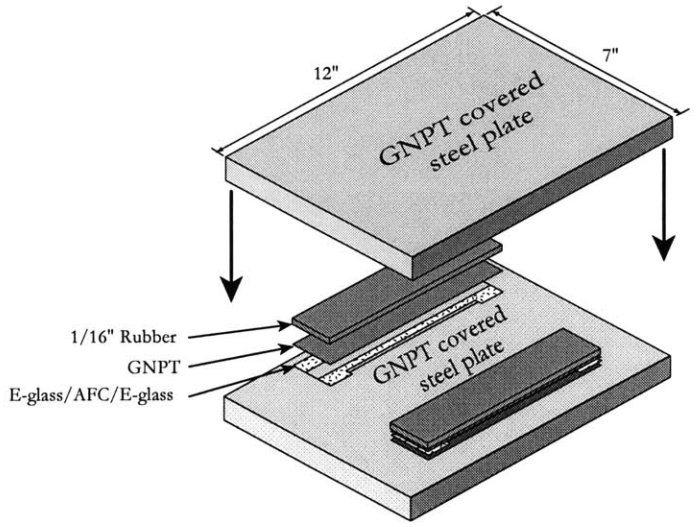

Figure 2-7: Setup used for AFC actuator lamination process with E-Glass

A piece of silicon rubber is cut from a 1/16" thick sheet and placed on top of the GNPT strip. This rubber is used to distribute the pressure evenly on across the laminate. The top cure plate is then placed on the silicon rubber and the whole assembly is place in the hotpress. The hotpress is closed with a force necessary to generate the curing pressure of 60psi and the temperature is set for 250°F. The hybrid laminate is cured for 2 hours. After the cure, the

[7]GNPT, American Durafilm Co., Holliston, MA, Ph: 888-809-2314.

hotpress is opened and the laminate is cooled in air.

Once the laminate is cooled, the test articles are trimmed carefully with a surgical blade or a sharp edge. A high degree of care is taken not to damage the electrodes. The nominal thickness of 0.01" diameter fiber AFC actuator symmetrically laminated with one ply (1 E120) or two plies (2 E120) of E-Glass is 0.0225" and 0.0315", respectively.

2.5.2 High Voltage Wire Connections

Connecting wires to electrode tabs are essential prior to testing of active test articles. The normal soldering technique is used to make the connections on copper padded electrode tabs. However, a more complicated wiring procedure is used on silver ink electrode tabs. The wiring connections to silver electrode tabs are made using a silver based conductive epoxy. The E-Solder No. 3026 Flexible Conductive Adhesive[8] is chosen as the best product for this purpose. The adhesive process involves mixing the E-Solder and the hardener with 100:6.5 ratio by weight. The actuators are laid on a steel cure plate wrapped in a GNPT sheet. The GNPT sheet prevents the epoxy from bonding to the cure plate, if the epoxy leaks out of the electrode tab. A drop of conductive epoxy is place on the electrode tab and the tinned wire leads are placed on it. The wires are held in place by taping them on to the steel plate. A 1.0" wide strip of GNPT sheet and a 1/16" thick rubber strip is laid on the electrode tab and to cover the whole actuator. The top GNPT strip prevents the conductive epoxy from bonding to the rubber and the rubber is used to distribute the pressure evenly across the actuator. Then the top cure plate is placed on the rubber and the assembly placed in the hotpress. The curing procedure is similar to the lamination process discussed in Section 2.5.1. The conductive epoxy is cured at 180°F for 2 hours at 60psi.

2.5.3 Strain Gage Application

The strain gages are bonded on to test articles that undergo mechanical loading. The gages on the passive test articles are used to measure the mechanical strain of the specimen. The gages on the active test articles are used to measure the mechanical strain as well the induced strain output of the actuator, when an excitation voltage is applied. The gages are bonded on both

[8]VonRoll Isola Isola USA Inc., Schenectandy, NY, Ph: 518-344-7100.

sides of the specimen in order to detect undesired bending or misalignment of the test article during mechanical loading. The strain data from both sides of the specimen are averaged to calculate the resultant strain.

Three types of strain gages and two types of adhesive materials produced by Micro-Measurements Group Inc.[9] are used in various tests. A unidirectional gage, CEA-00-125UW-350, is used in AFC performance under static tensile load tests. A bidirectional gage, CEA-00-125UT-35, is used for stress-strain tests in order to measure strains in both the longitudinal and the transverse directions. A fatigue rated unidirectional gage, WD-DY-125AD-350, is used for mechanical fatigue tests. This special gage is able to withstand high mechanical fatigue cycles. All three types of gages are shown in Figure 2-8.

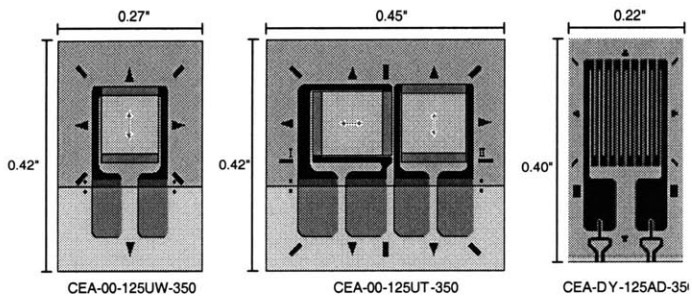

Figure 2-8: Strain gages used in AFC material characterization tests

The M-Bond 200, which uses thumb pressure and temperature for bonding, is used for quasi-static mechanical tests. The M-Bond 610, which uses high temperature and pressure for bonding, is used for mechanical fatigue tests.

2.5.4 Loading Tab Application

The loading tabs are mounted on to test articles when it is required to be gripped on the mechanical testing machine. The tabs are cut from 1/16" thick fiberglass[10] sheet with a 30° bevel angle as recommended in the ASTM testing standard for tensile properties of polymer matrix composite materials [ASTM, D3039]. The bevel angle facilitates a smooth load transfer

[9] Micro-Measurements Group Inc., Raleigh, NC, Ph: 919-365-3800.
[10] GPO-3 fiberglass sheets, McMaster-Carr Supply Company, New Bruncwick, NJ, Ph: 732-329-3200.

from the tensile testing machine to the specimen. For quasi-static tests, the tabs are bonded on both ends of the test article using 5-minute epoxy[11]. A high strength nitrile epoxy adhesive film, FM 123-2[12], is used to bond loading tabs on mechanical fatigue specimens. The FM 123-2 requires to be cured at 225°F for 1 hour at 60psi.

2.6 Actuator Stiffness Properties Model

A simple Rule of Mixture model using the Mechanics of Materials concept is used to determine the actuator fiber direction stiffness properties and the effect on the induced strain due to elastic constraints [Jones, 1999]. A schematic of the 0.010" fiber active test specimen is shown in Figure 2-9. The schematic include piezoceramic fibers, Kapton electrode, and matrix material. The analysis neglects the stiffness effect of silver ink interdigitated electrode pattern.

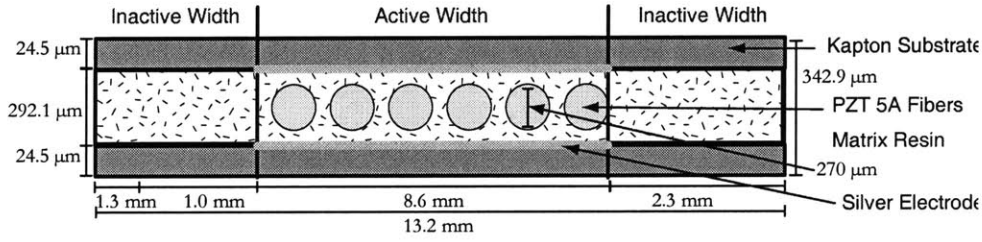

Figure 2-9: Cross-sectional schematic of the 0.01" fiber narrow AFC test coupon

As described in Section2.4.1, active test article cross-sectional area is divided into the active area in the middle and the inactive areas on the sides. This analysis assumes a total width of 0.52" and an active width of 0.34". The AFC actuator consists of 30 PZT-5A circular fibers of 0.010" in diameter, corresponding to 90% fiber line fraction. It assumes that all the fibers lie within the active width. The average diameter of a fiber is 270 μm and the modulus of the fiber is assumed to be 66.5GPa. This is an average modulus between the open circuit modulus (71GPa) and the close circuit modulus (62GPa) of the bulk PZT-5A[13] material. An average modulus is used since AFC actuator system can not be categorized as completely opened or

[11] 5 Minute Epoxy, ITW Devcon, Danvers, MA, Ph: 987-777-1000.
[12] FM 123-2 adhesive film, Cytec Fiberite Inc., Havre de Grace, MD, Ph: 410-939-1910.
[13] Piezoelectric Materials Specifications, Morgan Electro Ceramics Inc., Bedford, OH, Ph: 440-232-8600. http://www.morganelectroceramics.com/pzmat11.html#type2

completely closed circuit system. Material specification for each of the material components are shown in the Table 2.2.

				Area Fractions	
Component	**Modulus**	**Thickness**	**Width**	**Total Actuator**	**Active Area**
Kapton	2.5GPa	25.4 μm	13.2 mm	0.30	0.15
Fiber	66.5GPa	Diameter 270 μm		0.38	0.56
Matrix	2.9GPa	Not Applicable		0.32	0.29
Total	-	342.9 μm	13.2 mm	1.00	1.00

Table 2.2: AFC actuator material component specifications

The analysis of a 0.010" AFC actuator shows that the longitudinal modulus of the active area is 39.7GPa and the modulus of the whole active test coupon is 26.9GPa. It is important to note that these modulus estimations are for mechanically un-strained actuator. When the actuator is mechanically strained, fibers starts to break, decreasing the actuator modulus. Similar analysis conducted on a 0.005" fiber AFC with 66 total number of fibers, of which 54 fibers lie within the active width. The modulus of the active area in 0.005" fiber actuator is 30.8GPa and the modulus of the whole test coupon is 25.1GPa.

A slight modification to the model enabled to estimate the longitudinal Actuation Reduction Factor, the reduction in longitudinal strain performance due to constraint effect from [0/90] E-Glass lamination. Assumed modulus of [0/90] E-Glass is 21.7GPa. Lamination of 0.010" AFC actuator with one and two plies of [0/90] E-Glass on either side is expected to cut down the longitudinal induced strain performance of the actuator by approximately 37% and 53% from its unlaminated performance, respectively. Similarly modifications to the model can be utilized to estimate the actuator stiffness properties in the longitudinal direction in a variety of different configurations and in turn estimate the actuator induced strain performance.

Chapter 3

AFC Stress-Strain Tests

Important mechanical properties of composite materials include the stiffness and the static strength in the two in-plane directions plus the interlaminar strength. A sensitivity analysis of the active ply mechanical properties on the AMR blade using CLPT and FEM models showed that the longitudinal (fiber direction) modulus was by far the most important parameter, followed by the AFC transverse modulus [Weems, 2000]. The Poisson's ratio is also an important actuator mechanical property required for the blade design and prediction of the blade's mechanical properties. Therefore an accurate knowledge of the AFC stress-strain behavior in both the longitudinal and the transverse directions are essential.

The stress-strain tests are conducted based on the ASTM testing standard for tensile properties of polymer matrix composite materials [ASTM, D3039]. This standard provides guidelines for test article design, test procedure, apparatus, and calculations. These guidelines are incorporated into the stress-strain tests and they are discussed in detail in latter sections.

3.1 Longitudinal Modulus Tests

In longitudinal modulus tests, the mechanical load is applied to the actuator specimen in the fiber direction of the AFC. The purpose of the test is to extract the AFC longitudinal (fiber direction) modulus and the Poisson's ratio as a function of the mechanical strain. A deterioration in the longitudinal modulus is expected with higher mechanical strains due to fragmentation of the brittle piezoceramic fibers.

3.1.1 Test Articles

The tests are conducted on passive AFC test articles cut from the wide actuators illustrated in Section 2.4.3. A rectangular shape is chosen for the test article geometry in accordance to the ASTM standard [ASTM, D3039]. The overall dimensions of the longitudinal modulus specimens are: 5.2" long and 1.0" wide. The length of the test article is limited by the availability of the maximum fiber length. The maximum length of PZT-5A fibers available from the CeraNova Corporation[1] at the time of this research project is ~5.0". After bonding loading tabs, the remaining gage length of the test specimen is approximately 4.0". The width of the test article is derived from the aspect ratio recommended in the ASTM standard [ASTM, D3039]. The specimen width is selected to contain a sufficient number of fibers in the cross-section to be statistically representative of the AFC actuator. Another consideration in selecting the specimen width is to minimize the edge effects on the bidirectional strain gages. The bidirectional strain gages, CEA-00-125UT-350[2], are used to acquire the longitudinal and the transverse strain data from both sides of the specimen. Details of the bidirectional strain gage and the gage bonding procedure is described in Section 2.5.3. A longitudinal modulus test specimen with dimensions is shown in Figure 3-1. It is important to note that due to the lack of functional electrodes in these passive test specimens, the piezoceramic fibers in all stress-strain test specimens are assumed to have an open circuit electrical boundary condition.

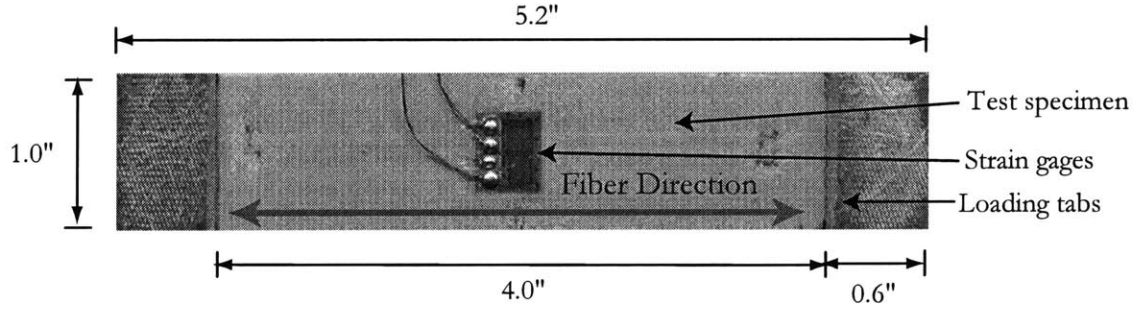

Figure 3-1: Longitudinal modulus test specimen

[1] CeraNova Corporation, Franklin, MA, Ph: 508-520-7600.
[2] Micro-Measurements Group Inc., Raleigh, NC, Ph: 919-365-3800.

3.1.2 Test Matrix

The longitudinal stress-strain tests are conducted on both bare or unlaminated actuators as well as [0/90] E-Glass (E120) laminated actuators because the AFCs are designed to be used in hybrid laminate configurations. The actuator specimens are laminated with one ply (1 E120) or two plies (2 E120) of [0/90] E-Glass cloth on either side of the AFC specimen to make a symmetric composite laminate. Details of the lamination procedure is explained in Section 2.5.1. The number of E-Glass plies used for lamination of the AFC specimens are varied in order to understand the variation in the actuator stress-strain behavior due the addition of passive structural material.

The longitudinal modulus tests are conducted on the 0.01" diameter fiber AFC material system with 75% and 90% fiber line fractions in order to characterize the variation in the fiber line fraction on the longitudinal stress-strain behavior. A line fraction of 90% is the standard for the 0.01" diameter fiber AFC actuators since it is easier to manufacture as fibers can be rolled together easily [Pizzochero, 2000]. Where as, 75% fiber line fraction actuators are more labor intensive because a comb-like apparatus must be used to keep fibers apart from each other to obtain the lower fiber line fraction [Pizzochero, 2000].

Therefore, a total of six longitudinal stress-strain specimen configurations are tested. The complete longitudinal modulus stress-strain test matrix for 0.01" diameter fiber AFC actuator system is shown in Table 3.1. The lay-up of each specimen configuration is described by the fiber line fraction and the number of [0/90] E-Glass plies used for lamination. More tests are conducted on the 90% fiber line fraction because it is the primary AFC actuator material system considered to be incorporated into the AMR blade.

Configuration	Specimen ID	Specimen lay-up
1	L0, L1	[AFC(90%)]
2	L10, L11, L12, L16, L17	[E120/AFC(90%)/E120]
3	L13, L14, L15, L20, L21	[E120/E120/AFC(90%)/E120/E120]
4	L2, L3	[AFC(75%)]
5	L18, L19	[E120/AFC(75%)/E120]
6	L22, L23	[E120/E120/AFC(75%)/E120/E120]

Table 3.1: Longitudinal modulus test matrix

3.1.3 Test Setup

An Instron 8501[3] series tensile testing machine with hydraulic grips is used to apply the desired mechanical load to the specimen during the stress-strain test. Strain gage conditioners are utilized to calibrate and condition strain data signal from bidirectional gages from both sides of the test specimen. A data acquisition computer with the LabVIEW[4] software is used to the record load and position data from the Instron machine as well as the strain data from the strain gage conditioners. A photo of the stress-strain test setup is shown in Figure 3-2.

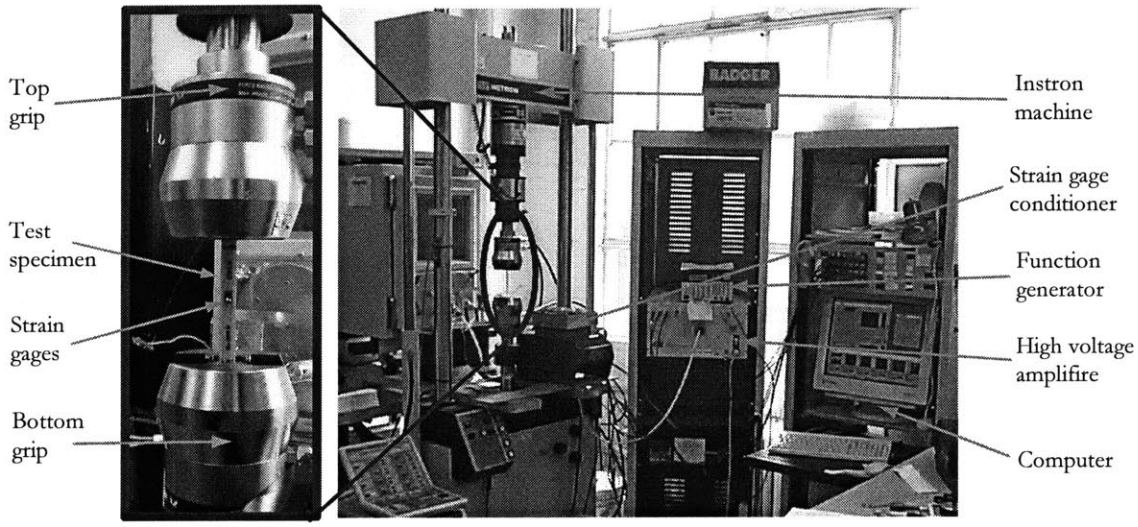

Figure 3-2: Stress-strain test setup with Instron 8501 tensile testing machine

3.1.4 Test Procedure

The specimens are loaded to simulate a quasi-static condition, in which the loading rate is slow enough that the rate sensitivity effects are negligible [ASTM, D3039]. The loading rate recommended by the ASTM standard is $10000\mu\varepsilon$/min. However, a slower rate of $5000\mu\varepsilon$/min is used in the AFC stress-strain tests in order to eliminate any possibilities of error due to rate effects. In order to accurately capture the nonlinearity in the stress-strain behavior, the specimens are loaded to incrementally higher maximum strain levels, starting from $500\mu\varepsilon$,

[3]Series 8501, Instron Corporation, Canton, MA, Ph: 800-564-8378.
[4]LabVIEW v5.1, National Instruments Corp., Austin, TX, Ph: 800-667-5347.

$1000\mu\varepsilon$, up to $6000\mu\varepsilon$ at $1000\mu\varepsilon$ increments. The stress-strain analysis is conducted only up to $6000\mu\varepsilon$ because the limit load expected in the AMR blade is during the forward flight condition is $\sim 4000\mu\varepsilon$.

According to the ASTM standard, the loading/unloading of the specimen must be conducted using the "strain control" mode or the "position control" mode [ASTM, D3039]. The "strain control" mode controls the load on the specimen based on the strain feedback and it is the best suited mode to be employed for this test because the specimens are loaded up to predetermined strain levels. However, the test setup described in Section 3.1.3 is not capable of loading the test specimen using the "strain control" mode. The setup is only capable of performing mechanical loading based on the "load control" mode or the "position control" mode. In the "load control" mode the specimen is loaded based on the load feedback reading from the machine's load cell. In the "position control" mode the specimen is loaded based on the displacement of the grips. It is important to note that the displacement of the grips can not be used directly to perform strain control tests due to the high compliance in the gripping system. The compliance in the system results in strains that are much lower than expected when the specimen is loaded by displacing the grips. Therefore, the challenge is to design a test procedure to load the specimen up to a predetermined strain level using the position control mode. The Table 3.2 outlines the step-by-step procedure developed to perform stress-strain tests efficiently while minimizing experimental errors.

Note 1: The top and the bottom grips must be aligned perfectly before mounting the test article. Even a slight misalignment in the grips causes the test article to twist and bend, making it impossible to apply a pure tensile load to the specimen. Extreme care is taken not to bend the test article when mounting on to the testing machine. The bending causes damage to the actuator specimen by introducing cracks in the brittle piezoceramic fibers. The unlaminated specimens can bend easily, leading to lower than expected initial longitudinal modulus values. Once the test specimen is gripped using the top grip an alignment apparatus is used to ensure that the specimen is vertical and aligned with the bottom grip.

Note 2: A delicate gripping procedure is used to close the lower grip. This procedure ensures that the test machine does not apply a compressive load on the test specimen when the bottom grip is closed. Without execution, the test machine is set to apply a small but positive

Step	Description
1	Record the specimen ID of the selected passive AFC test article with loading tabs and strain gages.
2	Mount the test coupon in the Instron tensile test machine using only the top hydraulic grip. See **Note 1** for details.
3	Enter calibration factors in to the LabVIEW. Load and position calibrations taken from the Instron output and strain gage calibrations from gage conditioners.
4	Balance strain gages to read zero strain when a specimen is gripped from the top and hanging free at the bottom.
5	Raise the bottom grip manually up to the specimen's lower loading tab using the position control mode.
6	Start the LabVIEW data acquisition system to acquire gripping data.
7	Close the lower grip while applying a tensile load of 5N instantaneously in the load control mode. See **Note 2** for more details.
8	Save gripping data and ensure that the applied load is stable at 5N.
9	Enter values to the waveform generator in the Instron machine's position controller to run the required load and unload cycle. See **Note 3** for details.
10	Enter the duration of the test and the number of data points to be taken in to the LabVIEW software. See **Note 4** for details.
11	Start the LabVIEW data acquisition system to take data during the loading/unloading cycle.
12	Wait for 2 seconds to take initial data before the loading cycle. The switch to position control and immediately begin the loading/unloading cycle by starting the Instron's waveform generator .
13	Observe the loading/unloading of the specimen on the LabVIEW real-time plot.
14	Before end of the unloading segment, ~10N, switch to load control mode immediately with 5N load. See **Note 5** for details.
15	Ensure that the applied load is stable at 5N level and save load/unload data.
16	Repeat Step 9 through 15 to obtain stress-strain data for higher maximum strain levels indicated in Table 3.3.

Table 3.2: Stress-strain test procedure

load of 5N in the load control mode. While the lower grip is closing, before it touches the loading tabs on the specimen, the application of the 5N load is executed instantaneously and maintained. If the application of the 5N load is not performed or delayed, the machine closes the lower grip with a compressive load on the specimen. This is undesirable because it bends the specimen, introducing damage to the AFC test article by cracking the brittle piezoceramic fibers. The data taken during the gripping procedure is used to determine the loads and strains seen by the specimen during this delicate gripping procedure.

Note 3: A dual ramp waveform function in the position controller is used to generate loading/unloading cycles. The Table 3.3 summarizes the maximum displacement values that are used in the ramping cycle to reach the expected maximum strain levels for specimens with a gage length of 4.0". A grip displacement rate of $10\mu m/s$ is chosen to load the specimen and it corresponds to a strain rate of approximately $5000\mu\varepsilon/\min$. The mechanical loading sequence followed to conduct stress-strain tests for incrementally higher maximum strain levels using the dual ramp function is illustrated in the Figure 3-3

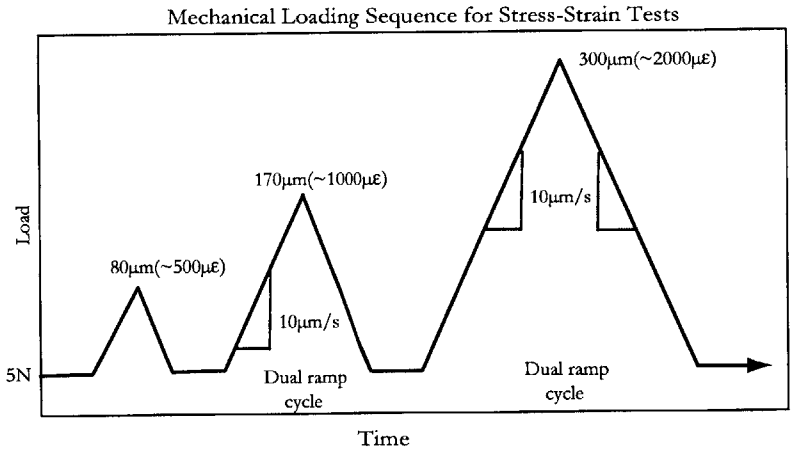

Figure 3-3: Mechanical loading sequence followlwed to perform stress-strain tests to incrementally higher maximum strain levels

Note 4: The total period to acquire the data is entered to the LabVIEW[5] software. The total period includes the duration of the dual ramp cycle and a buffer of 5 seconds. The buffer

[5]LabVIEW v5.1, National Instruments Corp., Austin, TX, Ph: 800-667-5347.

time is to collect few seconds of data before and after the ramping cycle. The number of data points to be taken for each cycle is determined so that a data point is taken after every 2-3$\mu\varepsilon$. This rate of data acquisition produces clear and useful data. The input values used in the LabVIEW software for each of the maximum strain level are shown in Table 3.3.

	Instron wave generator		**LabVIEW**	
Maximum Strain ($\mu\varepsilon$)	**Displacement (μm)**	**Rate ($\mu m/s$)**	**Time (s)**	**Data Points**
500	80	10	21	400
1000	170	10	39	700
2000	300	10	65	1100
3000	420	10	89	1600
4000	540	10	113	2100
5000	680	10	141	2600
6000	800	10	165	3100

Table 3.3: Instron and LabVIEW input values for longitudinal stress-strain tests

Note 5: This action is necessary in order to stop the unloading cycle before the Instron machine applies a compressive load to the specimen. Before the end of unloading segment, ~10N, the unloading cycle is forced to stop by switching the machine to load control mode immediately with 5N load.

The load data acquired from the Instron machine is converted to stress values using the specimen width and the nominal thickness of each specimen configuration. The nominal thicknesses for unlaminated, 1 E120, and 2 E120 E-Glass laminate configurations are 0.0135", 0.0225", and 0.315", respectively. The strain data from both sides of the specimen are averaged to calculate the absolute mechanical strain of the specimen.

3.1.5 Test Results

The longitudinal stress versus strain behavior for the 0.010" diameter AFC actuators with 90% and 75% fiber line fractions laminated with one ply of [0/90] E-Glass is shown in Figure 3-4.

As expected, the 0.01" diameter fiber AFC material system shows a highly nonlinear stress versus strain behavior in the longitudinal direction and the modulus decreases rapidly with higher mechanical strain. High mechanical strains induce cracking in brittle piezoceramic fibers in the actuator material system, decreasing the AFC modulus. A "knee" in the stress-strain locus is observable, indicating the onset of catastrophic damage to the actuator. As seen

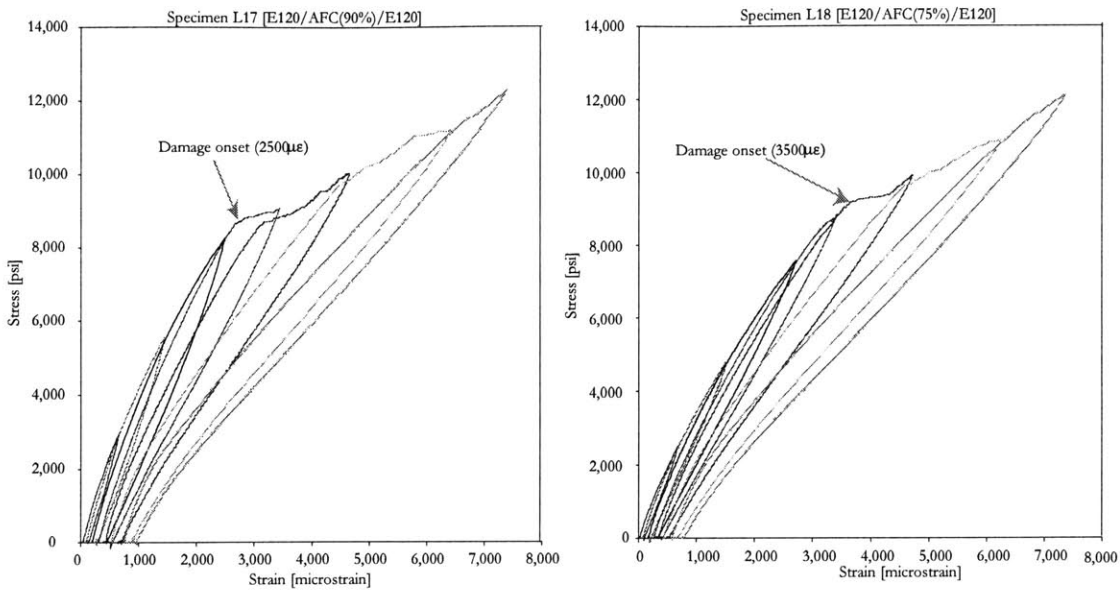

Figure 3-4: Longitudinal stress-strain behavior of 90% and 75% fiber line fraction AFCs symmetrically laminated with one ply of [0/90] E-Glass

from Figure 3-4, the onset of catastrophic damage for 90% and 75% fiber line fraction AFCs laminated with one ply of [0/90] E-Glass are $\sim 2500\mu\varepsilon$ and $\sim 3500\mu\varepsilon$, respectively. In 75% fiber line fraction AFCs, the onset of catastrophic damage is delayed due to higher matrix volume fraction that improves the load transfer capability around damaged fibers [Jones, 1999].

The stress-strain behavior of the same actuator material systems symmetrically laminated with two plies of [0/90] E-Glass is shown in Figure 3-5. The Figure 3-5 indicates that the onset of catastrophic damage is delayed on actuators laminated with two plies of [0/90] E-Glass. The catastrophic damage onset for 90% and 75% fiber line fraction AFCs laminated with two plies of [0/90] E-Glass are $\sim 2800\mu\varepsilon$ and $\sim 3800\mu\varepsilon$, respectively. The delay in the catastrophic damage onset is due to higher amounts of passive composite structure around the AFCs that enhances the load transfer capability.

In order to capture the nonlinearity, the modulus is calculated as "chord modulus" values for various strain ranges as recommended by the ASTM standard [ASTM, D3039]. The the chord modulus are calculated for various strain ranges from $100\mu\varepsilon$ to a specified upper strain limit such as $500\mu\varepsilon$, $1000\mu\varepsilon$, $2000\mu\varepsilon$, up to $6000\mu\varepsilon$. When the data is not available at the

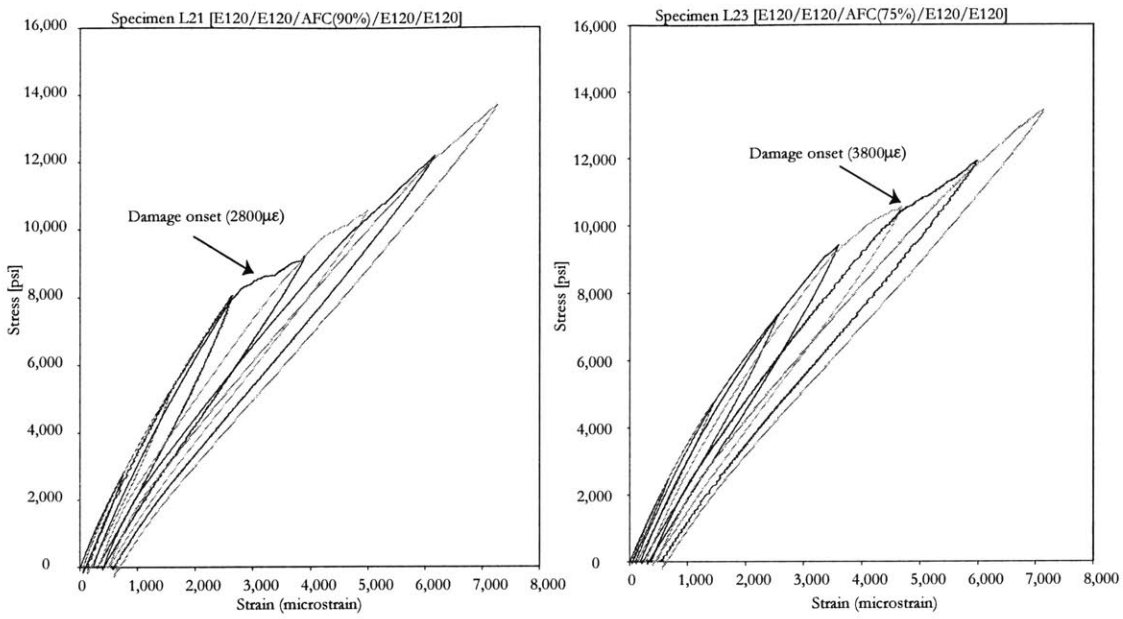

Figure 3-5: Longitudinal stress-strain behavior of 90% and 75% fiber line fraction AFCs symmetrically laminated with two plies of [0/90] E-Glass

exact end points of the strain range, the closest available data point is used to calculate the chord modulus [ASTM, D3039]. The summary of chord modulus and Poisson's ratio values for all six longitudinal specimen configurations are shown in Table 3.8. The tabulated data is averaged over all the samples tested for each configuration as listed in Table 3.1.

Approximately $1000\mu\varepsilon$ and $800\mu\varepsilon$ of residual strains are observed when 90% and 75% line fraction actuators laminated with 1 E120 are strained up to $7000\mu\varepsilon$. The residual strains are considerably reduced when the actuators are laminated with two plies of E120 per side. The stress-strain plots more for 0.01" diameter fiber AFC specimens are shown in Appendix B.

3.1.6 Results Discussion

As expected, the 0.01" diameter fiber AFC material system shows a highly nonlinear stress versus strain behavior in the longitudinal direction and the actuator modulus decreases rapidly with higher mechanical strain. The brittle piezoceramic fibers with high fiber volume fraction cause catastrophic damage to AFC actuators at higher strains. A "knee" in the longitudinal stress-strain locus is observed, indicating the onset of catastrophic damage to the actuator at

	90% fiber line fraction			75% fiber line fraction		
# of E-Glass plies/side	**none**	**1 E120**	**2 E120**	**none**	**1 E120**	**2 E120**
# of samples tested	**2**	**5**	**5**	**2**	**2**	**2**
Strain Ranges	**Average Chord Modulus (GPa)**					
100$\mu\varepsilon$ - 500$\mu\varepsilon$	30.5	32.9	28.7	30.6	26.5	25.8
100$\mu\varepsilon$ - 1000$\mu\varepsilon$	22.1	28.5	27.1	27.2	23.7	23.7
100$\mu\varepsilon$ - 2000$\mu\varepsilon$	11.8	23.6	22.8	16.7	20.5	20.6
100$\mu\varepsilon$ - 3000$\mu\varepsilon$	10.2	18.3	18.7	12.9	18.5	18.7
100$\mu\varepsilon$ - 4000$\mu\varepsilon$	8.5	14.8	16.0	10.1	15.7	16.5
100$\mu\varepsilon$ - 5000$\mu\varepsilon$	7.1	13.0	14.2	No	13.5	14.5
100$\mu\varepsilon$ - 6000$\mu\varepsilon$	6.1	12.0	13.5	Data	12.1	13.4
Strain Ranges	**Average Poisson's Ratio**					
100$\mu\varepsilon$ - 500$\mu\varepsilon$	0.260	0.247	0.194	0.342	0.224	0.177
100$\mu\varepsilon$ - 1000$\mu\varepsilon$	0.210	0.246	0.204	0.335	0.222	0.180
100$\mu\varepsilon$ - 2000$\mu\varepsilon$	0.019	0.238	0.201	0.288	0.219	0.172
100$\mu\varepsilon$ - 3000$\mu\varepsilon$	0.068	0.184	0.171	0.123	0.216	0.172
100$\mu\varepsilon$ - 4000$\mu\varepsilon$	0.033	0.143	0.138	0.068	0.186	0.155
100$\mu\varepsilon$ - 5000$\mu\varepsilon$	0.034	0.116	0.120	No	0.161	0.140
100$\mu\varepsilon$ - 6000$\mu\varepsilon$	0.036	0.108	0.111	Data	0.151	0.129

Table 3.4: Test specimen longitudinal chord modulus and Poisson's ratios

$\sim$2500$\mu\varepsilon$ and $\sim$3500$\mu\varepsilon$, for 90% and 75% fiber line fraction AFC laminated with one ply of [0/90] E-Glass, respectively. The onset of catastrophic damage is delayed on 75% fiber line fraction actuators due to higher matrix volume fraction. The onset of catastrophic damage is further delayed on specimens laminated with two plies of [0/90] E-Glass. However, the longitudinal stress-strain tests conducted on 0.005" diameter fiber AFC material system does not indicate such an onset of rapid damage. This is due to the smaller fiber diameter and lower fiber line fraction. Smaller fibers with higher matrix volume fraction enable more efficient load transfer capability around fiber cracks in the 0.005" diameter fiber AFC material system. The longitudinal stress-strain data for the 0.005" diameter fiber AFC material system is shown in Appendix B.

The longitudinal modulus data for the [0/90] E-Glass laminated specimens shown in Table 3.8, are used to extract the AFC modulus indirectly. The modulus of the AFC actuator is extracted from E-Glass laminated specimens by removing the contribution of the [0/90] E-Glass analytically. The Mechanics of Material approach discussed in Section 2.6 is used to extract the AFC longitudinal modulus by using the known laminate specimen modulus and the pure

E-Glass modulus at various strain ranges. Therefore, a complete stress-strain analysis of pure E-Glass is also conducted at corresponding mechanical strain levels. The chord modulus and the Poisson's ratio values for pure E-Glass at various configurations and strain ranges are shown in the Appendix A. The extracted AFC longitudinal modulus from indirect analysis is shown in the Table 3.5.

	90% fiber line fraction			75% fiber line fraction		
# of E-Glass plies/side	**1 E120**	**2 E120**	**Avg**	**1 E120**	**2 E120**	**Avg**
# of samples tested	**5**	**5**	**10**	**2**	**2**	**4**
Strain Ranges	**Average Chord Modulus (GPa)**					
100$\mu\varepsilon$ - 500$\mu\varepsilon$	40.2	39.5	39.9	29.6	32.8	31.2
100$\mu\varepsilon$ - 1000$\mu\varepsilon$	33.5	35.9	34.7	25.6	27.9	26.7
100$\mu\varepsilon$ - 2000$\mu\varepsilon$	25.2	26.5	25.9	20.1	21.3	20.7
100$\mu\varepsilon$ - 3000$\mu\varepsilon$	16.7	17.0	16.9	17.1	17.1	17.1
100$\mu\varepsilon$ - 4000$\mu\varepsilon$	11.1	11.2	11.1	12.5	12.4	12.5
100$\mu\varepsilon$ - 5000$\mu\varepsilon$	8.2	7.6	7.9	9.1	8.2	8.6
100$\mu\varepsilon$ - 6000$\mu\varepsilon$	6.7	6.3	6.5	6.9	6.0	6.5

Table 3.5: Indirectly extracted AFC longitudinal chord modulus from E-Glass laminated actuator specimens

The Figure 3-6 compares the longitudinal chord modulus for the 0.01" diameter fiber AFC material system shown in the Table 3.5 with the 0.005" diameter fiber AFC material system. The modulus of the 0.01" diameter fiber actuators decreases more rapidly than the 0.005" diameter fiber actuators. Furthermore, the rate of modulus reduction is lower in the 75% fiber line fraction actuators than the 90% line fraction actuators.

The measured "initial modulus", the chord modulus in value for 100$\mu\varepsilon$ - 500$\mu\varepsilon$ range, is compared with the modulus predicted by the Mechanics of Materials model described in Section 2.6 show good correlation. The theoretical AFC longitudinal modulus calculated using the model for 90% and 75% fiber line fraction actuators are 41.0GPa and 34.4GPa, respectively. These calculations are based on 71GPa modulus for PZT-5A piezoceramic fibers, assuming an open circuit electrical boundary condition in test specimens. Experimentally extracted initial modulus are 39.9GPa and 31.2GPa, corresponding to an error of approximately 2.7% and 9.4% for 90% and 75% fiber line fraction AFC material systems, respectively.

The actuator material configuration with 90% fiber line fraction is chosen for the AMR blade application because the mechanical strain on the blade in the fiber direction is not expected to

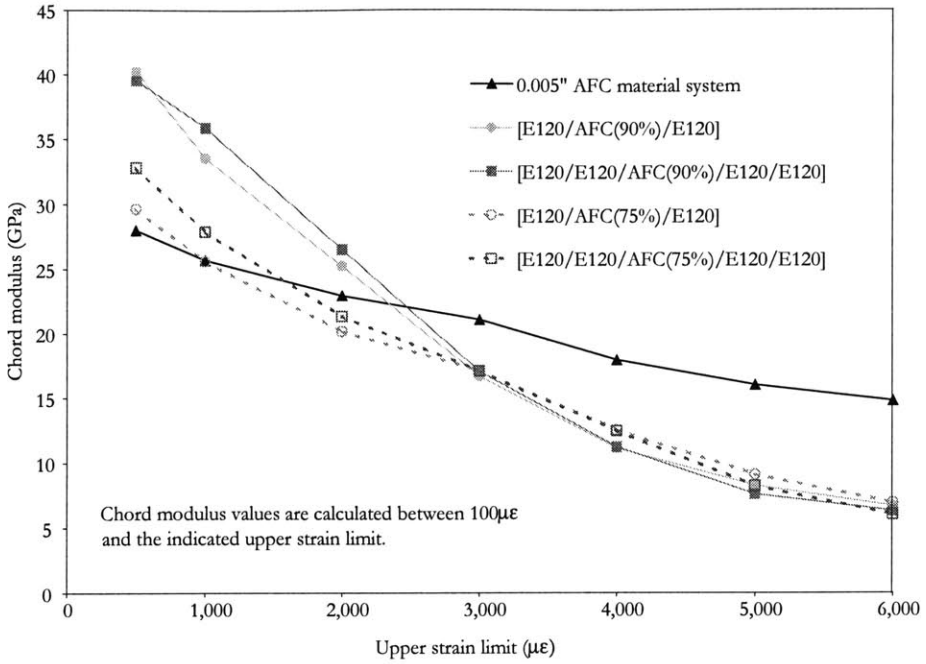

Figure 3-6: Extracted longitudinal chord modulus for 0.01" diameter fiber AFC material system

be higher than $1900\mu\varepsilon$ in the forward flight condition. Thus, it provides an adequate safety buffer for the blade actuators which showed an onset of catastrophic damage at $\sim 2500\mu\varepsilon$ and $\sim 2800\mu\varepsilon$ when laminated with one and two plies of [0/90] E-Glass, respectively. Furthermore, larger fiber diameter in the 0.01" AFCs and higher fiber volume fraction in the 90% line fraction actuators system significantly improve the actuation capability of the AMR blade

3.2 Transverse Modulus Tests

In transverse modulus tests, the mechanical load is applied to the specimen in the direction normal to the piezoceramic fibers. The purpose of the test is to extract the AFC transverse modulus and the minor Poisson's ratio as a function of the mechanical strain. A highly non-linear stress-strain behavior is expected in the transverse modulus tests because the load is primarily carried by the AFC resin matrix in shear.

3.2.1 Test Articles

The tests are conducted on passive AFC test articles cut from wide actuators illustrated in Section 2.4.3. A rectangular shape is chosen in accordance to the ASTM standard [ASTM, D3039]. The overall dimensions of the longitudinal modulus specimens are: 2.0" long and 1.0" wide. The length of the test article is limited to the width of widest AFC actuators produced by Continuum Control Corporation[6]. After bonding loading tabs, the remaining gage length of the test specimen is approximately 1.5". The specimen width is selected to be statistically representative of the AFC actuator. Another consideration in selecting the specimen width is to minimize the edge effects on the bidirectional strain gages. Details of the bidirectional strain gage and the application procedure is described in Section 2.5.3. Similar to the longitudinal modulus specimens, strain from both sides of the specimen is observed to detect undesired bending or misalignment of the test article during mechanical loading. Strain data from both sides of the specimen is averaged to determine the resultant mechanical strain of the test article. A transverse modulus test specimen with dimensions is shown in Figure 3-7.

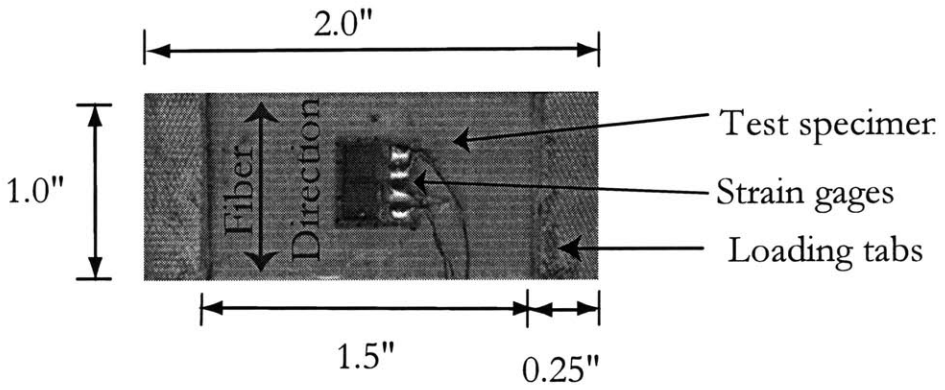

Figure 3-7: Transverse modulus test specimen

3.2.2 Test Matrix

Transverse stress-strain testing is conducted on 0.01" diameter fiber actuators with 90% fiber line fraction. The tests are conducted on both unlaminated as well as [0/90] E-Glass (E120)

[6]Continuum Control Corporation, Billerica, MA, Ph: 978-670-4910.

laminated specimens. Details of the lamination procedure is explained in Section 2.5.1. Lamination is conducted using only one ply of E-Glass per side (1 E120) in order to minimize the effect of passive composite plies on the actuator's transverse stress-strain behavior. The complete transverse modulus stress-strain test matrix for 0.01" diameter fiber AFC actuator system is shown in Table 3.6.

Configuration	Specimen ID	Specimen lay-up
1	T1, T2, T3	[AFC]
2	T4, T5, T6, T7, T8, T9	[E120/AFC/E120]

Table 3.6: Transverse modulus test matrix

3.2.3 Test Setup

The test setup used for longitudinal modulus test is also utilized for transverse modulus tests. Detailed of the test setup is discussed in Section 3.1.3. A photo of the stress-strain test setup is shown in Figure 3-2.

3.2.4 Test Procedure

The test procedure followed in the longitudinal modulus tests discussed in Section 3.1.4 is slightly modified to conduct transverse modulus tests. The step-by-step procedure developed for stress-strain testing is outlined in the Table 3.2. The only difference is the values entered to the Instron 8501[7] machine's waveform function generator in Step 9 and values entered in LabVIEW in Step 10 of the test procedure. The modified input values used in the transverse modulus test procedure are shown in Table 3.7. The displacement values used in the ramping cycle to reach the expected maximum strain levels is lower due to the fact that the transverse modulus specimens has a shorter gage length of 1.5". A shorter specimen gage length also requires the grip displacement rate to be lowered to $4\mu m/s$ in order to produce a quasi-static loading condition by maintaining a strain rate of $\sim 5000\mu\varepsilon/\min$. The input values entered in to the LabVIEW[8] software also changed accordingly for each maximum strain level.

[7] Series 8501, Instron Corporation, Canton, MA, Ph: 800-564-8378.
[8] LabVIEW v5.1, National Instruments Corp., Austin, TX, Ph: 800-667-5347.

	Instron wave generator		LabVIEW	
Maximum Strain ($\mu\varepsilon$)	**Displacement (μm)**	**Rate ($\mu m/s$)**	**Time (s)**	**Data Points**
500	40	4	25	400
1000	80	4	45	800
2000	120	4	65	1200
3000	170	4	90	1600
4000	210	4	110	2000
5000	250	4	130	2400
6000	300	4	155	2800

Table 3.7: Instron and LabVIEW input values for transverse stress-strain tests

3.2.5 Test Results

A nonlinear stress versus strain behavior is observed for 0.01" diameter AFC actuator material system in the transverse direction. Figure 3-8 shows the transverse stress-strain behavior of an unlaminated actuator and an actuator symmetrically laminated with one ply of [0/90] E-Glass.

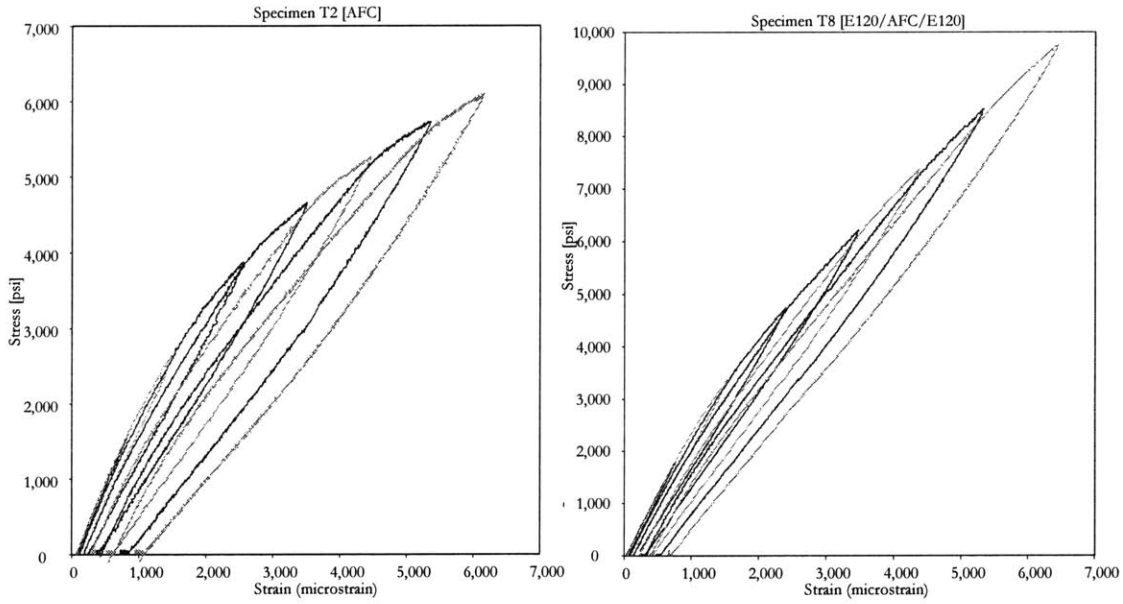

Figure 3-8: Transverse stress-strain behavior of unlaminated and [0/90] E-Glass laminated AFC actuator

The summary of chord modulus and Poisson's ratio values for each transverse specimen configuration is shown in Table 3.9. The data is averaged over all the samples tested for each

configuration listed in the Table 3.6. The transverse modulus and the minor Poisson's ratios are also quoted as chord values for various strain ranges from $100\mu\varepsilon$ to a specified upper limit, such as $500\mu\varepsilon$, $1000\mu\varepsilon$, up to $6000\mu\varepsilon$.

	Chord Modulus (GPa)		Poisson's Ratio	
# of E-Glass plies/side	**none**	**1 E120**	**none**	**1 E120**
# of samples tested	**3**	**6**	**3**	**6**
$100\mu\varepsilon$ - $500\mu\varepsilon$	14.5	17.5	0.105	0.117
$100\mu\varepsilon$ - $1000\mu\varepsilon$	12.9	15.8	0.122	0.117
$100\mu\varepsilon$ - $2000\mu\varepsilon$	11.0	14.1	0.100	0.089
$100\mu\varepsilon$ - $3000\mu\varepsilon$	9.3	12.9	0.081	0.071
$100\mu\varepsilon$ - $4000\mu\varepsilon$	8.1	11.9	0.063	0.061
$100\mu\varepsilon$ - $5000\mu\varepsilon$	7.1	11.3	0.055	0.055
$100\mu\varepsilon$ - $6000\mu\varepsilon$	6.5	10.9	0.065	0.051

Table 3.8: Test specimen transverse chord modulus and Poisson's ratios

A high residual strain, over $1000\mu\varepsilon$, is observed when the unlaminated transverse actuator specimens are strained up to $6000\mu\varepsilon$. Much lower residual strain, $\sim 800\mu\varepsilon$, is observed when the [0/90] E-Glass laminated transverse actuator specimens are strained over $6000\mu\varepsilon$. Transverse stress-strain plots for more for 0.01" diameter fiber AFC specimens are shown in Appendix B.

3.2.6 Results Discussion

The transverse stress versus strain behavior in the AFC actuator is also highly nonlinear because the load is primarily carried by epoxy resin in shear. The unlaminated transverse specimens show a high residual strain and a large hysteric behavior. A significant decrease in the residual strain and the hysteric behavior is observed in [0/90] E-Glass laminated actuators. The chord modulus data for laminated transverse specimens shown in the Table 3.9, are used to extract the transverse modulus of the AFC actuator. The transverse modulus of the AFC is extracted from the E-Glass laminated specimens by removing the contribution of the [0/90] E-Glass analytically. The Mechanics of Material approach discussed in Section 2.6 is used to extract the AFC transverse modulus by using the known laminate specimen modulus and the pure E-Glass modulus at various strain ranges. Therefore, a complete stress-strain analysis of pure E-Glass is also conducted at corresponding mechanical strain levels. The chord modulus and the Poisson's ratio values for pure E-Glass at various configurations and strain ranges are shown

in the Appendix A. Analytically extracted AFC transverse modulus for unlaminated and 1 E120 configurations are shown in Table 3.9.

# of E-Glass plies	none	1 E120	Avg
# of samples tested	3	6	9
Strain Ranges	Average Chord Modulus (GPa)		
100$\mu\varepsilon$ - 500$\mu\varepsilon$	14.5	14.6	14.5
100$\mu\varepsilon$ - 1000$\mu\varepsilon$	12.9	12.3	12.6
100$\mu\varepsilon$ - 2000$\mu\varepsilon$	11.0	9.4	10.2
100$\mu\varepsilon$ - 3000$\mu\varepsilon$	9.3	7.7	8.5
100$\mu\varepsilon$ - 4000$\mu\varepsilon$	8.1	6.2	7.1
100$\mu\varepsilon$ - 5000$\mu\varepsilon$	7.1	5.4	6.3
100$\mu\varepsilon$ - 6000$\mu\varepsilon$	6.5	4.8	5.7

Table 3.9: Indirectly extracted AFC transverse chord modulus from E-Glass laminated actuator specimens

The Figure 3-9 illustrates the nonlinear transverse chord modulus for AFC actuators shown in Table 3.9. The transverse modulus of 0.01" diameter fiber AFC actuators decreases nonlinearly with mechanical strain. The nominal AFC transverse modulus used in the AMR blade design in 10.2GPa. This is the extracted AFC transverse modulus at 2000$\mu\varepsilon$.

3.3 Summary

The longitudinal and transverse stress-strain tests enabled to extract four important tensile properties of standard 0.01" diameter fiber AFC material system with 90% fiber line fraction. The longitudinal (fiber direction) modulus is by far the most important material property extracted from the tests, followed by the transverse modulus. Both the major and minor Poisson's ratios were also extracted from tests by employing bidirectional strain gages on test articles. Table 3.10 summarizes the nominal tensile properties of 0.01" diameter fiber AFC material system with 90% fiber line fraction.

A nominal longitudinal modulus of 16.9GPa, corresponding 100$\mu\varepsilon$ - 3000$\mu\varepsilon$, and a transverse modulus of 10.2GPa, corresponding 100$\mu\varepsilon$ - 3000$\mu\varepsilon$, were used in the blade design. The measured "initial modulus" in the longitudinal direction, the chord modulus in value for 100$\mu\varepsilon$ - 500$\mu\varepsilon$ range, correlates well with the predicted modulus of 41.0GPa. The tests provided a thorough understanding of the highly non-linear stress versus strain behavior exhibited by the

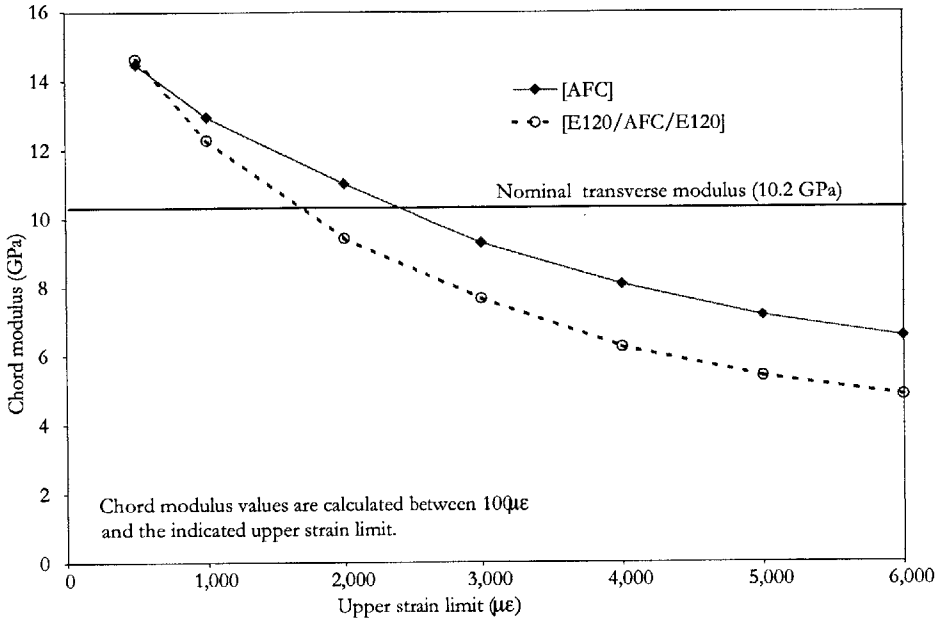

Figure 3-9: Extracted transverse chord modulus for 0.01" diameter fiber AFC material system

	Chord Modulus (GPa)		Poisson's Ratio	
Strain Ranges	**Longitudinal**	**Transverse**	**Major**	**Minor**
100$\mu\varepsilon$ - 500$\mu\varepsilon$	39.9	14.5	0.260	0.105
100$\mu\varepsilon$ - 1000$\mu\varepsilon$	34.7	12.6	0.210	0.122
100$\mu\varepsilon$ - 2000$\mu\varepsilon$	25.9	10.2	0.019	0.100
100$\mu\varepsilon$ - 3000$\mu\varepsilon$	16.9	8.5	0.068	0.081
100$\mu\varepsilon$ - 4000$\mu\varepsilon$	11.1	7.1	0.033	0.063
100$\mu\varepsilon$ - 5000$\mu\varepsilon$	7.9	6.3	0.034	0.055
100$\mu\varepsilon$ - 6000$\mu\varepsilon$	6.5	5.7	0.036	0.065

Table 3.10: Summary of AFC nominal tensile material properties

AFC actuator material system. A "knee" in the longitudinal stress-strain locus was observed on the 90% fiber line fraction material system at $\sim 2500\mu\varepsilon$, indicating an onset of catastrophic damage to the actuator. The 75% fiber line fraction material system was able to delay the onset of catastrophic failure until $\sim 3500\mu\varepsilon$. The actuator material configuration with 90% fiber line fraction was chosen for the AMR blade application because the mechanical strains on the blade in the fiber direction is not expected to be higher than $1900\mu\varepsilon$ in the forward flight condition. However, it is recommended to investigate the use of smaller piezoceramic fibers in future AFC material systems in order to retain the actuator strength at higher mechanical load levels.

The shear modulus is also an important tensile material property required for the blade design. However, the shear modulus is less important than the longitudinal or the transverse modulus. The stress-strain tests necessary to extract the shear modulus were not conducted due time constraints as well as the unavailability of the required actuator configuration.

Chapter 4

Free Strain Performance Tests

The free strain performance tests are designed to measure the induced strain output of the actuator due to electrical excitation, which is generally used to describe most active material systems. The free strain performance, defined as the in-plane strain output of the actuator with no external load, is used as one of the primary metric to measure AFC capability. A sinusoidal electrical cycle is utilized and the actuator performance is measured for a range of peak-to-peak voltages (Vpp), DC bias voltages (Vdc) and frequencies to understand the non-linear variation in actuator strain output.

The free strain test results are carefully analyzed in order to select the optimum voltage cycle to be used in the AMR blade application. The optimized operating voltage cycle is selected to maximize the induced strain of the actuator while staying within certain practical limits of piezoceramic fibers in AFCs. The interdigitated electrode pattern enables the fibers to be poled in the fiber-direction in order to take advantage of the primary piezoelectric effect. Thus a negative voltage in the operating cycle applies an electric field opposite to the direction of poling and the highest negative voltage is limited by the coercive field of the fibers. Operating beyond than the coercive voltage leads to repolarization of the actuator. The positive end of the voltage cycle is limited by saturation, the point at which an increase in the electric field no longer increases the strain output. In practice, the upper voltage level is limited by the risk of dielectric breakdown of the actuator and also by driving amplifiers with limited current capabilities.

4.1 Test Articles

All of the tests are conducted on the 0.01" diameter fiber AFC material system with 90% fiber line fraction. More details of the material system is found in Section 2.3. A combination of wide actuators described in Section 2.4.2 and narrow coupons described in Section 2.4.1 are utilized in order to optimize the free strain performance characterization. The test are performed on both unlaminated and E-Glass laminated actuators to identify the performance variation due to various elastic constraint levels. Furthermore, the free strain performance variation due to various elastic constraint levels are characterized by symmetrically laminating the actuator with one ply (1 E120) or two plies (2 E120) of [0/90] E-Glass.

4.2 Test Matrix

A comprehensive test matrix is developed to capture the longitudinal and the transverse actuator performance due to variations in many parameters. The variation in actuator strain performance is characterized for peak-to-peak voltages (Vpp), DC bias voltages (Vdc), frequency, and various elastic constraint levels.

		Voltage Cycle		
Performance vs.	**Specimen ID**	**Vpp (kV)**	**Vdc (kV)**	**Frequency (Hz)**
Vpp and Vdc	S1,S2,S3	0.2-4.0	0,0.4,0.8	1
Lamination-wide actuator	B51,B52,B53	0.5-3.0	0.0	1,10,50,100
Lamination-narrow coupons	B13,B14,B15	0.2-4.0	0.0	1
Frequency and Vpp	B19,B20,B21	0.5-3.0	0.0	1,10,50,100

Table 4.1: Test matrix for free strain performance tests

4.3 Test Setup

The design of the free strain performance test setup is optimized to measure the induced strain of the AFC while minimizing the undesired external loads that could affect the measurement, for example, the frictional loads. In order to facilitate the "free" condition, the actuator is placed horizontally on an AFC test rig custom made out of Plexiglas for this purpose. The test rig is designed to clamp the actuator at one end using a clamping mechanism and allowing the

other end to move freely. The rig surface is prepared to minimize the friction loads between the actuator and the rig. The surface is covered with Guaranteed Non-Porous Teflon[1] (GNPT) tape for this purpose and a thin layer of silicone oil is applied on the GNPT to further reduce friction. A set of customized guides are placed along the edges of the AFC to minimize the out-of-plane movement of the actuator during actuation. The guides are also covered with GNPT to minimize friction. A set of carefully customized guides allow the AFC to move freely in-plane while minimizing out-of-plane movements during actuation. The out-of-plane movement of the actuator leads to lower measurements in the induced strain output. A picture of the custom made test rig is shown in Figure 4-1.

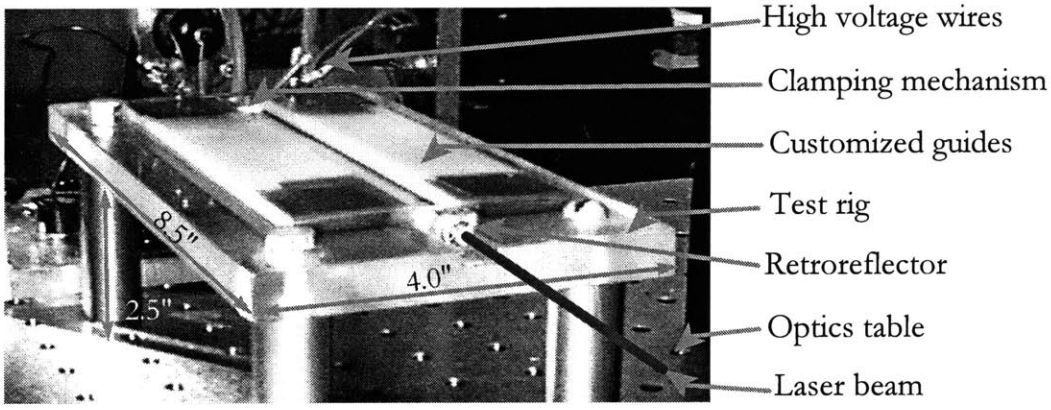

Figure 4-1: Custom made test rig used for AFC free strain performance tests

The strain output of the actuator is measured using a laser displacement measuring interferometer system[2] and the test rig is installed on an optics table. A retroreflector is attached to the free end of the actuator in order to reflect the measurement laser beam back to the interferometer. The laser system measures the displacement of the actuator by using the interference pattern between the measurement beam reflected by the retroreflector and the reference beam from the laser source. The digital displacement measurement signal is fed to the data acquisition computer through a GPIB (General Purpose Interface Board) card installed in the computer. The layout of the AFC free strain performance test setup is shown in Figure 4-2.

[1] GNPT, American Durafilm Co., Holliston, MA, Ph: 888-809-2314.
[2] ZMI 1000, Zygo Corporation, Middlefield, CT, Ph: 860-347-8506.

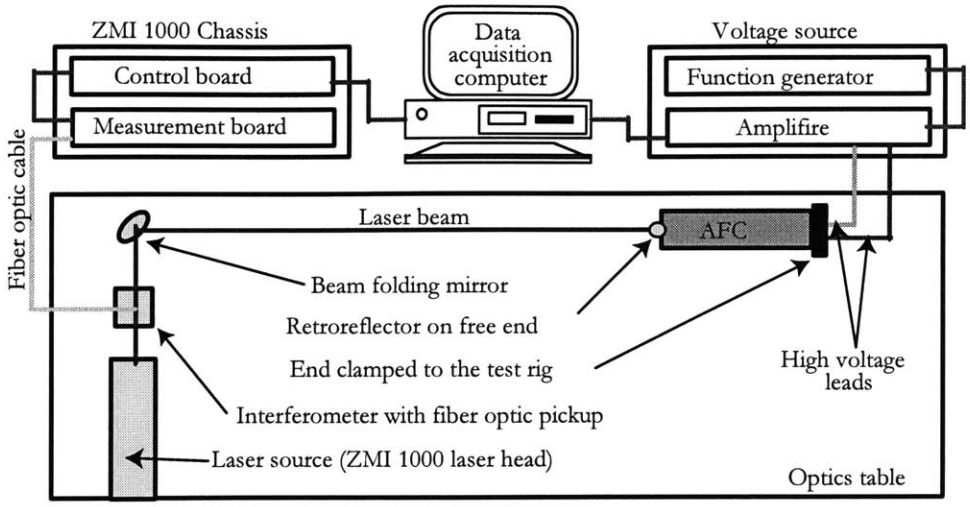

Figure 4-2: Layout of the laser interferometer system used for free strain performance tests

The voltage is applied to the actuator using a high voltage amplifier[3] capable of 1000x amplification. A function generator[4] is utilized to generate the required input signal to the amplifier. A safety circuit employing a variable resistor is connected in series with the function generator signal. This is necessary to avoid high current spikes that could occur due to discontinuities in the voltage signal while adjusting the function generator. The high current spikes cause damage to the actuator by inducing dielectric breakdown in the AFC. A simple procedure is followed to avoid such high current spikes. First, the variable resistor is set to the open circuit setting which inhibits the function generator signal from reaching the amplifier. Then the required electrical cycle is set in the function generator. Next, the high voltage is enabled and the variable resistor is used to feed the function generator signal gradually to the set level. The voltage and current are monitored with two analog signals generated by the amplifier. These analog signals are fed to the computer through a dedicated data acquisition card. A trigger signal is generated using the LabVIEW[5] to command the computer to acquire both the digital displacement data and the analog electrical data at the same time. This trigger function in essential to correlate the actuator induced strain output to the applied voltage.

[3]Model 664 10kV 20mA amplifire, Trek Inc., Medina NY, Ph: 716-798-3140.
[4]0.1mHz-100MHz PM 5138 Fuction Generator, Philips, Germany.
[5]LabVIEW v5.1, National Instruments Corp., Austin, TX, Ph: 800-667-5347.

4.4 Test Procedure

A standard test procedure is developed to measure the induced strain output of the actuator in an efficient and methodical manner while minimizing experimental errors. Extreme care is taken to reduce the out-of-plane movement of the actuator while minimizing the friction between the test rig and test specimen. The retroreflector is cleaned using acetone to remove oil or other residues from its reflecting surface. Table 4.2 outlines the step-by-step procedure to be followed when conducting free strain performance tests on AFCs.

Step	Description
1	Record the specimen ID of the selected active AFC test article.
2	Mount the test coupon in the custom made test rig and clamp one end of the specimen to the rig using the clamping mechanism.
3	Attach the retroreflector assembly to the free end of the actuator. Ensure that the retroreflector surface is clean and it moves smoothly along the groove.
4	Customized guides are placed along both edges of the actuator.
5	Ensure that the variable resistor is at the open circuit setting.
6	Attach high voltage wire leads from the amplifier to the appropriate electrode tabs on the actuator.
7	Set the function generator to the desired sinusoidal electrical cycle.
8	Switch the amplifier on and enable the high voltage application.
9	Enter calibration factors for voltage (1000V/V) and current (2mA/V) measurement signals to the LabVIEW data acquisition software.
10	Set the LabVIEW to take 1000 data points for a period of ten cycles. Total period depends on the cycle frequency: 1Hz = 10s, 10Hz=1s, 100Hz=0.1s, etc.
11	Turn the variable resistor gradually to feed the set electrical cycle from the function generator to the high voltage amplifier.
12	Start the LabVIEW software to record and save data.
13	Turn the variable resistor gradually back to the open circuit setting.
14	Switch the high voltage amplifier to the stand-by position.
15	Repeat Steps 7-14 to acquire free strain data for more electrical cycles.

Table 4.2: Free strain performance test procedure

The free strain performance is calculated by the actuator displacement measured from laser interferometer system for a specific voltage cycle. The active length of the actuator is used to normalize the actuator induced displacement to determine the induced strain. The active length is defined as the distance between the last electrode finger at each end of the electrode pattern as illustrated in Figure 2-3. The induced strain output of AFCs are presented in microstrain and always correlated with the applied voltage level.

4.5 Test Results

The excitation of the AFC actuator with a sinusoidal voltage cycle produces a non-linear hysteresis behavior between the applied voltage and the strain output. This type of hysteresis behavior due to the applied electrical field is expected from piezoceramic based actuators. The Figure 4-3 shows the typical hysteresis behavior observed on a narrow AFC test coupon B19. The data is presented for unlaminated and laminated configurations. The actuator is laminated with two plies of [0/90] E-Glass and actuated with 2000Vpp and 3000Vpp voltage cycle at 1Hz, 10Hz, and 100Hz frequencies.

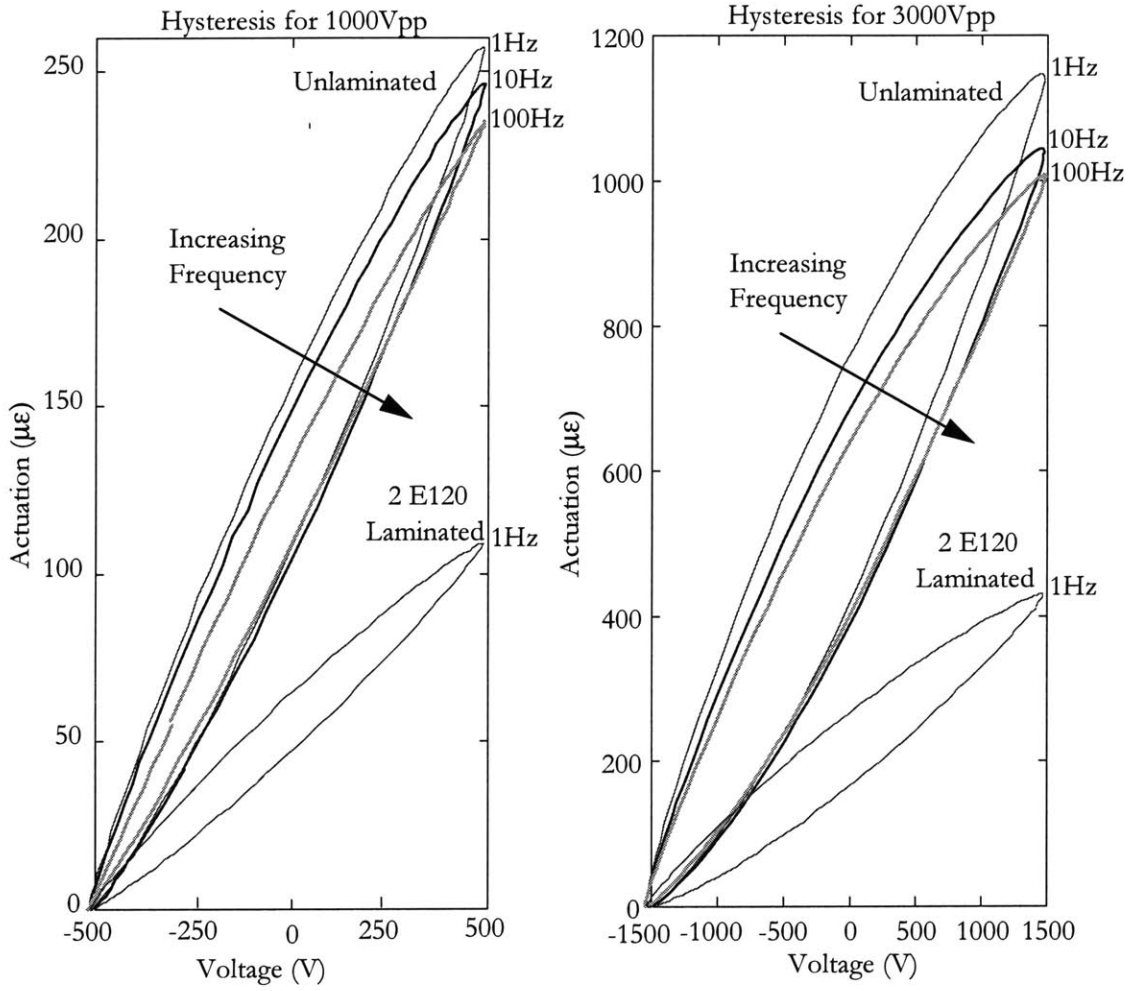

Figure 4-3: Hysteresis behavior of actuator induced strain

As seen from the Figure 4-3 the hysteresis behavior changes slightly due to various voltage levels, operating frequencies and elastic constraint conditions. It is important to note that as the AFC actuator elongates in the fiber-direction (longitudinal direction) it contracts in the transverse direction and vice versa. The fiber-direction strain output is defined as positive and the transverse strain output is defined as negative. This sign convention is used only to indicate that the transverse actuation is completely out of phase from the longitudinal actuation direction. The Actuation Ratio, the ratio between the transverse actuation and the longitudinal actuation is calculated for AFC actuators because it is an important parameter in determining performance capabilities of the AMR blade. E-Glass laminated actuator configurations are used to measure the Actuation Reduction Factor, the percentage reduction in the actuator free strain output due to added elastic constraints levels.

4.5.1 Performance Variation due to Vpp and Vdc

The longitudinal and the transverse strain performance variation is measured for various Vpp and Vdc on unlaminated actuators. The measurements are taken from 200Vpp up to 4000Vpp in 200Vpp increments at 0Vdc, 400Vdc, and 800Vdc levels. The Vdc has a small effect on actuator induced strain performance. Thus the test is conducted only on unlaminated actuators to capture the effect of Vdc. The wide actuators discussed in Section 2.4.2 are used in this test to measure the performance variation in both the longitudinal and the transverse directions. The active lengths used to normalized actuator displacement data to calculate induced strain in the longitudinal and the transverse directions are 129mm and 48mm, respectively.

The Figure 4-4 shows the longitudinal and the transverse performance measured on unlaminated AFC actuators. The presented data is the average of three unlaminated wide actuators identified in Table 4.1. The details of wide AFC actuators used in the test are found in Section 2.4.2. It is clear that the free strain in AFC actuators has a highly non-linearly relationship with Vpp. Furthermore, after 3400Vpp, the increase in the free strain performance starts to diminish in the zero Vdc cycle. This phenomenon is discussed in Section 4.6 as it relates to the optimum operating voltage cycle selection. The variation in Vdc shows almost no effect at low Vpp values, however it shows a some effect for voltages higher than 2500Vpp. At a given Vpp level, the maximum actuator performance is observed at the zero Vdc cycle and the free strain

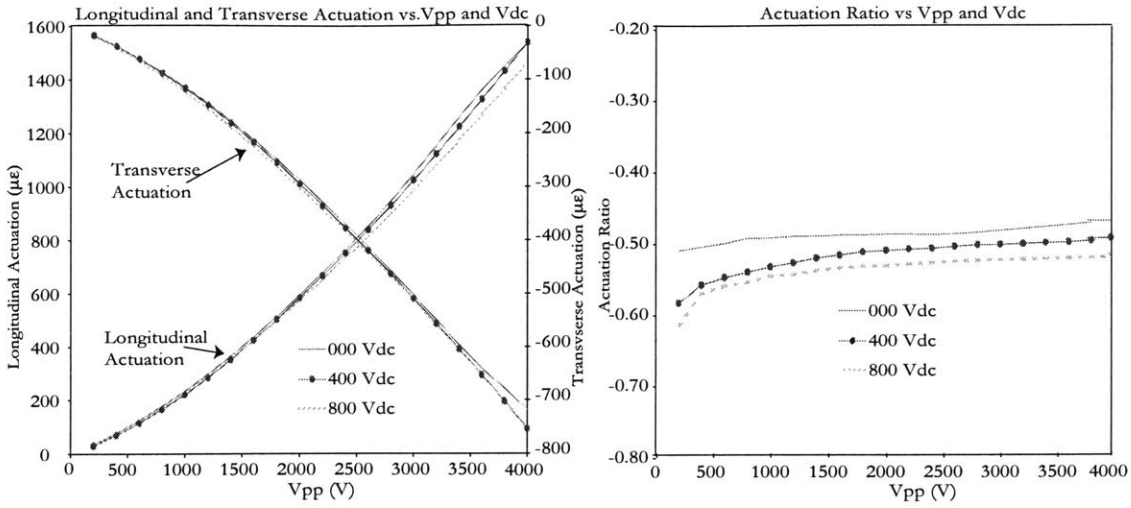

Figure 4-4: Longitudinal and transverse actuation variation on Vpp and Vdc (unalminated)

performance decreases with higher Vdc levels. Furthermore, it is observed that the actuation ratio varies slightly with Vpp and Vdc levels. The averaged actuation ratio for unlaminated actuator calculated for the whole range of Vpp and Vdc is -0.50.

4.5.2 Performance Variation due to Lamination

The AFC actuators are laminated with [0/90] E-Glass to measure the variation in the free strain performance at various levels of elastic constraints. The longitudinal and the transverse performance variation due to E-Glass lamination are measured using both wide actuators discussed in Section 2.4.2 and narrow test coupons discussed in Section 2.4.1.

In tests utilizing the wide actuators, the voltage cycle is varied from 500Vpp up to 3000Vpp in 500Vpp increments with 0Vdc at 1Hz. At 3000Vpp level, the strain performance is measured not only at 1Hz but also at 10Hz, 50Hz, and 100Hz. The test is conducted for each AFC actuator at three elastic constraint configurations, namely, unlaminated, laminated with one ply (1 E120) and laminated with two plies (2 E120) of [0/90] E-Glass on either side. The same set of three actuators are tested at all three configurations in order to isolate the effect of elastic constraint on the actuation capabilities of AFCs. The Figure 4-5 shows the effect of various levels of lamination on both the longitudinal and the transverse strain output on wide

actuators identified in Table 4.1. The actuation reduction factor is also calculated for both the longitudinal as well as the transverse directions. Furthermore, the actuation ratio for various levels of lamination is compared.

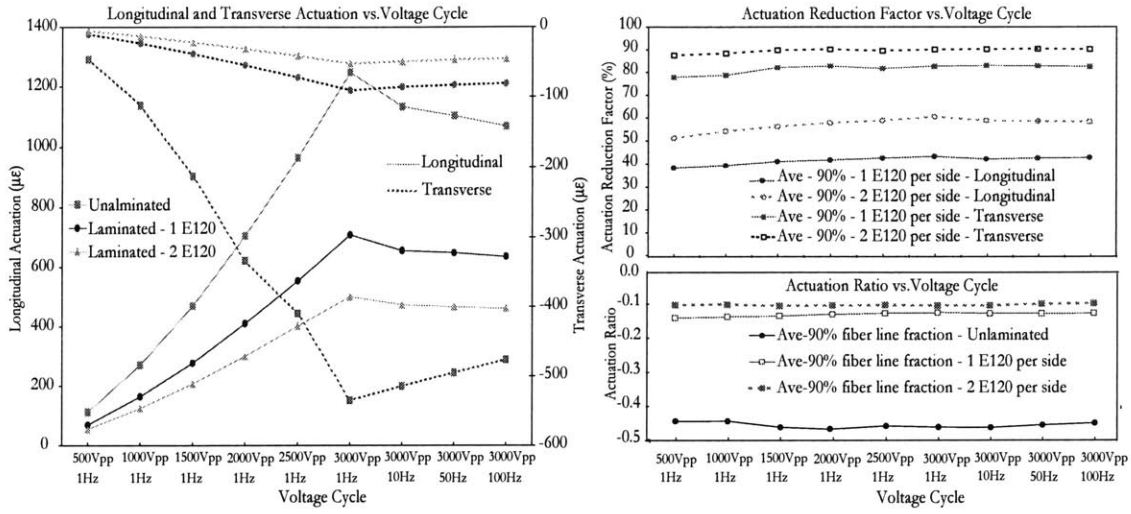

Figure 4-5: Longitudinal and tranverse actuation variation due to lamination (wide actuators)

As seen from Figure 4-5 the actuator longitudinal and transverse strain performance varies non-linearly with Vpp. However, the degree of non-linearity is reduced in laminated actuators. The actuation reduction factors due to [0/90] E-Glass lamination are almost constant with variation in the Vpp and the frequency. The average actuation reduction factor in the longitudinal direction due to 1 E120 and 2 E120 lamination are ~41% and ~57%, respectively. The actuation reduction factor in the transverse direction due to 1 E120 and 2 E120 lamination are ~82% and ~90%, respectively. The calculated actuation ratio for the unlaminated actuators are -0.47 for all electrical cycles. The average actuation ratio for 1 E120 and 2 E120 laminated actuators are -0.13 and -0.10, respectively.

A similar free strain performance test is conducted using narrow test coupons discussed in Section 2.4.1. The voltage cycle is varied from 200Vpp up to 4000Vpp in 200Vpp increments with 0Vdc at 1Hz. The Figure 4-5 shows the effect of lamination on the longitudinal strain output of narrow actuator coupons identified in Table 4.1. The longitudinal actuation reduction factor for 1 E120 and 2 E120 lamination is calculated.

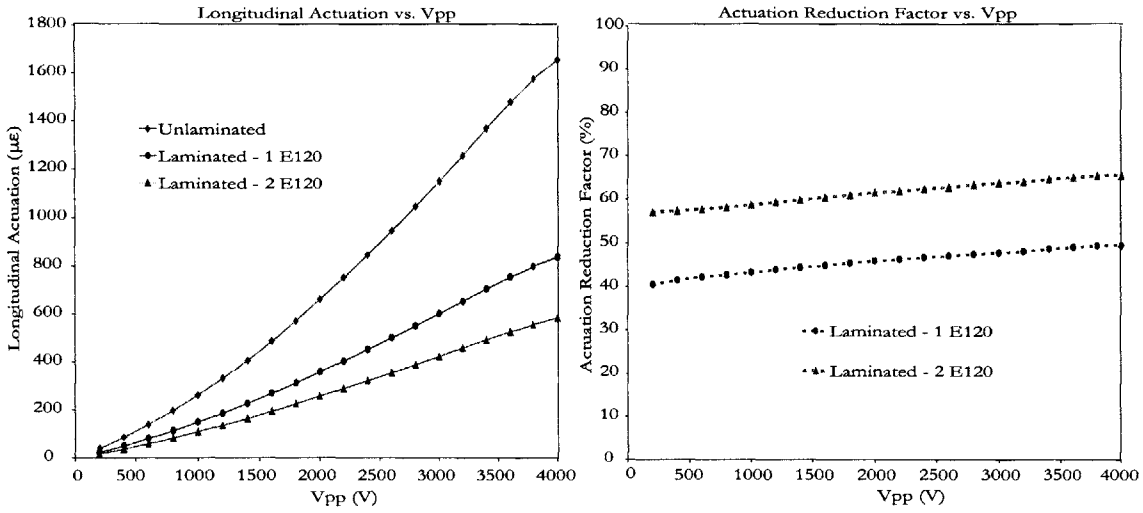

Figure 4-6: Longitudinal actuation variation due to lamination (narrow test coupons)

As seen from Figure 4-6 the actuator longitudinal performance vary non-linearly with Vpp. Furthermore, it is also observed that the degree of non-linearity is lower when laminated with [0/90] E-Glass. The actuation reduction factors varies slightly with the Vpp on narrow test coupons. The actuation reduction factor is in the range of 40%-50% for 1 E120 and 57%-65% for 2 E120 lamination. Similar to the results seen in Figure 4-4 on wide actuators, the strain output of narrow actuators also starts to diminish as Vpp is raised beyond 3400Vpp with 0Vdc. This phenomenon is discussed further in Section 4.6.

4.5.3 Performance Variation due to Frequency and Vpp

The actuator induced strain performance variation due to the variation in the electrical cycle frequency is observed on unlaminated and 2 E120 laminated narrow test coupons identified in Table 4.1 at 1Hz, 10Hz, 50Hz, and 100Hz. The same set of actuators are used in both laminated and unlaminated conditions. The voltage cycle is varied from 500Vpp up to 3000Vpp in 500Vpp increments with 0Vdc bias. The Figure 4-7 shows the variation in the longitudinal actuator performance averaged over three samples. The actuator free strain at each Vpp level is normalized by the performance at 1Hz frequency.

The Figure 4-7 shows the actuator longitudinal induced strain performance of AFCs roll-off

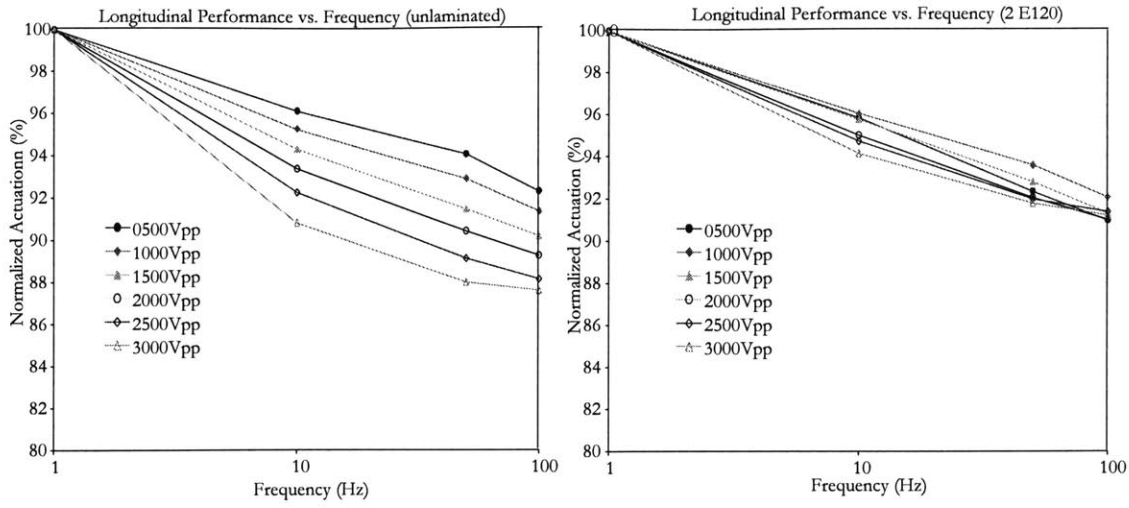

Figure 4-7: Longitudinal performance variation due to frequency on unlaminated and E-Glass laminated actuators

with the frequency of the electrical cycle. This type of roll-off with frequency is also observed in bulk PZT piezoceramic materials [Bent, 1997]. The actuation variation due to frequency is more pronounced in unlaminated actuators than in E-Glass laminated actuators. Compared to laminated actuators, the actuation performance of unlaminated actuators at a given frequency varies considerably with the Vpp level. It is observed that the induced strain performance roll-off on 2 E120 laminated actuators is less than 10% at 100Hz, for all Vpp levels.

4.6 Results Discussion

The free strain performance tests are designed to measure the induced strain of the actuators due to electrical excitation. The free strain performance is used as the primary metric of the AFCs' actuation capability. As expected in piezoceramic based actuators, a hysteresis behavior is observed between the applied voltage and the induced free strain output. In unlaminated actuators, the induced strain shows a highly non-linear relationship with the Vpp. The Vdc shows a small effect for voltages higher than 2500Vpp. The laminated actuators show a lower degree of non-linearity in the induced strain performance with Vpp.

Utilizing wide actuators, the average actuation reduction factors calculated in the longitu-

dinal direction due to 1 E120 and 2 E120 lamination are ~41% and ~57%, respectively. These values correlate well with the longitudinal actuation reduction factors estimated with the Mechanics of Materials model described in Section 2.6. The estimated longitudinal actuation reduction factors are 37% and 53% for 1 E120 and 2 E120 lamination, respectively. In the transverse direction, the actuation reduction factor due to 1 E120 and 2 E120 lamination are ~82% and ~90%, respectively. Compared to the longitudinal direction, a much higher transverse actuation reduction factor is observed due to E-Glass lamination. One of the reasons for a higher actuation reduction in the transverse direction is due to the mismatch in the AFC longitudinal and transverse modulus compared to E-Glass. The AFC actuators has a significantly lower transverse modulus (14.5 GPa) compared to the longitudinal modulus (39.7 GPa). Whereas, the [0/90] E120 cloth has identical modulus (21.7 GPa) in both directions. Therefore, laminating the AFC with E-Glass leads to higher actuation reduction in the transverse direction than in the longitudinal direction.

The average actuation ratio for the unlaminated, 1 E120, and 2 E120 laminated actuators are -0.47, -0.13 and -0.10, respectively. Lower actuation ratios are observed on laminated actuators due to the mismatch in the AFC longitudinal and transverse modulus compared to the [0/90] E-Glass.

It is also observed that the longitudinal performance on both the unlaminated and the 2 E120 laminated actuators roll-off with the electrical frequency. The induced strain performance roll-off on 2 E120 laminated actuators is less than 10% at 100Hz, for all Vpp levels.

A detailed analysis of the actuator performance in the zero Vdc cycle indicated that the increase in the free strain output starts to diminish at voltages higher than 3200Vpp. Such a behavior in the actuator performance could be the result of saturation at the positive end of the voltage cycle or repolarization at the negative end of the cycle. In order to identify the exact cause of this phenomenon, a calculation of ΔActuation/ΔVpp is made using the performance data shown in Figure 4-4 and 4-6 for unlaminated wide actuators and laminated test coupons, respectively. The Figure 4-8 shows the ΔActuation/ΔVpp calculated for wide actuators and test coupons.

In unlaminated wide actuators, the ΔActuation/ΔVpp for the 0Vdc cycle peaks at 3200Vpp and starts to decrease at higher voltages. This indicates that the AFC reaches the saturation

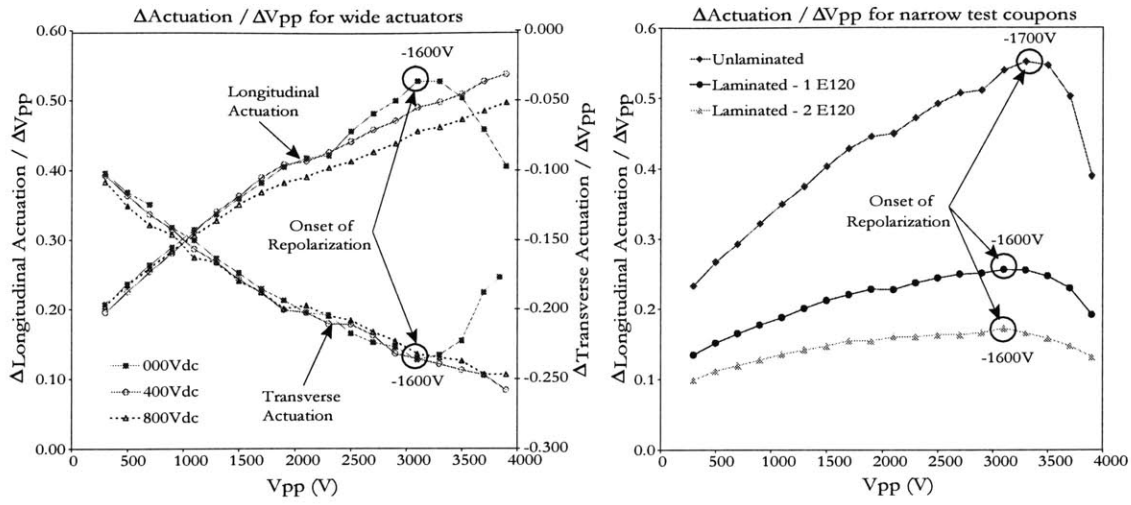

Figure 4-8: Calculated ΔActuation/ΔVpp for unlaminated wide actuators and laminated narrow test coupons

voltage at +1600V or the critical repolarization voltage at -1600V. However, the addition of 400Vdc or 800Vdc eliminates the roll-off in the actuator performance for voltage higher than 3200Vpp, further increasing the positive end of the operating cycle. This proves that the saturation at the positive end of the voltage cycle is not the cause for the reduction in performance seen in the zero Vdc level. Therefore, it can be concluded that the roll-off in performance observed in the non-bias cycle is due to voltages lower than -1600V, forcing the actuator to operate beyond the repolarization voltage. Thus a DC bias must be used for voltages over 3200Vpp in order to maintain the operating cycle above the critical repolarization voltage.

A similar analysis using narrow coupons showed that the ΔActuation/ΔVpp peaks at 3400Vpp for unlaminated actuators and the peak shifts to 3200Vpp for laminated (1 E120 and 2 E120) actuators. The shift in the ΔActuation/ΔVpp peak suggest that the repolarization voltage increases from -1700V to -1600V due to the higher constraint levels on the laminated actuators.

After analyzing the complete set of free strain performance data, the 3000Vpp with 0Vdc cycle is selected as the optimized operating voltage cycle for the AMR blade application. This voltage cycle is selected as it provides an adequate induced strain output from AFCs to perform

structural control. Furthermore, the minimum voltage of the selected cycle is -1500V, which is higher than the measured repolarization voltage of -1600V. Also, the +1500V upper end of the voltage cycle minimizes the risk of dielectric breakdown in the actuator. Furthermore, a non-bias voltage cycle simplifies the driving amplifier electronics used in the AMR blade operation.

4.7 Summary

The free strain performance is used as the primary metric of the AFCs' actuation capability and the actuator induced free strain output in unlaminated actuators showed a highly non-linear relationship with Vpp. The average free strain performance of the AFC actuator system was $\sim 300\mu\varepsilon$, $\sim 700\mu\varepsilon$, $\sim 1200\mu\varepsilon$, $\sim 1700\mu\varepsilon$, respectively, for 1000Vpp, 2000Vpp, 3000Vpp and 4000Vpp with 0Vdc at 1Hz. The actuation reduction factors in the longitudinal direction due to 1 E120 and 2 E120 lamination were $\sim 41\%$ and $\sim 57\%$, respectively. The actuation ratios determined for unlaminated, 1 E120, and 2 E120 laminated actuators were -0.47, -0.13 and -0.10, respectively. The optimum operating voltage cycle select for AMR blade application is 3000Vpp with 0Vdc. This voltage cycle provided an adequate actuation capability to perform vibration control and the minimum voltage was above the critical repolarization voltage of -1600V.

Chapter 5

Performance Under Tensile Loads

The performance under tensile load tests are designed to characterize the actuator induced strain performance during and after high mechanical tensile loading. It is essential to evaluate the actuator robustness and the performance under such conditions because the AFCs embedded in the AMR blade are expected undergo high mechanical loading. The predicted nominal and the limit tensile loads in the blade in the fiber-direction are $1900\mu\varepsilon$ and $4000\mu\varepsilon$, respectively [Weems, 2000]. Such high mechanical loads cause damage to AFC actuators by inducing cracks in the brittle piezoceramic fibers. Therefore it is important to evaluate the ability of the AFC actuators to withstand high mechanical loads and retain sufficient residual performance in damaged actuators to perform structural control.

Testing of AFC performance under tensile loads involves the application of a voltage cycle to measure the actuator performance while applying a controllable tensile load to the actuator. The AFC actuator specimens are incrementally loaded to a predetermined maximum strain limit and the induced strain performance is measured at discrete loads levels. After reaching the maximum mechanical strain, the specimens are unloaded gradually while measuring the actuator performance. The mechanical load cycles are repeated three times on the same specimen up to the maximum strain level.

5.1 Test Articles

The narrow AFC test coupons described in Section 2.4.1 are used in all AFC performance under tensile load tests in the E-Glass laminated configuration. The E-Glass lamination procedure is discussed in Section 2.5.1. The high voltage wires are connected to the actuator electrode tabs in accordance to the procedure explained in Section 2.5.2. The wiring is necessary to supply the excitation voltage into the actuator when the specimen is mounted on the tensile testing machine. The unidirectional strain gages, CEA-00-125UW-350[1], are bonded on both sides of the specimen to measure the mechanical strain and the induced strain of the actuator. The details of the strain gage and the application procedure is discussed in Section 2.5.3. The loading tabs necessary to grip the specimen on the tensile testing machine are bonded as explained in Section 2.5.4. An actuator test coupon prepared for the AFC performance under tensile load testing is shown in Figure 5-1.

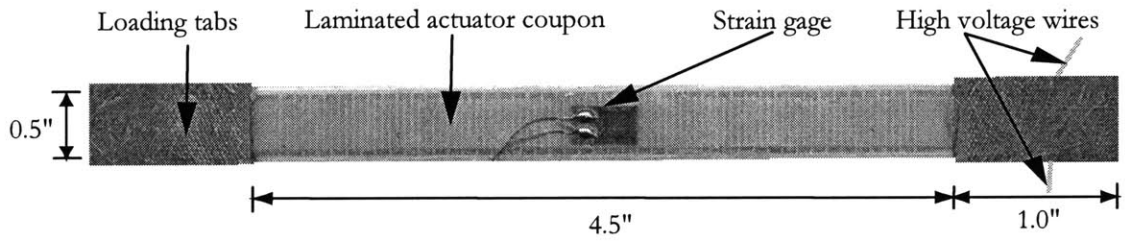

Figure 5-1: Actuator coupon prepaired for performance under tensile load tests

5.2 Test Matrix

The actuator coupons consisted of 0.01" diameter fiber AFC material system with 90% fiber line fraction. More details of the AFC material system is found in Section 2.3. All test coupons are symmetrically laminated with two plies of [0/90] E-Glass to mimic the constraint condition expected on 0.01" fiber actuators in the blade. The actuators are tested for three maximum strain limits, namely, 2000$\mu\varepsilon$, 4000$\mu\varepsilon$, and 6000$\mu\varepsilon$. These maximum strain limits are selected to be within the expected mechanical load levels in the AMR blade. Three actuator specimens

[1]Micro-Measurements Group Inc., Raleigh, NC, Ph: 919-365-3800.

are tested for each maximum strain level and each specimen is loaded/unloaded three times up to the maximum strain to observe the accumulation of damage due to repeated mechanical cycles. The complete test matrix for the AFC performance under tensile load test is shown in Table 5.1.

Maximum Strain Level	Specimen ID	Specimen lay-up
$2000\mu\varepsilon$	B13, B28, B42	[E120/E120/AFC/E120/E120]
$4000\mu\varepsilon$	B14, B29, B43	[E120/E120/AFC/E120/E120]
$6000\mu\varepsilon$	B15, B30, B44	[E120/E120/AFC/E120/E120]

Table 5.1: Test matrix for AFC performance under tensile loads

5.3 Test Setup

A setup similar to the stress-strain test detailed in Section 3.1.3 is utilized to apply the necessary mechanical load to the actuator. Additionally, a high voltage amplifier is used supply the required voltage for actuation. A photo of the test setup is shown in Section 3.1.3 in Figure 3-2. Special strain gage conditioners are used to electrically isolate the strain gages from the computer. This type of electrical protection is necessary because the high voltage in the actuator could leak to the gages bonded on the actuator surfaces and damage the expensive data acquisition equipment.

5.3.1 Mechanical Loading Sequence

The test setup is designed to mechanically load the actuator incrementally and measure the induced strain at discrete load levels while maintaining a load constant. Therefore, the AFC performance under tensile load tests are run utilizing the "load control" mode in the Instron[2] test machine. In the "load control" mode, the mechanical load on the test specimen is controlled based on the load feedback readings from the machine's load cell. The specimen is incrementally loaded/unloaded using the single ramp function in the load controller. In order establish a quasi-static loading condition, a slow rate of 2N/second is used in the ramping cycle. As the ramping function is completed, a constant load is maintained in order to measure the

[2]Series 8501, Instron Corporation, Canton, MA, Ph: 800-564-8378.

actuation performance at the particular load level. A computerized data acquisition system with the LabVIEW[3] software is used to record and save data during the actuation process. The acquired data include, the load and position measurements from the Instron, the voltage and current measurements from the amplifier and the strain gage readings from gage conditioners. Once the required data is acquired, the single ramp function in the load controller is used again to mechanically load the specimen to the next load level. The mechanical loading sequence is illustrated in Figure 5-2.

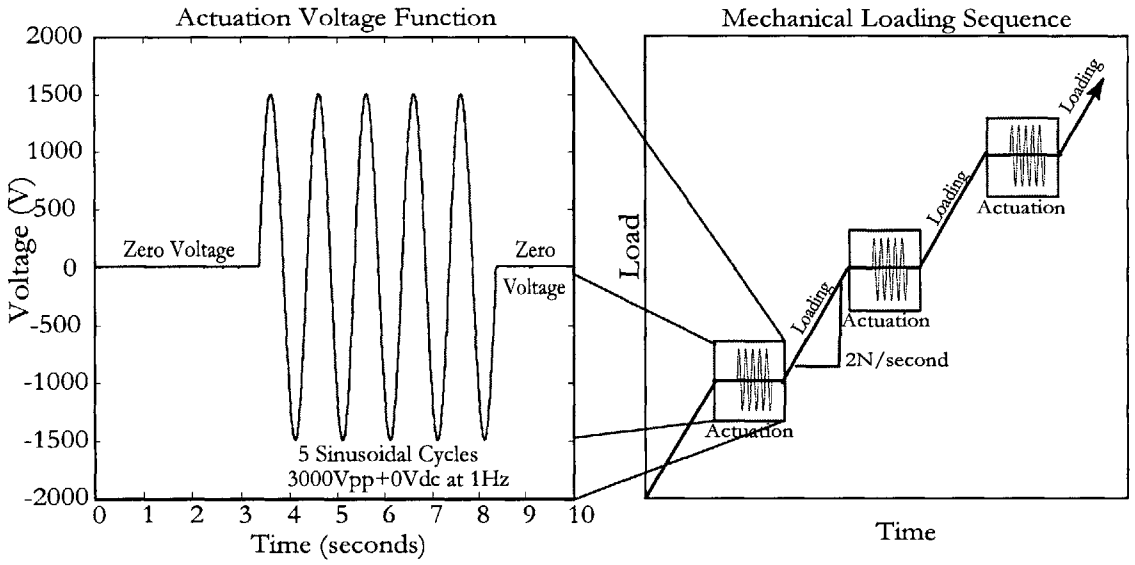

Figure 5-2: Customized voltage function and mechanical loading sequence used in performance under tenstile load tests

5.3.2 Customized Voltage Function

The actuator induced strain performance at all load levels are measured by applying a 3000Vpp sinusoidal voltage cycle with 0Vdc at 1Hz. A high voltage amplifier[4] capable of 2000x amplification is used to supply the required voltage to the actuator. The LabVIEW software is used to generate the input signal to the amplifier while simultaneously acquiring data from the necessary sources. The voltage function is customized to apply five electrical cycles to the

[3]LabVIEW v5.1, National Instruments Corp., Austin, TX, Ph: 800-667-5347.
[4]Model 20/20B 20kV, 20mA amplifire, Trek Inc., Medina NY, Ph: 716-798-3140.

actuator at the required voltage and frequency. In addition, two zero voltage segments are added to the beginning and the end of the sinusoidal segment. The strain gage data acquired during the initial zero voltage segment is used to determine the static mechanical strain on the test specimen. The zero voltage segment at the end is to reset the short circuit electrical boundary condition in the actuator before the next ramping cycle. The total duration of the voltage function is 10 seconds and 1000 data points are recorded from each source during this period. The customized voltage function is illustrated in Figure 5-2.

5.3.3 Load Controller Tuning

An important part of the test setup is to tune the load controller in the Instron machine in order to maintain a constant load on the specimen during the actuation process. As mentioned, the "load control" mode is used to control and maintain the mechanical load on the specimen. However, during the actuation process the specimen induces a displacement and the load controller must react efficiently to maintain a constant load by displacing the machine's actuator to compensate the specimen displacement. It is observed that the ability of the load controller to maintain a constant load is largely depended on the PID (Proportional, Integral and Differential) gain-constants used in the machine's load controller. Therefore, tuning the load controller with a correct set of gain-constants are essential to enable the Instron machine to maintain a relatively constant load during the actuation process. An incorrect set of gain-constants makes the machine incapable of maintaining a constant load during the actuation process. The appropriate set of PID gain constants largely depended upon the specimen stiffness, the amount of induced strain and the actuation frequency.

The gain-constants used for 0.01" diameter fiber AFC test coupons laminate with two plies of [0/90] E-Glass actuated at 3000Vpp at 1Hz are: P=14.0, I=14.0 and D=0.0. A trial and error method is used to tune the PID load controller in the Instron machine. The tuning is performed by actuating a sample actuator specimen while holding the load constant at 10N. Then the specimen is continuously actuated while monitoring the variation in the constant load using the LabVIEW. The controller is tuned by making small adjustments to the PID gain-constants to minimize the variation in the constant load. The Figure 5-3 illustrates the importance in tuning the load controller with the correct set of PID gain-constants to maintain

the desired constant load of 100N during the actuation process.

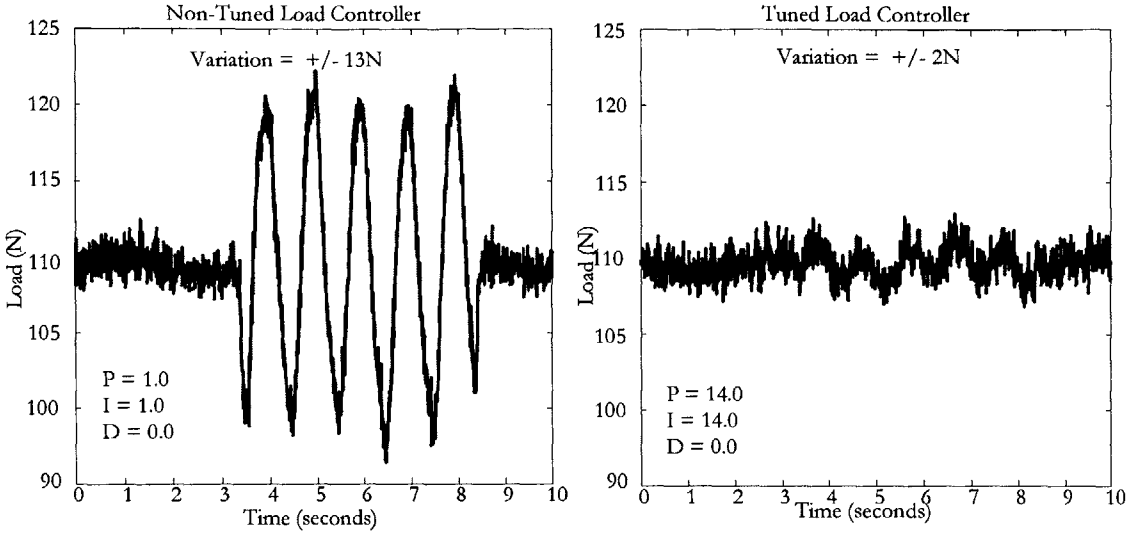

Figure 5-3: Variation in constant load due to a tuned and a non-tuned load controller

As seen in Figure 5-3 the tuned load controller maintains the desired constant load of 100N with an acceptable variation ±2N during the actuation process. However, the non-tuned load controller results in an unacceptable variation of ±13N as it tries to maintain the constant load.

5.4 Test Procedure

The Table 5.2 outlines the step-by-step procedure developed to conduct the AFC performance under tensile load tests efficiently while minimizing experimental errors.

Note 1: The top and bottom grips of the Instron machine must be aligned before mounting the test article. Even a slight misalignment in the grips causes the test article to twist and bend, making it impossible to apply a pure tensile load to the specimen. Extreme care is taken not to bend the test article when mounting on to the testing machine. The bending causes damage to the actuator test specimen by introducing cracks in the piezoceramic fibers. Once the test specimen is gripped using the top grip, an alignment apparatus is used to ensure that the specimen is vertical and aligned with the bottom grip.

Note 2: The calibration factors for the load and position readings are set in the Instron

Step	Description
1	Record the specimen ID of the prepared active AFC test coupon.
2	Mount the test coupon in the Instron tensile test machine using only the top hydraulic grip. See **Note 1** for details.
3	Enter calibration factors to the LabVIEW software. See **Note 2** for details.
4	Balance strain gages to read zero strain when a specimen is gripped from the top and hanging free at the bottom.
5	Use the LabVIEW to apply the customized voltage function while acquiring and recording data at the zero load level.
6	Use position control to raise the bottom grip up to the coupon's lower loading tab.
7	Use the LabVIEW, without the voltage function, to acquire gripping data.
8	Close the lower grip while applying a tensile load of 5N instantaneously in load control mode. See **Note 3** for more details.
9	Save gripping data and ensure that the applied load is stable at 5N.
10	Use the LabVIEW with the customized voltage function to apply the high voltage to test coupon in order to measure the actuation performance at 5N load.
11	Select the single ramp waveform function in the Instron machine's load controller with a 2N/second rate of loading.
12	Load the specimen using the ramp function to the next predetermined load level corresponding to an increase of $\sim 200\mu\varepsilon$.
13	Once the load is settled, use the LabVIEW to apply the customized voltage function to measure actuator performance at this constant load level and record data.
14	Repeat Steps 12-13 to incrementally load the specimen until it reaches the maximum strain level defined in the test matrix. See **Note 4** for more details
15	After reaching the maximum strain level, incrementally unload the specimen using the ramp function to the next predetermined level corresponding to a decrease of $\sim 200\mu\varepsilon$.
16	Once the load is settled, use the LabVIEW to apply the customized high voltage function to measure actuation at this constant load level.
17	Repeat Steps 15-16 to incrementally unload the specimen until it reaches 5N load.
18	Switch to the position control mode and ungrip the specimen from the bottom grip.
19	Use the LabVIEW to apply the customized high voltage function to measure actuation at zero load level after unloading.
20	Repeat Steps 6-19 to conduct repeated loading/unloading cycles on the specimen.

Table 5.2: Test procedure for AFC performance under tensile loads

machine's data output. The calibration factors for the voltage (2000V/V) and current (2mA/V) are specified in the high voltage amplifier. The strain gages are calibrated to read $1000\mu\varepsilon$/V and the LabVIEW is set to acquire 1000 data points during a total period 10 seconds.

Note 3: A delicate gripping procedure is used to close the lower grip to ensure that the machine does not apply a compressive load on to the test specimen when the bottom grip is closed. Without execution, the test machine is set to apply a small but positive load of 5N in the load control mode. While the lower grip is closing, before it touches the loading tabs on the specimen, the application of 5N load is executed instantaneously and maintained. If the application of the 5N load is not performed or delayed, the machine closes the lower grip with a compressive load on the specimen. This is undesirable because it bends the specimen, introducing damage to the AFC test article by cracking the brittle piezoceramic fibers. The data taken during the gripping procedure is used to determine the loads and strains seen by the specimen during this delicate procedure.

Note 4: This test is conducted under the load control mode. Therefore, the strain gage readings must be observed constantly and the loading must be manually halted when the specimen load reaches the maximum mechanical strain defined the test matrix.

The load data acquired from the Instron machine is converted to stress values using the specimen width and the nominal thickness of the test articles. The strain data from gages on both sides of the specimen are averaged to calculate the mechanical strain and the induced strain performance at a particular load level. The induced strain performance is extracted by taking the difference between the maximum and the minimum strains measured during the sinusoidal segment of the voltage function.

5.5 Test Results

In AFC performance under tensile load tests, both the mechanical strain and the induced strain of the actuator at various load levels are measured in microstrain. For comparison reasons, the actuation performance is normalized by the initial induced strain of the virgin specimen.

5.5.1 Tensile Loading up to 2000$\mu\varepsilon$

The actuator induced strain performance of the specimen B13 which is gradually strained up to 2000$\mu\varepsilon$ tensile load is shown in Figure 5-4.

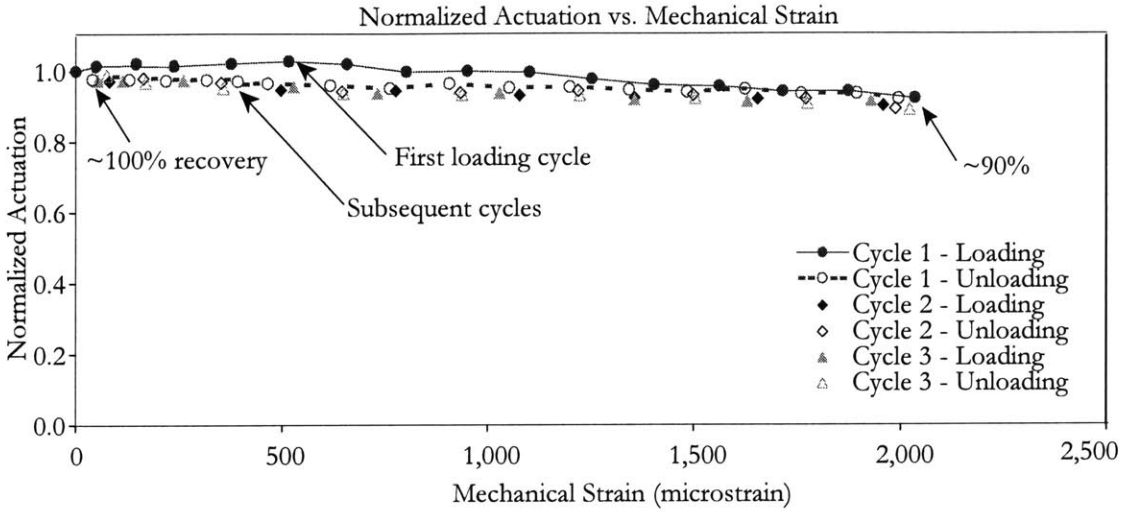

Figure 5-4: Actuation performance under tensile load (Maximum Strain = 2000$\mu\varepsilon$)

As seen in Figure 5-4, a near-linear reduction in actuation performance is observed as the specimen is loaded incrementally up to the maximum tensile load of 2000$\mu\varepsilon$. A slight difference between the first loading cycle and the subsequent cycles are observed. This indicates that the virgin actuator has accumulated a little damage during the first loading cycle. At the maximum mechanical strain level of 2000$\mu\varepsilon$ the actuator retains ~90% of its original performance. Almost all of the deteriorated performance due to loading is recovered as the specimen is unloaded gradually to the zero load level. The residual actuator performance at the zero load is ~100% after undergoing three mechanical loading/unloading cycles. The actuator performance during the loading/unloading of the second and third cycles are approximately equal to the unloading segment of the first mechanical cycle. This indicates that the actuator has not accumulated any additional damage due to the repeated mechanical cycles. However, the loading of the actuator up to the maximum mechanical strain of 2000$\mu\varepsilon$ resulted in ~100$\mu\varepsilon$ of permanent strain. Similar results are observed with specimens B28 and B42 that underwent performance under tensile load tests up to a maximum load level of 2000$\mu\varepsilon$. The normalized actuation plots

for the above specimens are found in Appendix C.

5.5.2 Tensile Loading up to 4000$\mu\varepsilon$

A much higher variation in the actuator performance due to mechanical tensile loading is observed when an actuator coupon is strained up to a maximum strain level of 4000$\mu\varepsilon$. The data shown in Figure 5-5 is obtained with the specimen B43.

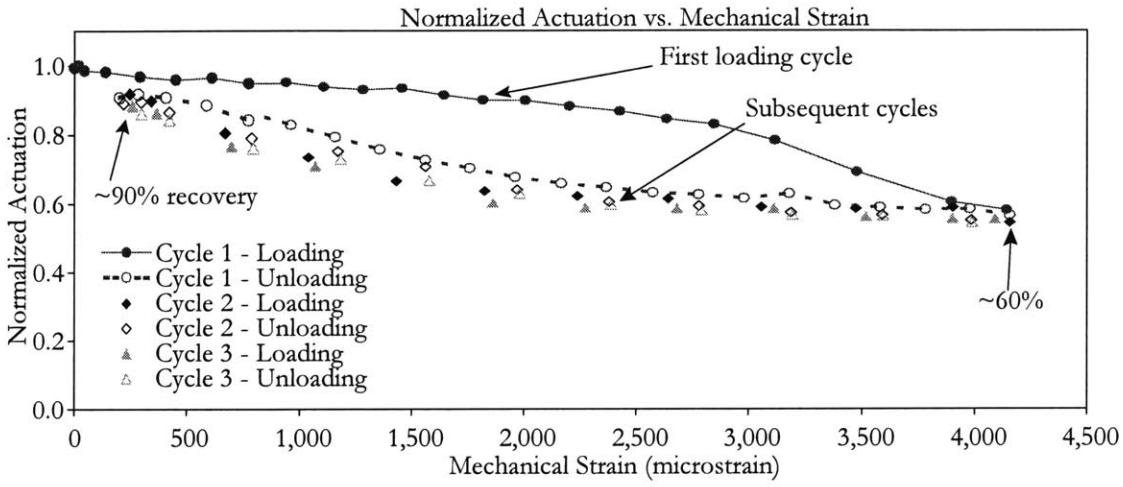

Figure 5-5: Actuation performance under tensile load (Maximum Strain = 4000$\mu\varepsilon$)

As the actuator is gradually loaded up to a maximum tensile strain of 4000$\mu\varepsilon$ a significant difference in actuator performance is observed between the first loading cycle and the subsequent cycles. This indicates the damage to piezoceramic fibers occurred during the first loading cycle. The rate of reduction in the actuation is low at the beginning of the first loading cycle, ~10% reduction at 2000$\mu\varepsilon$. However, a faster rate of reduction in the performance is observed at higher strains, with only ~60% of the initial performance remaining at the maximum strain level of 4000$\mu\varepsilon$. During the unloading cycle, the actuator performance recovered slowly until 2000$\mu\varepsilon$ and a faster rate of recovery is observed at lower strain with ~90% of the original performance is recovered at the zero load level. The actuator performance during the subsequent load/unload cycles tend to follow the first unloading cycle and ~70% of the actuation is retained at the 2000$\mu\varepsilon$ level. A small difference in the performance is observed between the first unloading cycle and the second and third mechanical cycles. This shows that a little progressive damage

is accumulated during the second mechanical cycle. The actuator performance during the third cycle lies on top of the second cycle, indicating no further accumulation of damage. It is also observed that a mechanical load of $4000\mu\varepsilon$ introduces a permanent strain of $\sim 250\mu\varepsilon$ in the test coupon. Similar results are observed with specimens B14 and B29 that underwent performance under tensile load tests up to a maximum load level of $4000\mu\varepsilon$. The normalized actuation plots for the above specimens are found in Appendix C.

5.5.3 Tensile Loading up to $6000\mu\varepsilon$

A more drastic deterioration in the actuator performance is observed when an AFC actuator is loaded up to a maximum strain level of $6000\mu\varepsilon$. The data shown in Figure 5-6 is obtained by loading the specimen B30.

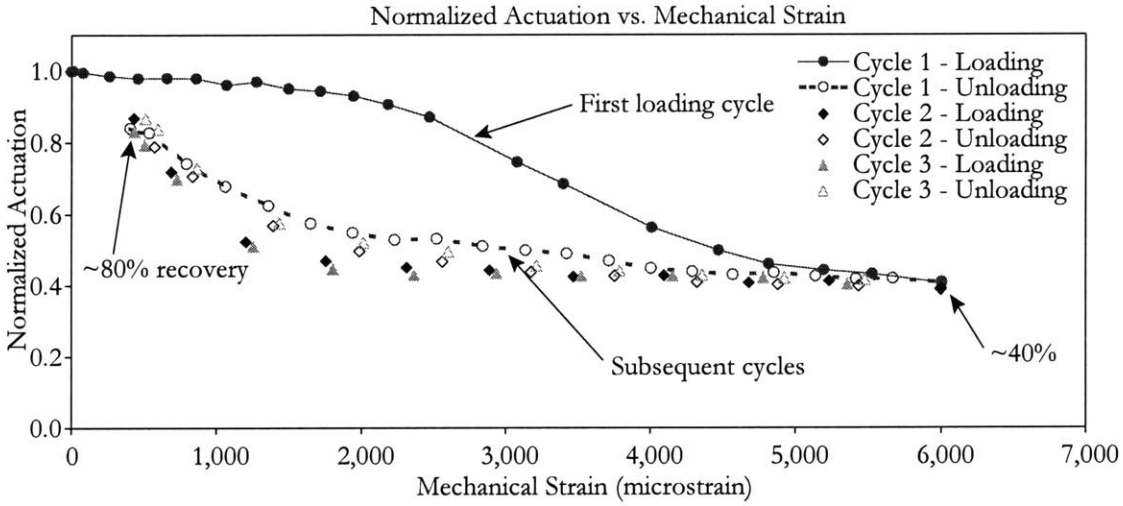

Figure 5-6: Actuation performance under tensile load (Maximum Strain $= 6000\mu\varepsilon$)

A large difference between the first loading cycle and the subsequent cycles is observed when the actuator is loaded up to a maximum strain of $6000\mu\varepsilon$. It indicates a significant damage accumulation in the actuator during the first loading cycle. During the first loading cycle, the rate of reduction in the actuator performance is slow at the beginning, only $\sim 10\%$ reduction at $2000\mu\varepsilon$. However, a faster rate of reduction in performance is observed at higher strains, with only $\sim 50\%$ of the initial performance retained at $4000\mu\varepsilon$ level. After $4000\mu\varepsilon$, the

deterioration in performance appears to plateau with ~40% of the initial performance retained at the maximum load of 6000$\mu\varepsilon$. The rapid rate of performance degradation observed after ~2500$\mu\varepsilon$ corresponds to the onset of catastrophic damage observed in the stress-strain tests conducted on the 0.01" diameter AFC actuator system. The Details of the stress-strain tests are found in Chapter 3. During the first unloading cycle, the actuator performance remained low, compared to the first loading cycle, but recovered faster at lower mechanical strain levels. Up to ~80% of the initial performance is recovered as the specimen is unloaded to the zero load. The actuator performance during the subsequent load/unload cycles tend to follow the first unloading cycle with ~50% and ~45% of the performance retrained at 2000$\mu\varepsilon$ and 4000$\mu\varepsilon$, respectively. A slight difference in the performance is observed between the first unloading cycle and the loading/unloading of the second and third cycles. This indicates a little progressive damage accumulated during the second mechanical cycle. However, the performance during the third mechanical cycle lies approximately on top of the second cycle indicating no accumulation of further damage during the repeated cycles. The mechanical loading of the actuator specimen up to 6000$\mu\varepsilon$ has induced a permanent strain of ~400$\mu\varepsilon$ in the specimen. Similar results are observed with specimens B15 and B44 that underwent performance under tensile load tests up to a maximum load level of 6000$\mu\varepsilon$. The normalized actuation plots for the above specimens are found in Appendix C.

5.6 Results Discussion

In performance under tensile load tests, the induced strain of AFCs due a 3000Vpp sinusoidal voltage cycle with 0Vdc at 1Hz is measured as a function of the static mechanical tensile load on specimen. The AFC actuator specimens were incrementally loaded to a predetermined maximum strain limit and the induced strain performance was measured at discrete loads levels. The fragmentation of piezoceramic fibers due to mechanical strain on the AFC resulted in a reduction in actuator performance. The extend of the total accumulated damage depended on the maximum mechanical strain undergone by the actuator. Higher maximum mechanical loads resulted in more damage accumulated in the actuator.

After reaching the maximum mechanical strain, the specimens were unloaded gradually

	Actuation ($\mu\varepsilon$)		First Loading Cycle				Third Loading Cycle			
ID	**Free**	**2 E120**	**2000**	**4000**	**6000**	**0 Load**	**2000**	**4000**	**6000**	**0 Load**
B13	1133	530	0.90	-	-	0.94	0.88	-	-	0.92
B28	1195	447	0.90	-	-	1.00	0.88	-	-	0.98
B42	1012	373	0.85	-	-	0.97	0.82	-	-	0.95
B14	1166	445	0.94	0.64	-	1.02	0.69	0.55	-	1.00
B29	1123	430	0.88	0.58	-	1.00	0.60	0.53	-	0.97
B43	1068	429	0.88	0.49	-	0.93	0.51	0.44	-	0.87
B15	1145	363	0.95	0.74	0.40	1.03	0.61	0.50	0.43	1.03
B30	987	378	0.93	0.56	0.41	0.83	0.44	0.43	0.41	0.87
B44	1007	475	0.87	0.56	0.40	0.85	0.48	0.40	0.37	0.76

Table 5.3: Summary of performance under tensile load test data

while measuring the actuator performance. Once completely unloaded, the actuator performance at the zero load level represented the residual actuation capability of the AFC after accumulation of damage due to loading. Most of the deteriorated performance was recovered. The mechanical load cycles were repeated on the same specimen up to the maximum strain level to observe any further accumulation of damage and no further deterioration in actuator performance was observed during repeated loading up to the maximum strain level.

It was observed that the extend of the total accumulated damage, the residual actuation at various strain levels, the percentage of performance recovery, and the rate of degradation in actuation depended on the maximum mechanical load undergone by the actuator. The Table 5.3 summarizes the normalized actuator performance at $2000\mu\varepsilon$, $4000\mu\varepsilon$, and $6000\mu\varepsilon$ at the first and the third loading cycles for all the specimens tested. The '0 Load' data corresponds to the retained actuator performance after completely unloading the specimen.

5.7 Summary

AFC performance tests under tensile loads demonstrated th deterioration in actuator performance with higher mechanical loads. For a virgin actuator, a specimen never before strained mechanically, the first loading cycle introduces damage to the piezoceramic fibers resulting in a gradual reduction in actuation at higher strain levels. Approximately 90%, 60% and 40% of the actuation was retained at the maximum load levels of $2000\mu\varepsilon$, $4000\mu\varepsilon$, and $6000\mu\varepsilon$, respectively. However, most of the deteriorated performance was recovered as the actuator

was unloaded back to the zero load level. Approximately 100%, 90% and 80% of the original performance was retained at the zero load level after loading the actuator up to maximum load levels of $2000\mu\varepsilon$, $4000\mu\varepsilon$, and $6000\mu\varepsilon$, respectively. It was also observed that only a little progressive damage is accumulated due to repeated loading if the maximum strain level is not exceeded.

This test provided an invaluable insight into the AFC actuators' ability to operate successfully under high tensile load conditions that exist in the rotor blade environment. The tests demonstrate the capability of the actuators to retains sufficient residual actuation to perform vibration control after withstanding high mechanical tensile loads in the AMR blade operation.

Chapter 6

Electrical Fatigue Tests

The electrical fatigue tests are designed to simulate the repeated actuation of AFCs during the AMR blade operation. It is important to determine the ability of the AFC material system to operate reliably for long durations while sustaining performance. The repeated actuation may lead to degradation in the actuator induced strain performance, heating of the actuator, or even catastrophic electrical failure. Therefore, electrical fatigue tests are used to characterize the performance of the actuator under high frequency actuation conditions.

The actuators are electrically fatigued using a 3000Vpp sinusoidal voltage cycle with 0Vdc, the highest voltage cycle expected in the AMR blade operation. The ideal fatigue frequency is 100Hz, as it would be the highest actuation frequency used in the AMR blade for vibration control. However, some of the tests are conducted at 200Hz frequency in order to accelerate time consuming tests. The tests are conducted under two mechanical loading conditions. In free strain condition tests, the actuators are tested up to 20 million electrical cycles without any external mechanical load applied to the actuator. In tensile load condition tests, the actuators are electrically fatigued up to 10 million electrical cycles while a constant tensile load applied to the actuator.

6.1 Electrical Fatigue Under Free Strain Condition

In electrical fatigue tests under free strain condition, the AFCs are repeatedly actuated without any external mechanical loads applied to the actuator. The tests are conducted at 100Hz and 200Hz frequencies using a 3000Vpp with a 0Vdc voltage cycle up to 20 million cycles. The total duration for a 20 million cycle fatigue test at 100Hz is 60hrs and for 200Hz is 30hrs. The induced strain of the actuator is measured at logarithmic electrical cycle intervals in order to identify the variation in actuator performance. Also, at more infrequent intervals, the actuators are inspected under a microscope in order to detect damages that could not be observed with the naked eye.

6.1.1 Test Articles

The narrow actuator coupons described in Section 2.4.1 with 0.01" diameter fiber AFC material system are used for electrical fatigue tests under free strain condition. Four unlaminated coupons are tested in order to facilitate inspection of piezoceramic fibers inside the actuator using a microscope. Two actuators symmetrically laminated with two plies of [0/90] E-Glass[1] (2 E120) are tested to simulate the constraint condition expected in the AMR blade. The E-Glass lamination procedure is discussed in Section 2.5.1. It is also important to note that half of the specimens had extra piezoelectric fibers. The extra fibers are used in order to have fibers underneath the electrode fingertips. See Figure 2-4 for details of the interdigitated electrode pattern used in AFCs. It is expected that having fibers underneath the electrode fingertips increases the actuators' venerability for electrical fatigue damage. This configuration is tested as it simulates the AMR blade actuators. Due to the current manufacturing limitations, one edge of the blade actuators always have fibers underneath the electrode fingertips. The addition of fibers outside the active area increases the stiffness of the inactive area, consequently reducing the induced strain performance of the actuator.

[1] Hexcel E120-155 prepreg cloth, Pleasanton, CA, Ph: 925-847-9500.

6.1.2 Test Matrix

The Table 6.1 shows the complete test matrix of the electrical fatigue tests conducted under free strain condition.

Constraint condition	Unlaminated	Unlaminated	Laminated
Electrical fatigue frequency	**100Hz**	**200Hz**	**200Hz**
Without fibers under electrode fingertips	B25	B26	B47
With fibers under electrode fingertips	B39	B40	B41

Table 6.1: Test matrix for electrical fatigue under free strain condition

6.1.3 Test Setup

The free strain performance test setup described in Section 4.3 is used for electrical fatigue tests under free strain condition. In addition, a Type K thermocouple is placed on the actuator surface to monitor heating due to repeated actuation. The thermocouple is attached to the actuator surface using tape. The required voltage signal is generated using a function generator[2] and the signal is amplified by 1000x using a high voltage amplifier[3]. The actuator is placed horizontally on the custom made AFC testing rig installed on an optics table. Actuator induced strain performance is measured using the laser displacement measuring interferometer system[4]. A microscope[5] is used to inspect the actuators during the test in order to detect microscopic damages inside the actuator due to electrical fatigue.

6.1.4 Test Procedure

The Table 6.2 outlines the step-by-step procedure for electrical fatigue tests under free strain condition.

[2] 0.1mHz-100MHz PM 5138 Fuction Generator, Philips, Germany.
[3] Model 664 10kV 20mA amplifire, Trek Inc., Medina NY, Ph: 716-798-3140.
[4] ZMI 1000, Zygo Corporation, Middlefield, CT, Ph: 860-347-8506.
[5] ZIESS Axiatech Microscopes, Germany.

Step	Description
1	Record the specimen ID of the selected active AFC test article.
2	Mount the test coupon in the custom made test rig and clamp one end of the specimen to the rig using the clamping mechanism.
3	Attach the retroreflector assembly to the free end of the actuator. Ensure that the retroreflector surface is clean and assembly moves smoothly along the groove.
4	Place the customized guides along both edges of the actuator.
5	Attach the thermocouple on to the actuator coupon using flash tape.
6	Ensure that the variable resistor is at the open circuit setting.
7	Attach high voltage wire leads to the appropriate electrode tabs on the actuator.
8	Set the function generator produce 3000Vpp signal with 0Vdc offset at 1Hz.
9	Switch the amplifier on and enable the high voltage application.
10	Enter calibration factors to the LabVIEW. (V=1kV/V, I=2mA/V)
11	Set the LabVIEW to take 1000 data points for a period of 10 seconds.
12	Turn the variable resistor gradually to feed the set electrical cycle from the function generator to the high voltage amplifier.
13	Use the LabVIEW to record and save actuator performance data for 1Hz frequency.
14	Increase the electrical cycle frequency in the function generator up to the fatigue frequency of 100Hz or 200Hz.
15	Use the LabVIEW record and save actuator displacement data for a duration of 10 cycles. (100Hz=0.1s and 200Hz=0.05s).
16	Monitor and record the temperature of the specimen using the thermocouple.
17	Repeat Steps 15-16 to record the induced strain performance of the actuator at logarithmic cycles intervals up to 20 million electrical cycles.

Table 6.2: Test procedure for electrical fatigue under free strain condition

6.1.5 Test Results

The actuator induced strain is calculated by normalizing the actuator displacement measured by the laser interferometer system[6] using the active length of 100mm. The active length is defined as the distance between the last electrode finger at each end of the electrode pattern as illustrated in Figure 2-3. In order to compare the performance variation among test samples, the induced strain output for each test coupon is normalized by the initial actuation at the fatigue frequency. The Figure 6-1 shows the variation in normalized actuator performance with the number of electrical cycles.

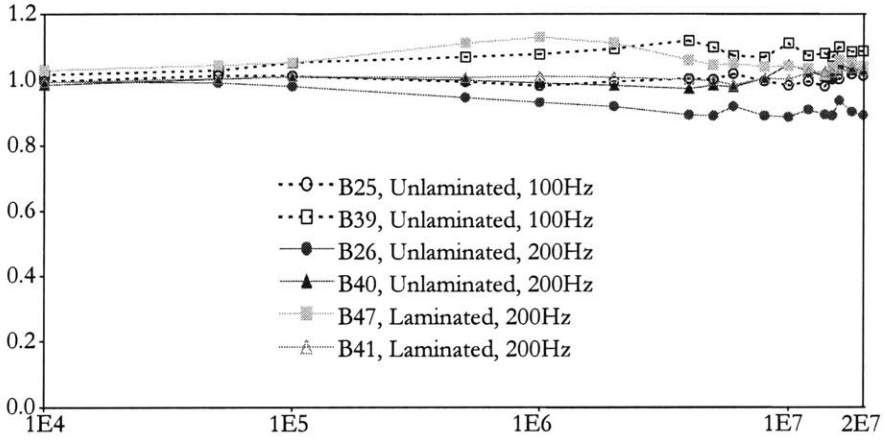

Figure 6-1: Actuator performance results of electrical fatigue tests under free strain condition

All actuator specimens tested under free strain condition survived the electrical fatigue test up to 20 million cycles and no significant heating is observed during the test. Most coupons showed no degradation in actuation performance and only one coupon showed a slight reduction in performance. The highest variation in the induced strain performance in any actuator is less than $\pm 10\%$ of the initial performance.

The specimen B25, which had no fibers underneath electrode fingertips, showed no loss in actuation during the test. However, after 1 million electrical cycles, the inspection of the actuator under the microscope enabled to detect $\sim$20 microscopic burn sites along few of the electrode fingers. These electrical fatigues burns are observed to occur on piezoceramic fiber

[6]ZMI 1000, Zygo Corporation, Middlefield, CT, Ph: 860-347-8506.

surface closest to the electrode finger. The locations of the detected burns are marked on the actuator specimen and the same burn sites are observed repeatedly at logarithmic various cycle intervals during the test in order to evaluate their growth. As seen in the Figure 6-2, two of those burns (B25-A and B25-B) showed steady growth along the electrode finger.

The specimen B26, which also had no fibers underneath electrode fingertips, showed a gradual reduction in actuation with higher number of electrical cycles. Approximately 10% reduction in performance is measured at the end of the 20 million cycle test. On B26, three microscopic burns that are observed before the fatigue test did not grow during the test. However, other burns formed along few of the electrodes fingers during the test and some of them grew along the finger. The Figure 6-2 shows the time history of two of the burns (B26-A and B26-B) observed along electrode fingers. It is observed that fatigue burns do not tend to grow from one electrode finger to the adjacent finger with the opposite polarity but they grow along the edge of the same electrode finger. Furthermore, none of these fatigue burns extended a significant distance away from the electrode finger to cause catastrophic failure to the actuator.

Both B39 and B40 are unlaminated specimens that had extra piezoelectric fibers embedded in the actuators to have fibers under electrode fingertips. Both specimens showed lower initial actuation performance due to the clamping effect from fibers in the inactive area. The electrical fatigue test results showed no reduction in actuation performance in both B39 and B40 specimens. However, after 1 million electrical cycles, the microscope inspection enabled to detect a total of 8 sites of fatigue burning on the specimen B40 and most of them occurred on the fibers under the electrode fingertips. The burns along the electrode fingers showed a little growth, while those at the fingertips grew considerably. The B39 specimen also showed many burn sites at electrode fingertips and they also grew steadily during the test. However, none of the burns were large enough to cause catastrophic failure to the actuator. The time history of two electrical fatigue burns observed on electrode fingertips in B39 and B40 are shown in Figure 6-3.

The laminated specimens, B41 and B47, showed no loss in actuation performance up to 20 million electrical cycles. Specimen B47 also had fibers under the electrode fingertips, but neither specimen showed any fatigue burns severe enough to be visible through the layers of E-Glass.

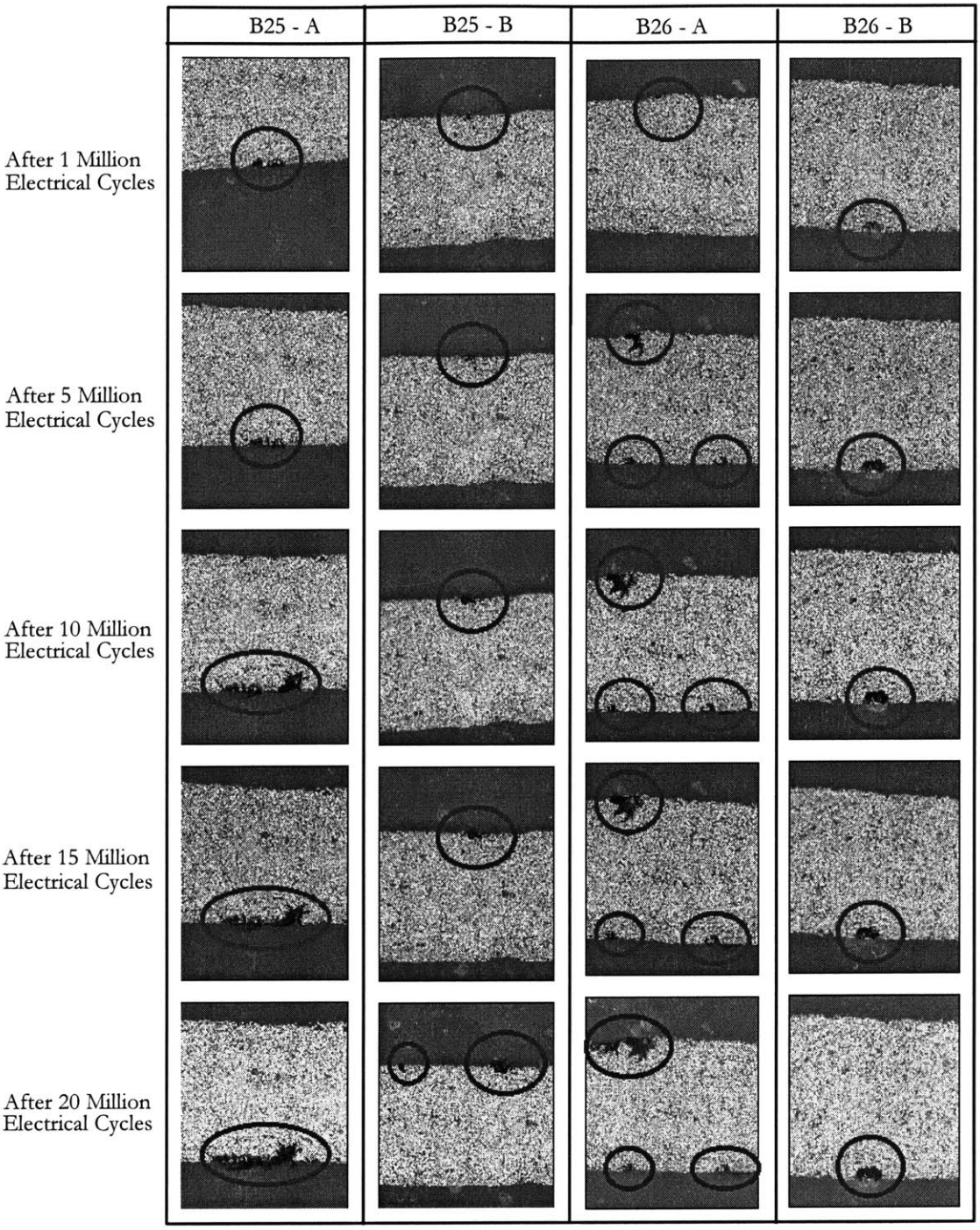

Figure 6-2: Electrical fatigue burns along electrode fingers

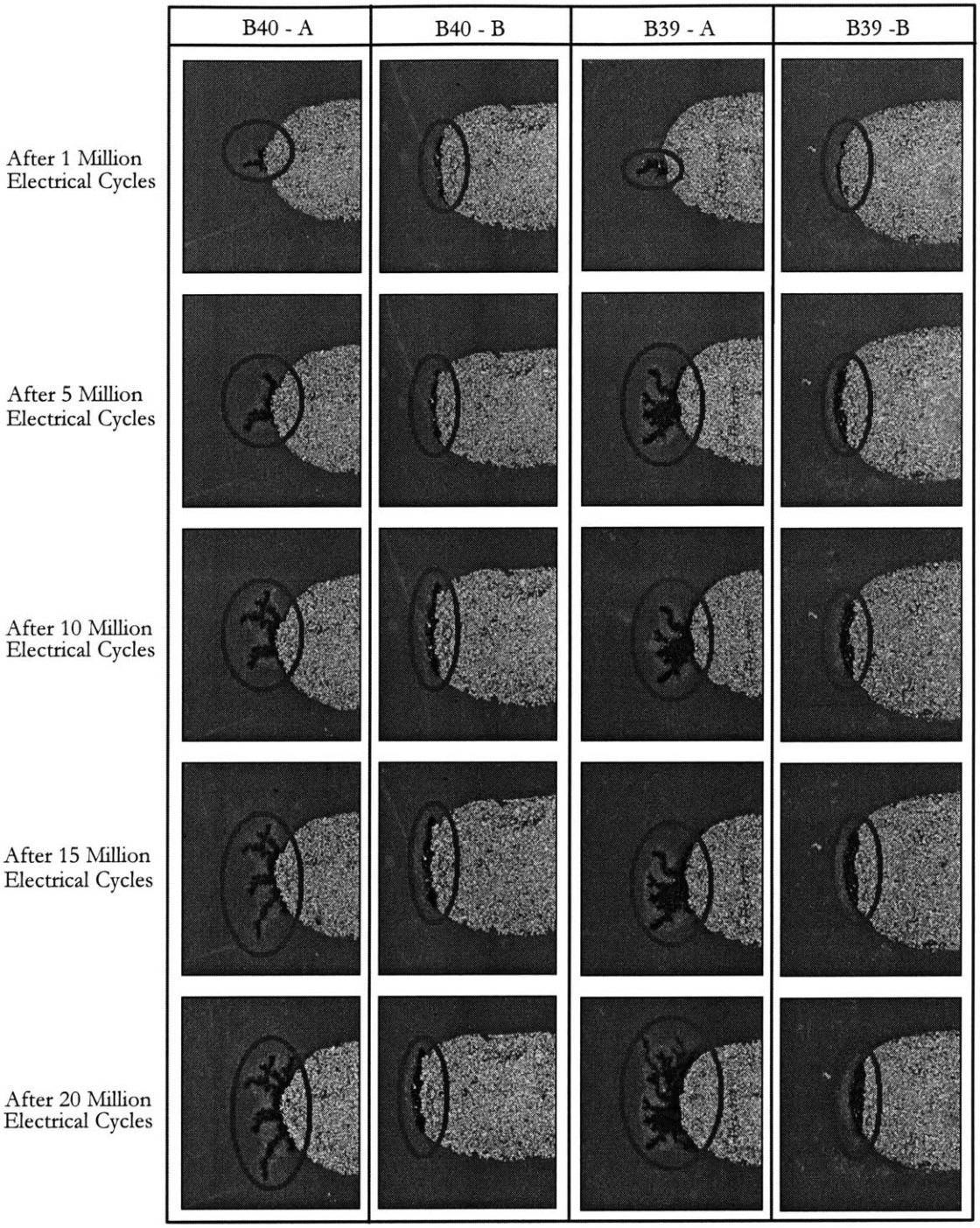

Figure 6-3: Electrical fatigue burns underneath electrode fingertips

6.1.6 Results Discussion

The electrical fatigue tests under free strain condition are conducted using narrow actuator coupons with 0.01" diameter fiber AFC material system. The actuator performance during the test and the test condition for each specimen is summarized in Table 6.3. Overall, the induced strain performance of five actuators out of a total of six showed no degradation under electrical fatigue under free strain condition, indicating no evidence of cumulative damage due to electrical fatigue. Only one actuator, B26, showed a slight deterioration in performance, retaining ~90% of the initial performance of the end of 20 million cycle test.

Specimen	E-Glass Lamination	Test Frequency	Initial Actuation	Normalized Actuation				
				1E4	1E5	1E6	1E7	2E7
B25	none	100 Hz	1064 $\mu\varepsilon$	1.00	1.01	0.98	0.98	1.01
B26	none	200 Hz	1047 $\mu\varepsilon$	1.00	0.98	0.93	0.89	0.89
B39	none	100 Hz	613 $\mu\varepsilon$	1.02	1.05	1.08	1.11	1.09
B40	none	200 Hz	623 $\mu\varepsilon$	1.03	1.06	1.04	1.09	1.07
B47	2 E120	200 Hz	523 $\mu\varepsilon$	1.03	1.05	1.13	1.04	1.04
B41	2 E120	200 Hz	326 $\mu\varepsilon$	0.99	1.01	1.01	1.00	1.03

Table 6.3: Actuator performance summary of electrical fatigue tests under free strain condition

However, detail inspection of the actuators under the microscope showed evidence of microscopic damage to the actuator in the form of fatigue burns. The fatigue burns generally occurs on the fiber surfaces closest to electrode fingers. It is observed that actuators with fibers underneath electrode fingertips showed more fatigue burn sites near fingertips than along the fingers. This may be due to higher concentration of electrical charge in the electrode fingertips due to its geometry and making those locations more vulnerable to initiate electrical fatigue damage. In the actuators without fibers underneath electrode fingertips, the fatigue burns occurred along electrode finger edges. Some of these fatigue burns grew steadily with the number of electrical cycles. However, at the end of the 20 million cycle test, none of the burns are large enough to cause catastrophic electrical failure in the actuator.

One possible explanation for the fatigue burn phenomenon is the charring of the matrix material due large current cycling between the fiber surface and the electrode finger. The large currents are generated from the high electric field between the fiber and the electrode. Once a burn is initiated, the charring creates a conductive material which further increases the

electric field by reducing the effective distance between the fiber and the electrode. Its is a compounding process that makes fatigue burns grow with the number of electrical cycles. The burning between the fiber and the electrode makes them grow along a electrode finger and not from one finger to the adjacent finger. Thus, the fatigue burns did not cause catastrophic failure on the actuators tested up to 20 million electrical cycle. However, the burning process makes it possible for the burns may grow larger and lead to catastrophic electrical failure in the actuator at higher electrical fatigue levels.

6.2 Electrical Fatigue Under Tensile Load Condition

In electrical fatigue tests under tensile loading condition, the AFCs are repeatedly actuated while applying a constant mechanical tensile load to the actuator. In order to accelerate time consuming fatigue tests, all the specimens are tested at 200Hz frequency using a 3000Vpp voltage cycle with 0Vdc up to 10 million cycles. The total duration for the fatigue test at 200Hz is 30hrs. The actuator induced strain performance is measured at logarithmic electrical cycle intervals to determine the variation in performance with the number of electrical cycles.

6.2.1 Test Articles

The electrical fatigue tests under tensile load condition are conducted using narrow actuator coupons described in Sections 2.4.1 with 0.01" diameter fiber AFC material system. All the actuator specimens are symmetrically laminated with two plies of [0/90] E-Glass utilizing the lamination procedure discussed in Section 2.5.1. The high voltage wires are connected to the actuator electrode tabs in accordance to the procedure explained in Section 2.5.2. Furthermore, unidirectional strain gages are bonded on both sides of the specimen to measure the mechanical strain and the induced strain of the actuator. Details of the strain gage and the application procedure is discussed in Section 2.5.3. The loading tabs necessary to mount the specimen on the tensile testing machine are bonded as explained in Section 2.5.4. An actuator test coupon prepared for electrical fatigue tests under tensile load condition is shown in Figure 5-1.

6.2.2 Test Matrix

The tests are conducted at three tensile load levels, namely, 2000$\mu\varepsilon$, 4000$\mu\varepsilon$, and 6000$\mu\varepsilon$. Due to time constraints and the limited availability of testing equipment for long duration tests, only one actuator specimen is electrically fatigued at each tensile load level. Table 6.4 shows the complete test matrix for the electrical fatigue tests conducted under tensile load condition.

Tensile Load	Specimen
2000$\mu\varepsilon$	B13
4000$\mu\varepsilon$	B29
6000$\mu\varepsilon$	B44

Table 6.4: Test matrix for electrical fatigue under tensile load condition

6.2.3 Test Setup

The test setup used for electrical fatigue under tensile load tests is identical to AFC performance tests conducted under tensile loads. The details of the test setup is found in Section 5.3. An Instron[7] tensile test machine is used to apply the constant tensile load to the actuator. The required voltage signal is generated using a function generator[8] and the signal is amplified by 2000x using a high voltage amplifier[9]. In addition, a Type K thermocouple is attached on the actuator surface using flash tape to monitor the heating due to electrical fatigue. Special strain gage conditioners are used to electrically isolate the strain gages from the computer. This type of electrical protection is necessary because the high voltage in the actuator could leak to the gages bonded on the actuator surfaces and damage the expensive data acquisition equipment.

The constant load is applied to the actuator specimen during the electrical fatigue tests utilizing the "load control" mode in the Instron machine. Therefore, it is important to tune the Instron machine's load controller to maintain a constant tensile load while the specimen is actuating continuously. The process of tuning the PID (Proportional, Integral and Differential) gain-constants in the machine's load controller is described in Section 5.3.3.

[7]Series 8501, Instron Corporation, Canton, MA, Ph: 800-564-8378.
[8]Wavetek Model 29, 10 MHz DDS Function Generator, Fluke Electronics, Everett, WA, Ph: 800-903-5853.
[9]Model 20/20B, 20kV and 20mA amplifire, Trek Inc., Medina NY, Ph: 716-798-3140.

6.2.4 Test Procedure

The Table 6.5 outlines the step-by-step procedure for electrical fatigue tests under tensile load condition.

Step	Description
1	Record the specimen ID of the prepared active AFC test coupon.
2	Mount the test coupon in the Instron tensile test machine using only the top hydraulic grip. See **Note 1** for details.
3	Attach the thermocouple on to the actuator coupon and connect high voltage wire leads to the amplifier output.
4	Balance strain gages to read zero strain when a specimen is gripped from the top and hanging free at the bottom.
5	Enter calibration factors to the LabVIEW software. See **Note 2** for details.
6	Use position control to raise the bottom grip up to the coupon's lower loading tab.
7	Close the lower grip while applying a tensile load of 5N instantaneously in load control mode. See **Note 3** for more details.
8	Select the single ramp waveform function in the Instron machine's position controller with a 2N/second rate of loading.
9	Load the specimen using the single ramp function to the predetermined constant load level. See **Note 4** for more details.
10	Hold the constant load and ensure the variable resistor is at the open circuit setting.
11	Set the function generator produce 3000Vpp signal with 0Vdc offset at 200Hz.
12	Switch the amplifier on and enable the high voltage application.
13	Turn the variable resistor gradually to feed the set electrical cycle from the function generator to the high voltage amplifier.
14	Use LabVIEW record and save 1000 data points for a period of 0.05 seconds.
15	Monitor and record the temperature of the specimen using the thermocouple.
16	Repeat Steps 15-16 to record the induced strain performance of the actuator at logarithmic cycles intervals up to 10 million electrical cycles.

Table 6.5: Test procedure for electrical fatigue tests under tensile load condition

Note 1: The top and bottom grips of the Instron machine must be aligned before mounting the test article. Even a slight misalignment in the grips causes the test article to twist and bend, making it impossible to apply a pure tensile load to the specimen. Extreme care is taken not to bend the test article when mounting on to the testing machine. The bending causes damage to the actuator test specimen by introducing cracks in the piezoceramic fibers. Once the test specimen is gripped using the top grip, an alignment apparatus is used to ensure that the specimen is vertical and aligned with the bottom grip.

Note 2: The calibration factors for the load and position readings are set in the Instron

machine's data output. The calibration factors for the voltage (2000V/V) and current (2mA/V) are specified in the high voltage amplifier. The strain gages are calibrated to read $1000\mu\varepsilon$/V.

Note 3: A delicate gripping procedure is used to close the lower grip to ensure that the machine does not apply a compressive load on to the test specimen when the bottom grip is closed. Without execution, the test machine is set to apply a small but positive load of 5N in the load control mode. While the lower grip is closing, before it touches the loading tabs on the specimen, the application of 5N load is executed instantaneously and maintained. If the application of the 5N load is not performed or delayed, the machine closes the lower grip with a compressive load on the specimen. This is undesirable because it bends the specimen, introducing damage to the AFC test article by cracking brittle piezoceramic fibers. The data taken during the gripping procedure is used to determine the loads and strains seen by the specimen during this delicate procedure.

Note 4: This test is conducted under the load control mode. Therefore, the strain gage readings must be observed constantly and the loading must be manually halted when the specimen load reaches the maximum mechanical strain defined the test matrix.

The strain data from gages on both sides of the specimen are averaged to calculate the mechanical strain and the induced strain performance at a particular load level. The induced strain performance is extracted by taking the difference between the maximum and the minimum strains measured to sinusoidal voltage application

6.2.5 Test Results

The induced strain performance measured in all specimens at logarithmic cycle intervals varied slightly with the number of electrical cycles. In order to compare the performance variation among test samples, the induced strain output for each test coupon is normalized by the initial actuation at the fatigue frequency of 200Hz. The Figure 6-1 shows the variation in the normalized actuator performance with the number of electrical cycles for each tensile load level.

6.2.6 Results Discussion

The electrical fatigue tests are conducted under tensile loading condition using narrow actuator coupons with 0.01" diameter fiber AFC material system. The actuators are symmetrically

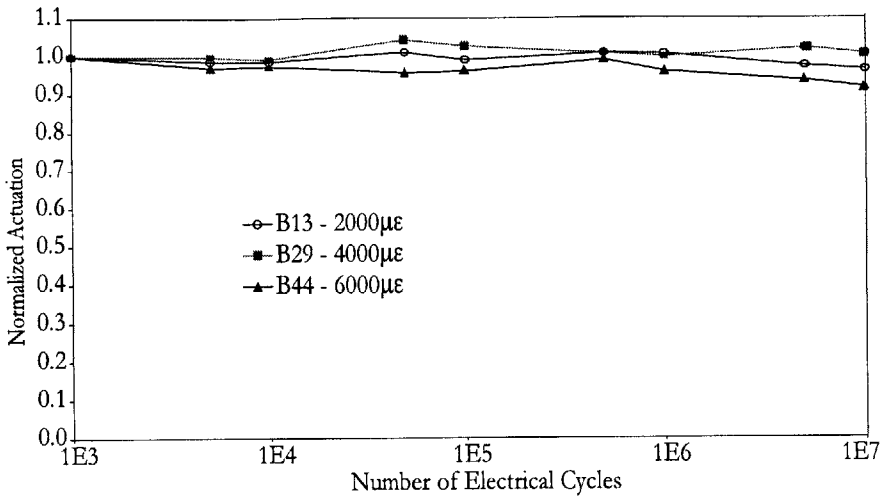

Figure 6-4: Actuator performance results of electrical fatigue tests under tensile load condition

laminated with two plies of [0/90] E-Glass. All three actuator specimens tested at three different constant tensile load levels survived the 10 million fatigue test. The actuator performance summary shown in Table 6.6.

Specimen	Mechanical Load	Initial Actuation	Normalized Actuation				
			1E3	1E4	1E5	1E6	1E7
B13	$2000\mu\varepsilon$	$335\mu\varepsilon$	1.00	0.99	0.99	1.01	0.97
B29	$4000\mu\varepsilon$	$349\mu\varepsilon$	1.00	0.99	1.03	1.00	1.01
B44	$6000\mu\varepsilon$	$297\mu\varepsilon$	1.00	0.97	0.96	0.96	0.92

Table 6.6: Actuator performance summary for electrical fatigue tests under tensile load condition

Overall, the actuation performance showed no significant degradation due to electrical fatigue under tensile load up to 10 million electrical cycles. The specimen B13, which is electrically fatigued under a constant load of $2000\mu\varepsilon$, showed less than 5% reduction in performance at end of the test. The specimen B29, which is electrically fatigued under a constant load of $4000\mu\varepsilon$, showed almost no loss in performance. The specimen B44, which is electrically fatigued under a constant load of $6000\mu\varepsilon$, showed less than 10% reduction performance at the end of the 10 million cycle test. None of the specimens failed during the test or showed any electrical fatigue burns severe enough to be visible through the layers of E-Glass.

6.3 Summary

The electrical fatigue tests were conducted to simulated the repeated actuation of AFCs during the blade operation. Five out of six actuators tested under the free strain condition showed no degradation in performance due to electrical fatigue. One actuator showed less than 10% reduction in performance at the end of 20 million cycle test. The microscopic inspection showed evidence of damage in the form of fatigue burns. However, none of the burns were large enough to cause catastrophic failure in actuators. Three specimens tested under $2000\mu\varepsilon$, $4000\mu\varepsilon$, and $6000\mu\varepsilon$ tensile loading conditions up to 10 million electrical cycles showed no significant degradation performance or large enough fatigue burns to be visible through E-Glass.

Electrical fatigue does not cause immediate problems in the AFC actuator system. However, fatigue burns observed during testing could lead to potential limitation in the actuator material system during the long term operation. In order to avoid electrical fatigue failures in blade actuators, the limitations are imposed on the AMR blade operation at high voltages and high frequencies. It is recommended to run electrical fatigue tests up to higher cycle levels in order to understand the potential issues due to fatigue burns. Furthermore, improvements to the AFC material system must be considered in future development to address the issue of electrical fatigue burns.

Chapter 7

Mechanical Fatigue Tests

The mechanical fatigue tests are designed to simulate the repeated mechanical loading on the embedded AFC actuators during the AMR blade operation. Mechanical fatigue on AFCs may lead to deterioration in performance, reduction in modulus, complete loss of actuation due to electrical failure or even catastrophic mechanical failure. Thus, it is of paramount important to determine the ability of the AFC material system to operate reliably under high mechanical fatigue conditions while sustaining actuation performance and maintaining mechanical strength. The tests are conducted using two types of AFC test articles, namely, actuators coupons and representative laminates. The actuator coupon specimens are made out of narrow AFC actuators laminated with [0/90] E-Glass to construct a simple symmetric composite. Both the induced strain performance and the modulus are used as degradation metric for these active specimens. The representative laminate specimens are passive test articles constructed to replicate the complex hybrid laminate structure in the AMR blade spar. Due to the passive nature, only the variation in modulus is used as the degradation metric in the representative laminate specimens.

7.1 Mechanical Fatigue Tests Using Actuator Coupons

The testing of AFC actuator coupons under mechanical fatigue involves the continuous application of a repetitive mechanical cycle while measuring the induced strain and the longitudinal modulus of the specimen at logarithmic mechanical cycle intervals. The tests are run at

23 Hz fatigue frequency to simulate the 1/rev mechanical loading condition expected in the AMR blade operation [Weems, 2000]. The actuators are tested up to 10 million cycles or the catastrophic mechanical failure according to the standard procedure [ASTM, D3479]. The induced strain performance of the actuator is measured at logarithmic mechanical cycle intervals by applying a 3000Vpp sinusoidal voltage cycle with 0Vdc at 1Hz. The fiber direction modulus is determined by conducting a load/unload cycle on the specimen at corresponding intervals. The electromechanical testing sequence is illustrated in Figure 7-1.

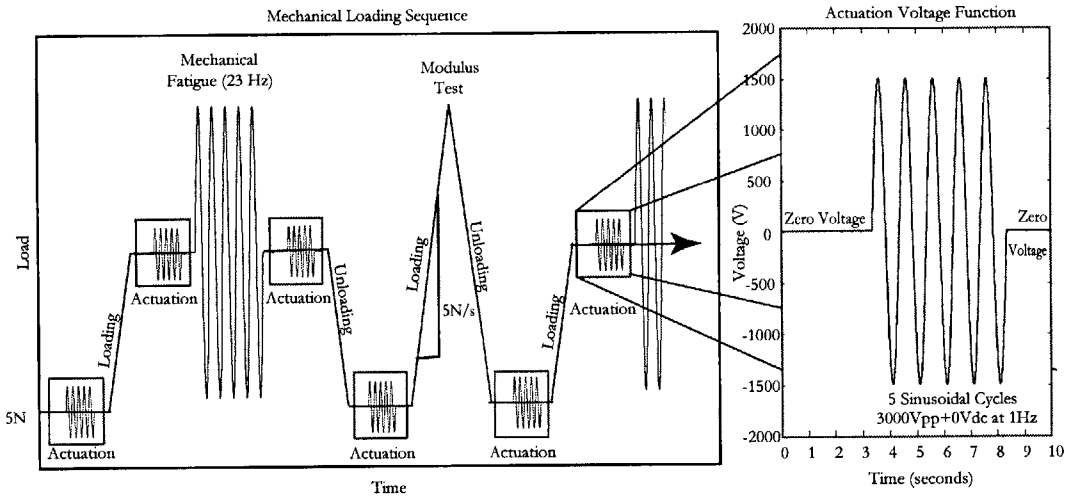

Figure 7-1: Mechanical fatigue testing sequence

7.1.1 Test Articles

The Narrow AFC actuator coupons with 0.01" diameter fiber material system described in Section 2.4.1 are used in mechanical fatigue tests. The specimens are constructed by symmetrically laminating the actuator with [0/90] E-Glass and the laminating procedure is explained in Section 2.5.1. The high voltage wires are attached to the actuator electrode tabs in accordance to the procedure discussed in Section 2.5.2. Furthermore, unidirectional strain gages rated for high mechanical fatigue loading, WD-DY-125AD-350[1], are bonded on both sides of the specimen to measure the mechanical strain and the induced strain. The details of the

[1]Micro-Measurements Group Inc., Raleigh, NC, Ph: 919-365-3800.

fatigue rated strain gage and the special application procedure is discussed in Section 2.5.3. The loading tabs necessary to grip the specimen on the tensile testing machine are bonded with a high strength adhesive film as explained in Section 2.5.4. An actuator coupon prepared for mechanical fatigue testing is shown in Figure 7-2.

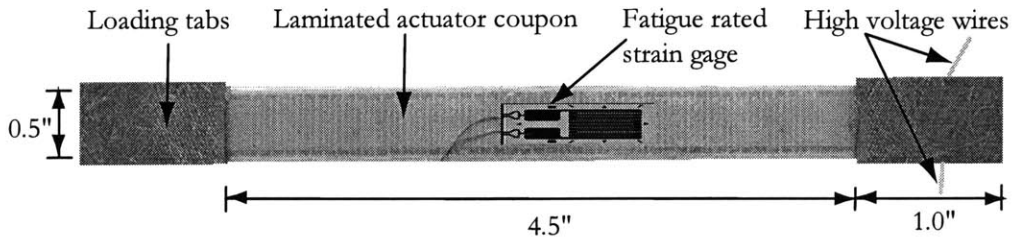

Figure 7-2: Actuator coupon prepaired for mechanical fatigue tests

7.1.2 Test Matrix

The actuator coupons are tested under mechanical fatigue using two mechanical fatigue load levels. Initially, the specimens are tested under the nominal fatigue load corresponding to a sinusoidal mechanical strain cycle of $1000\mu\varepsilon \pm 900\mu\varepsilon$. The nominal fatigue load level is selected to represent the operational loads expected in the AMR blade. Thus, a complete mechanical failure of the actuator is not expected at this load level. After completing the nominal fatigue test, a few of the specimens are tested again at a 50% higher load cycle. This extended fatigue load level corresponds to a strain cycle of $1500\mu\varepsilon \pm 1350\mu\varepsilon$. The tests are conducted at this extended fatigue cycle to determine the boundaries of the AFC material system under mechanical fatigue loading. The test specimens are symmetrically laminated with 1 ply (1 E120) or 2 plies (2 E120) of [0/90] E-Glass in order to understand the variation in the AFC fatigue behavior due to the passive structure. The complete mechanical fatigue test matrix using actuator coupons is shown in Table 7.1.

7.1.3 Test Setup

The test setup used for the mechanical fatigue tests is similar to the setup used for the AFC performance tests under tensile loads. The details of the test setup is found in Section 5.3. The

Fatigue Load Cycle	Specimen	# E-Glass plies
$1000\mu\varepsilon \pm 900\mu\varepsilon$	B24, B27	1 E120
$1000\mu\varepsilon \pm 900\mu\varepsilon$	B42	2 E120
$1500\mu\varepsilon \pm 1350\mu\varepsilon$	B27	1 E120
$1500\mu\varepsilon \pm 1350\mu\varepsilon$	B42	2 E120

Table 7.1: Mechanical fatigue test matrix for actuator coupons

repetitive mechanical loading to the actuator is applied using an Instron[2] tensile test machine. A high voltage amplifier[3] capable of 2000x amplification is used to supply the required voltage to the actuator. A customized electrical function corresponding to a 3000Vpp sinusoidal voltage cycle with 0Vdc at 1Hz is generated using the LabVIEW[4] software. The details of the customized voltage function is found in Section 5.3.2.

The test is conducted using the Instron machine's "load control" mode. The mechanical load on the specimen corresponding to the required mechanical strain cycle is set at the beginning of the test. Therefore, a permanent strain or a reduction in stiffness in the specimen leads to higher mechanical strains. An important part of the test setup is to tune the load controller in the Instron machine to maintain a constant tensile load during the actuation process and to maintain the appropriate mechanical loading cycle during the fatigue segment. This is achieved by tuning the load controller for each segment of the test separately with a corresponding set of PID (Proportional, Integral and Differential) gain-constants. Detailed discussion on the PID gain-constants and the process of tuning the load controller is found in Section 5.3.3. The two sets of PID gain-constants used for the mechanical fatigue tests are shown in Table 7.2.

	P	I	D
To maintain a constant load during actuation	14.0	14.0	0.0
To maintain a stable mechanical fatigue cycle	1.0	1.0	0.0

Table 7.2: PID gain-constants used for mechanical fatigue tests

It is important to note that an incorrect set of gain-constants used during the actuation process leads to an unacceptable variation in the constant load as seen in Figure 5-3. Similarly, an incorrect set of gain-constants used during the fatigue cycle leads to unstable loading

[2]Series 8501, Instron Corporation, Canton, MA, Ph: 800-564-8378.
[3]Model 20/20B 20kV, 20mA amplifire, Trek Inc., Medina NY, Ph: 716-798-3140.
[4]LabVIEW v5.1, National Instruments Corp., Austin, TX, Ph: 800-667-5347.

conditions. Thus, the minimum and maximum load limits in the Instron machine are set in order to protect the test specimen from undesired loading.

7.1.4 Test Procedure

The Table 7.3 outlines the step-by-step procedure developed to perform mechanical fatigue tests on actuator coupons while minimizing experimental errors.

Note 1: The top and bottom grips of the Instron machine must be aligned before mounting the test article. Even a slight misalignment in the grips causes the test article to twist and bend, making it impossible to apply a pure tensile load to the specimen. Extreme care is taken not to bend the test article when mounting on to the testing machine. The bending causes damage to the actuator test specimen by introducing cracks in the piezoceramic fibers. Once the test specimen is gripped using the top grip, an alignment apparatus is used to ensure that the specimen is vertical and aligned with the bottom grip.

Note 2: The calibration factors for the load and position readings are set in the Instron machine's data output. The calibration factors for the voltage (2000V/V) and current (2mA/V) are specified in the high voltage amplifier. The strain gages are calibrated to read $1000\mu\varepsilon$/V.

Note 3: A delicate gripping procedure is used to close the lower grip to ensure that the machine does not apply a compressive load on to the test specimen when the bottom grip is closed. Without execution, the test machine is set to apply a small but positive load of 5N in the load control mode. While the lower grip is closing, before it touches the loading tabs on the specimen, the application of 5N load is executed instantaneously and maintained. If the application of the 5N load is not performed or delayed, the machine closes the lower grip with a compressive load on the specimen. This is undesirable because it bends the specimen, introducing damage to the AFC test article by cracking the brittle piezoceramic fibers. The data taken during the gripping procedure is used to determine the loads and strains seen by the specimen during this delicate procedure.

Note 4: This test is conducted under the load control mode. Therefore, the correct loads must be determined in order to set the mechanical fatigue cycle corresponding to the desired mechanical strain levels shown in the test matrix. The loads are determined by loading the specimen to produce a strain ~10% higher than the maximum strain of the fatigue cycle

Step	Description
1	Record the specimen ID of the prepared AFC test coupon.
2	Mount the test coupon in the Instron tensile test machine using only the top hydraulic grip. See **Note 1** for details.
3	Enter calibration factors to the LabVIEW software. See **Note 2** for details.
4	Balance strain gages to read zero strain when a specimen is gripped from the top and hanging free at the bottom.
5	Raise the bottom grip up to the coupon's lower loading tab using the Instron machine's position control mode.
6	Enter appropriate PID gain-constants necessary to maintain a constant load.
7	Close the lower grip while applying a tensile load of 5N instantaneously in load control mode. See **Note 3** for more details.
8	Use the LabVIEW with the customized voltage function to measure the actuator induced strain performance at 5N load.
9	Start the LabVIEW to take data during the loading cycle to follow.
10	Load the specimen using the single ramp function to determine the loads corresponding to the strains of the mechanical fatigue cycle. See **Note 4** for details.
12	Unload the specimen back to 5N load using the single ramp waveform function at a 5N/second rate of unloading.
13	Select the loads corresponding to the static strain ($1000\mu\varepsilon$ or $1500\mu\varepsilon$) and the dynamic strains ($\pm 900\mu\varepsilon$ or $\pm 1350\mu\varepsilon$) of the mechanical fatigue cycle.
14	Use the LabVIEW with the customized voltage function to measure the induced strain performance of the actuator at 5N load.
15	Use the dual ramp function in the load controller to load/unload the specimen to the maximum strain expected during the fatigue cycle at a rate of 5N/second.
16	Use the LabVIEW with the customized voltage function to measure and record the induced strain performance of the actuator at 5N load.
17	Load specimen up to the static strain level ($1000\mu\varepsilon$ or $1500\mu\varepsilon$) using the single ramp waveform at a 5N/second rate of loading.
18	Set the sinusoidal waveform in the load controller to generate the mechanical fatigue cycle corresponding to dynamic strains ($\pm 900\mu\varepsilon$ or $\pm 1350\mu\varepsilon$) at 23Hz.
19	Enter the appropriate PID gain-constants necessary to maintain a stable mechanical fatigue loading cycle.
20	Start the mechanical fatigue cycle and ensure that the loading cycle is stable.
21	Stop the fatigue cycle at logarithmic cycle intervals and unload the specimen back to 5N at a rate of 5N/second using the single ramp waveform function.
22	Repeat Steps 14-21 up to 10 million mechanical cycles.

Table 7.3: Test procedure for mechanical fatigue tests using actuator coupons

(2100$\mu\varepsilon$ or 3150$\mu\varepsilon$) using the single ramp waveform with a 5N/second rate of loading. The strain gage readings are observed continuously during the loading process and the loading is halted manually when the specimen reaches the desired strain level.

The strain data from gages on both sides of the specimen are averaged to calculate the mechanical strain and the induced strain at a particular load level. The induced strain performance is extracted by taking the difference between the maximum and the minimum strains measured during the sinusoidal segment of the voltage function. The load data acquired from the Instron machine is converted to stress values using the specimen width and the nominal thickness of the test articles. The chord modulus is calculated for various mechanical strain ranges, from 100$\mu\varepsilon$ to a specified upper limit, such as 500$\mu\varepsilon$, 1000$\mu\varepsilon$, 2000$\mu\varepsilon$, and 3000$\mu\varepsilon$. The modulus of the AFC actuator is extracted from the [0/90] E-Glass laminated specimens by removing the contribution of the E-Glass analytically. The Mechanics of Material approach discussed in Section 2.6 is used to extract the actuator modulus. A fatigue test conducted on pure [0/90] E-Glass specimen at 1000$\mu\varepsilon$±900$\mu\varepsilon$ mechanical strain level indicated no degradation in modulus up to 10 million cycles.

7.1.5 Results for Nominal Fatigue Cycle (1000$\mu\varepsilon$±900$\mu\varepsilon$)

The variation in AFC longitudinal modulus and induced strain performance observed on the actuator coupon B24, which is symmetrically laminated with one ply of [0/90] E-Glass, is shown in Figure 7-3.

The AFC modulus extracted from the initial loading cycle is 32GPa for 100-500$\mu\varepsilon$ and 26GPa for 100-2000$\mu\varepsilon$. The modulus calculated from the second loading cycle is slightly higher, 35GPa for 100-500$\mu\varepsilon$ and 27GPa for 100-2000$\mu\varepsilon$. The modulus remained relatively constant throughout the 10 million fatigue cycles. At the end of the test, the modulus is 41GPa for 100-500$\mu\varepsilon$ and 28GPa for 100-2000$\mu\varepsilon$. A gradual accumulation of permanent strain is observed during the test and ~280$\mu\varepsilon$ of permanent deformation is recorded at the end of 10 million cycles. The induced strain of the actuator is measured at 5N and 135N before and after each loading/unloading conducted for modulus determination. The specimen induced strain is 611$\mu\varepsilon$ initially at 5N load and the actuation gradually rose to 670$\mu\varepsilon$ during the test.

The variation in AFC longitudinal modulus and induced strain performance observed on

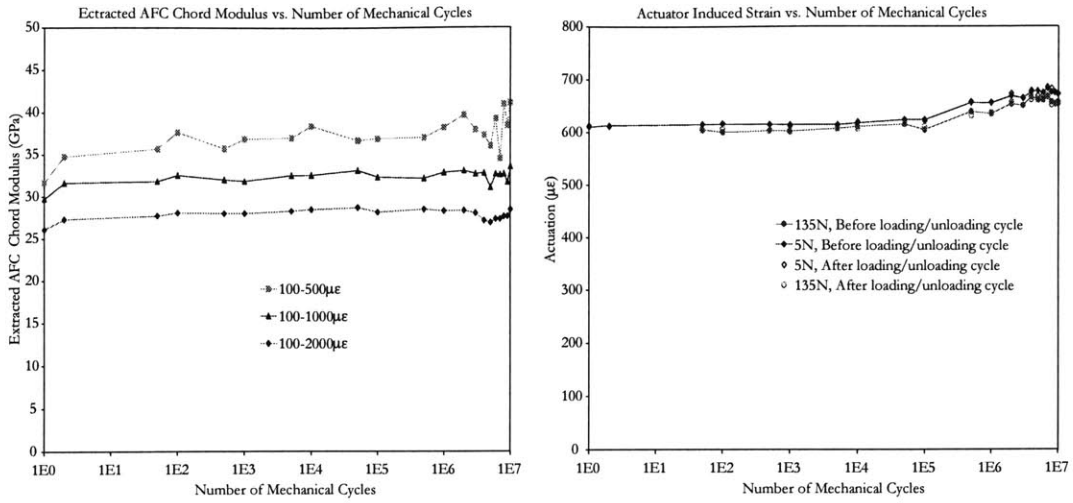

Figure 7-3: Actuation and modulus of B24 during the nominal mechanical fatigue test

the actuator coupon B27, which is also symmetrically laminated with one ply of [0/90] E-Glass, is shown in Figure 7-4.

The AFC modulus extracted from the specimen B27 during the initial loading cycle is 30GPa for 100-500$\mu\varepsilon$ and 23GPa for 100-2000$\mu\varepsilon$. The modulus calculated from the second loading cycle is 27GPa for 100-500$\mu\varepsilon$ and 24GPa for 100-2000$\mu\varepsilon$. The modulus remained relatively constant throughout the test. At the end of the test, the residual modulus is 29GPa for 100-500$\mu\varepsilon$ and 26GPa for 100-2000$\mu\varepsilon$. A gradual accumulation of permanent strain is observed during the test and $\sim$300$\mu\varepsilon$ of permanent deformation is recorded at the end of 10 million cycles. The induced strain of the actuator is measured at 5N and 135N before and after each loading/unloading segment conducted for modulus determination. The initial induced strain of the specimen is 692$\mu\varepsilon$ at 5N load and fluctuated between 670$\mu\varepsilon$ and 720$\mu\varepsilon$ during the test.

The specimen B42 also showed similar results. The variation in AFC longitudinal modulus and induced strain performance of the actuator coupon B42, laminated with two plies of [0/90] E-Glass per side, is shown in Figure 7-5.

The longitudinal AFC modulus extracted from the initial loading cycle is 23GPa for 100-500$\mu\varepsilon$ and 20GPa for 100-2000$\mu\varepsilon$. Subsequent loading/unloading cycles conducted at logarithmic cycle intervals showed similar or slightly higher modulus values throughout the test. At the end of the fatigue test, residual modulus at the end of the test 34GPa for 100-500$\mu\varepsilon$ and 23GPa

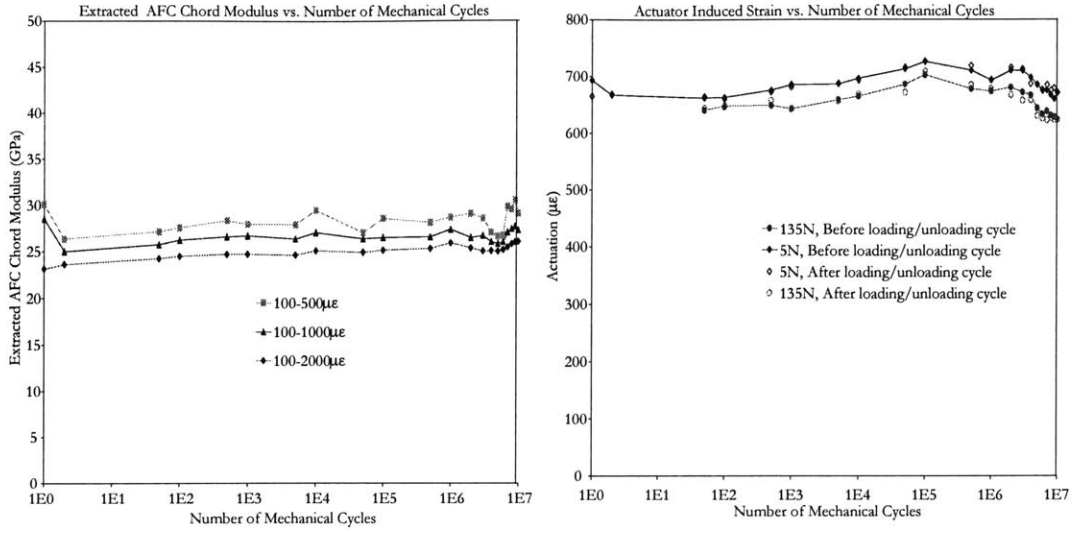

Figure 7-4: Actuation and modulus of B27 during the nominal mechanical fatigue test

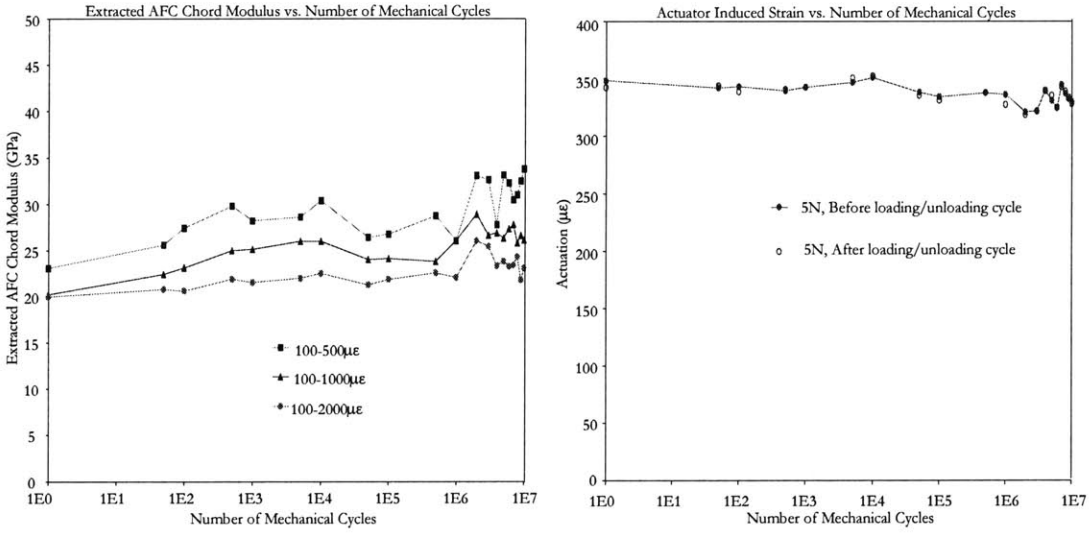

Figure 7-5: Actuation and modulus of B42 during the nominal mechanical fatigue test

for 100-2000$\mu\varepsilon$. A higher scattering in the modulus data for 100-500$\mu\varepsilon$ range is observed. The permanent strain accumulated in the specimen increases in the lower bound in the 100-500$\mu\varepsilon$ range, leading to higher uncertainly in the calculation. A gradual accumulation of permanent strain is observed during the test and ~230$\mu\varepsilon$ of permanent deformation is recorded at the end of 10 million cycles. A lower permanent strain is observed compared to the specimens B27 and B24 due to the presence of two E-Glass layers instead of one. The induced strain of the actuator is measured before and after each load/unload cycle at 5N load. The initial induced strain induced strain of the specimen is 348$\mu\varepsilon$ and fluctuated between 319$\mu\varepsilon$ and 351$\mu\varepsilon$ during the test. A lower induced strain is also observed due higher constraint condition introduced from lamination with 2 layers of E-Glass.

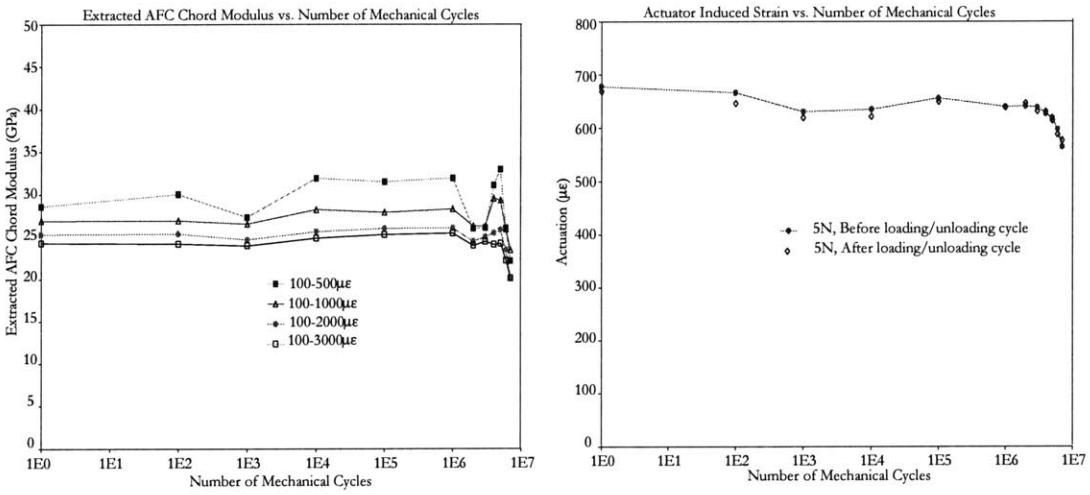

Figure 7-6: Actuation and modulus of B27 during the extended mechanical fatigue test

7.1.6 Results for Extended Fatigue Cycle of 1500$\mu\varepsilon$±1350$\mu\varepsilon$

After completing 10 million mechanical cycles at the nominal fatigue load level, further testing is conducted on two actuator coupons under the extended fatigue load. The variation in the AFC longitudinal modulus and induced strain performance recorded for the specimen B27 during the extended fatigue test is shown in Figure 7-6.

The AFC longitudinal modulus extracted from the initial loading cycle is 29GPa for 100-500$\mu\varepsilon$ and 25GPa for 100-2000$\mu\varepsilon$. The modulus for 100-2000$\mu\varepsilon$ range remained steady at

25-26GPa through 5 million cycles, then dropped to 23GPa at 6 million cycles and 20GPa at 7 million cycles. The induced strain of the actuator is measured at 5N load before and after each loading/unloading cycle performed to determine the modulus. The initially induced strain of the actuator is 672$\mu\varepsilon$ and stabilized between 620$\mu\varepsilon$ and 650$\mu\varepsilon$ up to 5 million mechanical cycles. The performance dropped to 592$\mu\varepsilon$ at 6 million cycles and 570$\mu\varepsilon$ at 7 million cycles. The specimen suffered two-part failure at the middle of the test section shortly after 7 million cycles. A picture of the mechanically failed actuator coupon is shown in Figure 7-7.

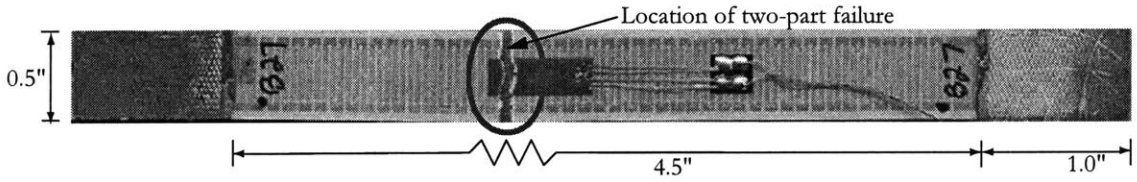

Figure 7-7: Two-part failure of B27 under the extended mechanical fatigue test

A similar mechanical fatigue test under the extended loading cycle is conducted on the specimen B42, which is laminated symmetrically with two plies of [0/90] E-Glass. The variation in the AFC longitudinal modulus and induced strain is shown in Figure 7-8.

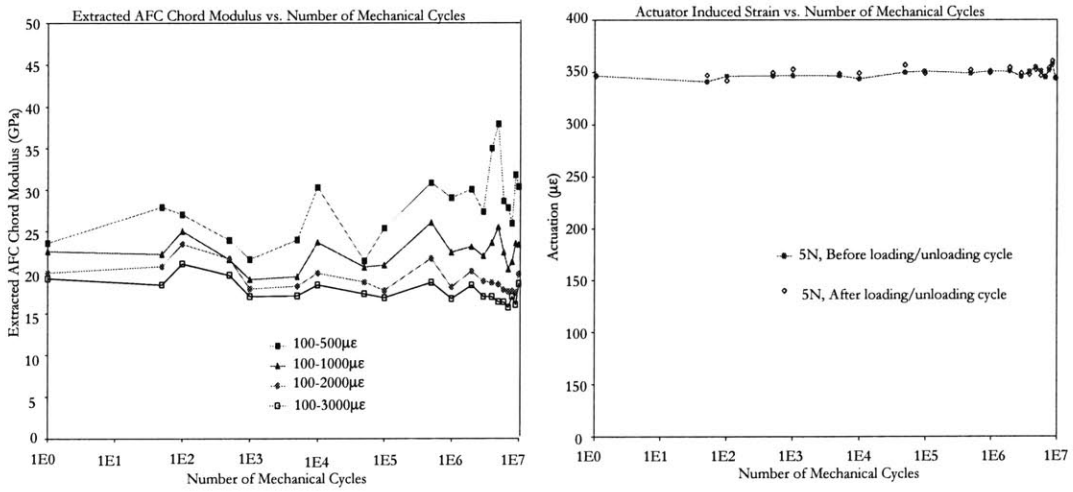

Figure 7-8: Actuation and modulus of B42 during the extended mechanical fatigue test

The extracted AFC longitudinal modulus from the initial loading cycle is 23GPa for 100-

500$\mu\varepsilon$ and 20GPa for 100-2000$\mu\varepsilon$. Subsequent loading/unloading cycles showed a large variation in the modulus calculated for 100-500$\mu\varepsilon$ range. The higher scattering in the modulus data for 100-500$\mu\varepsilon$ range is related to the permanent strain and the noisy signals from the strain gages. The modulus calculated for 100-2000$\mu\varepsilon$ remained steady at 23-18GPa through the 10 million cycle test. The induced strain of the actuator is measured before and after each loading/unloading cycle at 5N load and the induced strain performance remained steady. The initial induced strain is 344$\mu\varepsilon$ and remained between 340$\mu\varepsilon$ and 360$\mu\varepsilon$ during the 10 million cycle fatigue test under the extended load level.

7.1.7 Results Discussion

The mechanical fatigue tests performed on the actuator coupons provided an invaluable insight into the AFCs' behavior under dynamic mechanical loading conditions. All three mechanical fatigue tests conducted at the nominal fatigue load level of 1000$\mu\varepsilon$±900$\mu\varepsilon$ showed no reduction in the longitudinal modulus or a deterioration in the induced strain performance. After completing the fatigue test at the nominal load level, two actuators are tested at 50% higher loads corresponding to a strain cycle of 1500$\mu\varepsilon$±1350$\mu\varepsilon$. During the extended fatigue test, the actuator coupon laminated symmetrically with one ply of [0/90] E-Glass suffered two-part failure shortly after 7 million cycles. Under similar extended fatigue loading condition, the actuator coupon laminated symmetrically with two plies of [0/90] E-Glass showed no degradation in modulus or mechanical failure up to 10 million cycles. The summary of the extracted AFC chord modulus (in GPa) for 100-2000$\mu\varepsilon$ range is shown in Table 7.4.

		Number of Mechanical Cycles								
Specimen	**Fatigue Load**	**1**	**2**	**1E3**	**1E4**	**1E5**	**5E5**	**1E6**	**5E6**	**1E7**
B24	1000$\mu\varepsilon$±900$\mu\varepsilon$	26	27	28	29	28	29	28	27	29
B27	1000$\mu\varepsilon$±900$\mu\varepsilon$	23	24	25	25	25	25	26	25	26
B27	1500$\mu\varepsilon$±1350$\mu\varepsilon$	25	25	25	26	26	-	26	26	Failed
B42	1000$\mu\varepsilon$±900$\mu\varepsilon$	20	21	21	22	22	23	22	24	23
B42	1500$\mu\varepsilon$±1350$\mu\varepsilon$	20	21	18	20	18	22	18	19	20

Table 7.4: Variation in AFC modulus during mechanical fatigue tests

The induced strain performance of the actuator coupons tested under the nominal fatigue

load level did not deteriorate. The Figure 7-9 shows the variation in the actuator induced strain performance with the number of mechanical cycles. For comparison reasons, the actuation performance is normalized by the initial performance measured at 5N before the first loading cycle.

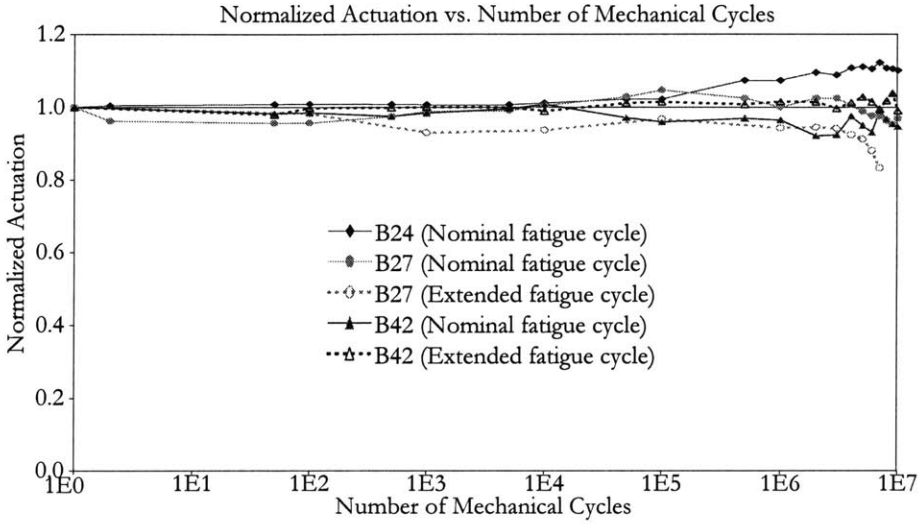

Figure 7-9: Normalized actuation results from mechanical fatigue tests

As seen in Figure 7-9, only the actuator B27 tested at the extended fatigue load showed a gradual degradation in performance after 5 million cycles. However, under similar mechanical fatigue loading conditions, the specimen B42 laminated symmetrically with 2 plies of [0/90] E-Glass did not show any deterioration in performance. The summary of the normalized performance data measured at 5N load is tabulated in Table 7.5. The initial strain value is the actuator induced strain performance measured before the first loading cycle.

		Initial	Number of Mechanical Cycles							
Specimen	**Fatigue Load**	**Strain**	**2**	**1E3**	**1E4**	**1E5**	**5E5**	**1E6**	**5E6**	**1E7**
B24	$1000\mu\varepsilon \pm 900\mu\varepsilon$	$611\mu\varepsilon$	1.00	0.99	1.00	0.99	1.04	1.04	1.08	1.07
B27	$1000\mu\varepsilon \pm 900\mu\varepsilon$	$692\mu\varepsilon$	0.96	0.93	0.96	1.02	0.98	0.98	0.92	0.90
B27	$1500\mu\varepsilon \pm 1350\mu\varepsilon$	$678\mu\varepsilon$	0.98	0.93	0.94	0.94	0.97	0.94	0.91	Failed
B42	$1000\mu\varepsilon \pm 900\mu\varepsilon$	$348\mu\varepsilon$	0.98	0.98	1.01	0.95	0.97	0.95	0.96	0.95
B42	$1500\mu\varepsilon \pm 1350\mu\varepsilon$	$345\mu\varepsilon$	0.98	1.00	0.99	1.01	1.01	1.02	1.02	0.99

Table 7.5: Variation in actuation during mechanical fatigue tests

7.2 Mechanical Fatigue Tests Using Representative Laminates

The mechanical fatigue tests are also performed on hybrid laminate specimens that are constructed to represent the composite structure of the AMR blade spar. The testing of such laminates are necessary to evaluate the modulus and the mechanical fatigue strength of the blade. The composite lay-up chosen to represent the blade spar is: $[E120/AFC/S2/S2/AFC/E120/S2]_S$. Where E120 is 0.0045" thick E-Glass[5] fabric, S2 is 0.0090" thick unidirectional S-Glass tape[6], and AFC[7] is 0.0135" thick actuators consist of 0.01" diameter fiber material system. The details of the AFC actuator material system is found in Section 2.3. The predicted nominal thickness of the total laminate is 0.126". An important difference between the blade spar and the lay-up chosen to construct the representative laminate test specimens is that the spar laminate is not symmetric. A symmetric laminate is chosen to construct the test coupons in order to minimize the warping of the laminate during the cooling process after curing.

7.2.1 Test Articles

The representative laminate test coupon geometry is designed in accordance to the Boeing standard for unnotched tension-tension fatigue testing of rotor blade laminates. The Boeing design is chosen because the testing of these representative laminate specimens are conducted at Boeing Helicopters. However, the standard Boeing specimen geometry is scaled downed in order to reduce the number of AFC actuators needed to construct the required number of representative laminate specimens. The representative laminate test coupon is 6" long by 0.75" wide and narrows to 0.60" in the center of the test section. The laminates are cured in the hotpress at 250°F for 2 hours. The lamination procedure is discussed in detail in Section 2.5.1. The hotpress is closed with a force appropriate for generating the desired cure pressure of 60psi. Following the cure, the pressure is released and the heat is turned off. The laminate is allowed to cool in air and it simulates the cool down period associated with the AMR blade cure. Once the laminates are cooled down, a water-jet machine is used to cut test coupons out of the laminate. The fiberglass loading tabs made out of 1/8" thick GPO-3 sheets[8] are

[5]Hexcel E120-155 prepreg cloth, Pleasanton, CA, Ph: 925-847-9500.
[6]3M SP 381 Scotchply S-Glass, 3M Adhesive Division, St. Paul, MN, Ph: 800-364-3577.
[7]Continuum Control Corporation, Billerica, MA, Ph: 978-670-4910.
[8]GPO-3 Fiberglass sheets, McMaster-Carr Supply Company, New Brunswick, NJ, Ph: 732-329-3200.

bonded on each end of the coupon. The tabs are cut with a 30° bevel angle to facilitate a smooth load transfer from testing machine to the test coupon [ASTM, D3039]. A high strength nitrile epoxy adhesive film, FM 123-2[9], is used to bond the loading tabs to the test coupons. The details of the loading tab bonding procedures is found in Section 2.5.4. The Figure 7-10 illustrates the geometry of the representative laminate test coupon.

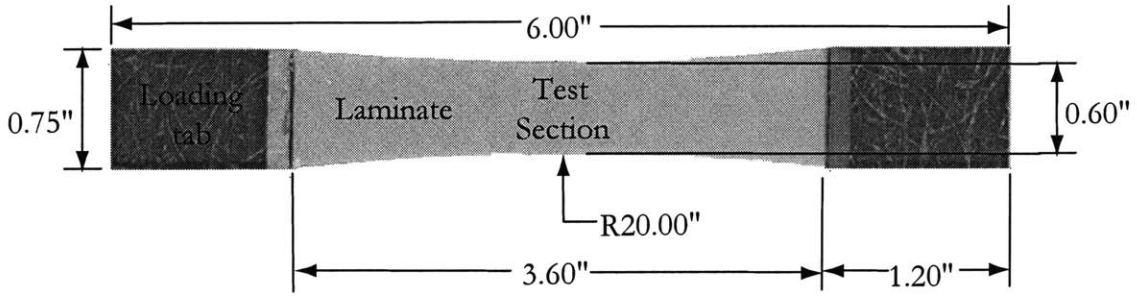

Figure 7-10: Dimentions of the representative laminate test coupon

The fatigue rated unidirectional strain gages, WD-DY-125AD-350[10], are bonded on both sides of the specimen to measure the mechanical strain. This special type of strain gage is able to withstand a high number of mechanical cycles. A high strength adhesive is used to bond the gages and details of the fatigue rated strain gages and the application procedure is discussed in Section 2.5.3.

Two configurations of hybrid laminate test coupons are designed to represent the AMR blade loads on the composite spar, namely, 0° configuration and 45° configuration.

The 0° laminate specimens are configured to replicate the axial strains on the blade due to flap bending, chord bending and CF loads [Weems, 2000]. These loads are replicated on the test specimen by aligning the direction of mechanical loading with the unidirectional S-Glass. Therefore, the orientation of composite plies in the 0° laminate is $[\pm 45^{E120}/+45^{AFC}/0^{S2}/0^{S2}/-45^{AFC}/0^{S2}]_S$. This configuration in 0° specimens aligns the piezoceramic fibers at ±45° to the direction of mechanical loading.

[9]FM 123-2 adhesive film, Cytec Fiberite Inc., Havre de Grace, MD, Ph: 410-939-1910.
[10]Micro-Measurements Group Inc., Raleigh, NC, Ph: 919-365-3800.

The 45° laminate specimens are designed to replicate the strains on the AMR blade due to torsion and components 0° loads. In this laminate configuration, the direction of mechanical loading is aligned in the direction of the piezoceramic fibers or 45° to the unidirectional S-Glass. The orientation of composite plies in the 45° laminate is $[0^{E120}/0^{AFC}/-45^{S2}/-45^{S2}/90^{AFC}/-45^{S2}]_S$. The Figure 7-11 shows the cross-sectional views of the 0° and the 45° laminates and illustrates the ply orientations.

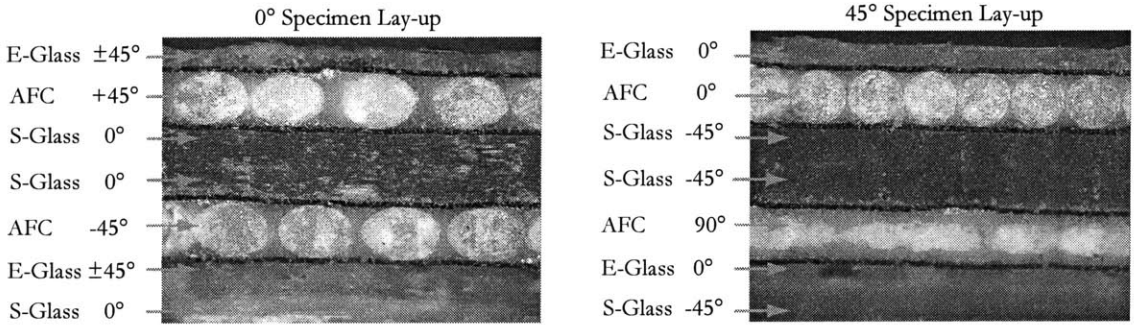

Figure 7-11: Representative laminate layup of 0° and 45° specimens

The trapezoidal 45° AFC actuators that are designed for the AMR blade application are used to construct the representative laminates. The actuators are placed among passive composite plies in the laminate exactly as in the AMR blade spar. The passive plies extends across the entire laminate and the area around the AFC actuators are filed with passive composites similar to the filler plies used in the blade design. The Figure 7-12 shows the process of extracting two 0° test specimens from a 2" x 10" laminate and four 45° test specimens from a 5" x 10" laminate.

7.2.2 Test Matrix

Four test coupons are produced from each type of representative laminate configuration. A static tension test is conducted up to the failure on one test coupon and the remaining three are used for mechanical fatigue tests. The complete test matrix for the representative laminate specimens are shown in Table 7.6.

The static tensile test is used to determine the laminate modulus and the laminate failure strength. The test requires the specimen to be loaded gradually until failure while recording

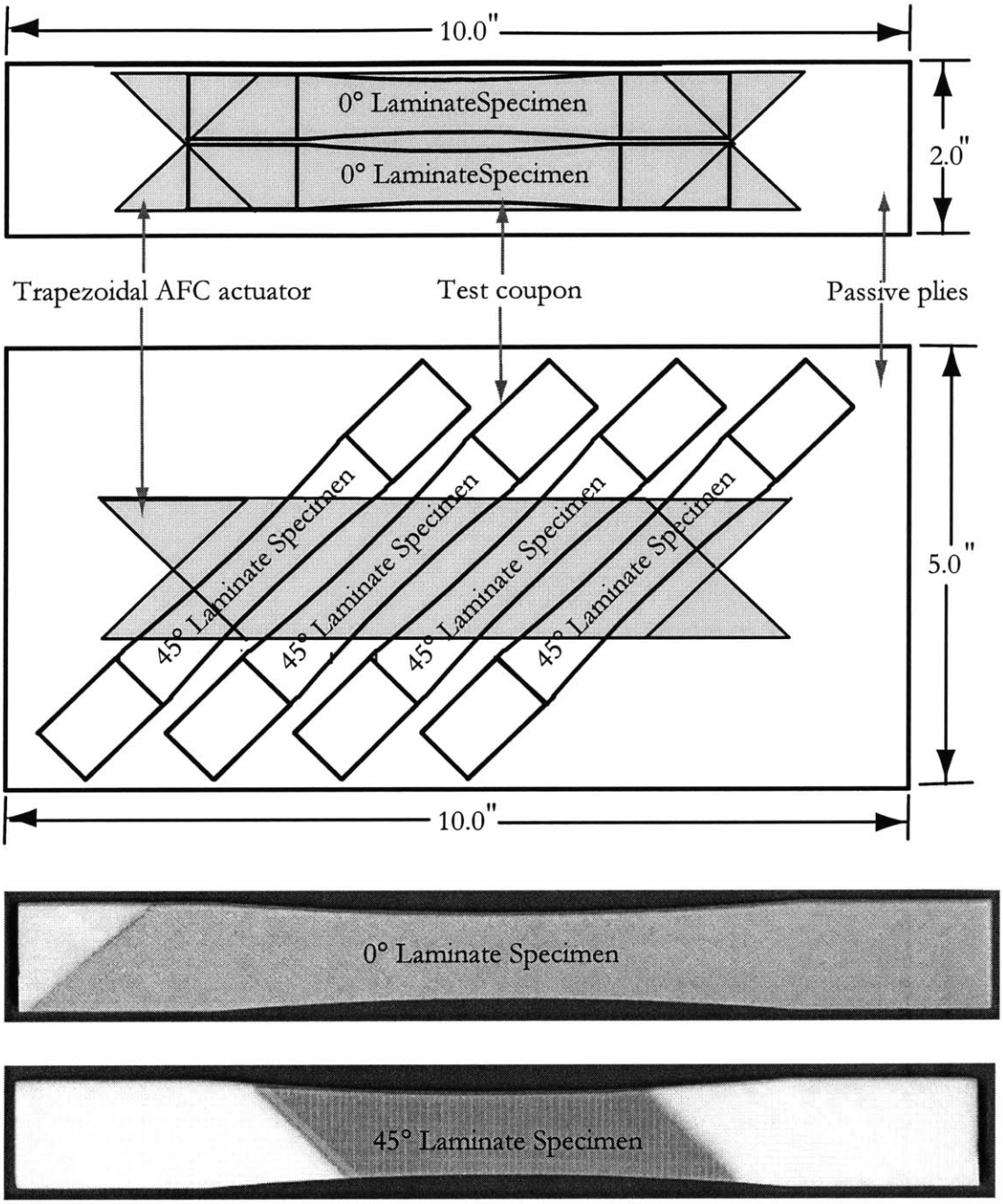

Figure 7-12: Process of extracting 0° and 45° representative laminate test coupons

Type of Test	Configuration	
	0°	45°
Static tension test	A	G
Mechanical fatigue test	B, C, D	E, F, H

Table 7.6: Test matrix for representative laminate tests

the applied load and the strain. The specimen test section width and the nominal thickness are used to convert the load data to stress at the test section. The mechanical fatigue tests are used to determine the fatigue strength of the laminate and also used to verify the laminate modulus determined by the static test. The mechanical fatigue test involves continuous application of a repetitive mechanical loading to the specimen up to 10 million cycles while measuring the modulus.

7.2.3 Test Setup and Test Procedure

The representative laminates specimens are tested at Boeing Helicopters. Therefore, the test setup and the test procedures are not discussed in this thesis.

7.2.4 Test Results for 0° Representative Laminate Tests

The Figure 7-13 shows the stress-strain results of the static tension tests compared with the predicted nominal modulus for the 0° representative laminate. The specimen A is loaded until failure and the specimens B, C, and D are loaded only up the maximum strain level expected during the mechanical fatigue test.

The predicted modulus for the 0° representative laminate is 25.6GPa and the modulus of all tested specimens closely matches the predicted value at strain levels less than $5000\mu\varepsilon$. The stress-strain data recorded from all four specimens lie on top of each other, indicating a high certainty in the experimental modulus results. The fiber breakages in the composite laminate at strains higher than $5000\mu\varepsilon$ resulted in a gradual reduction in modulus. During the loading of specimen A up to failure, one of the strain gages failed at $\sim 14000\mu\varepsilon$ and the other failed at $\sim 19000\mu\varepsilon$. It is estimated that the specimen A failed catastrophically at $\sim 30000\mu\varepsilon$ (3%) under a failure stress of 110ksi [Weems, 2000]. A picture of the specimen A after failure is shown as an insert in Figure 7-13.

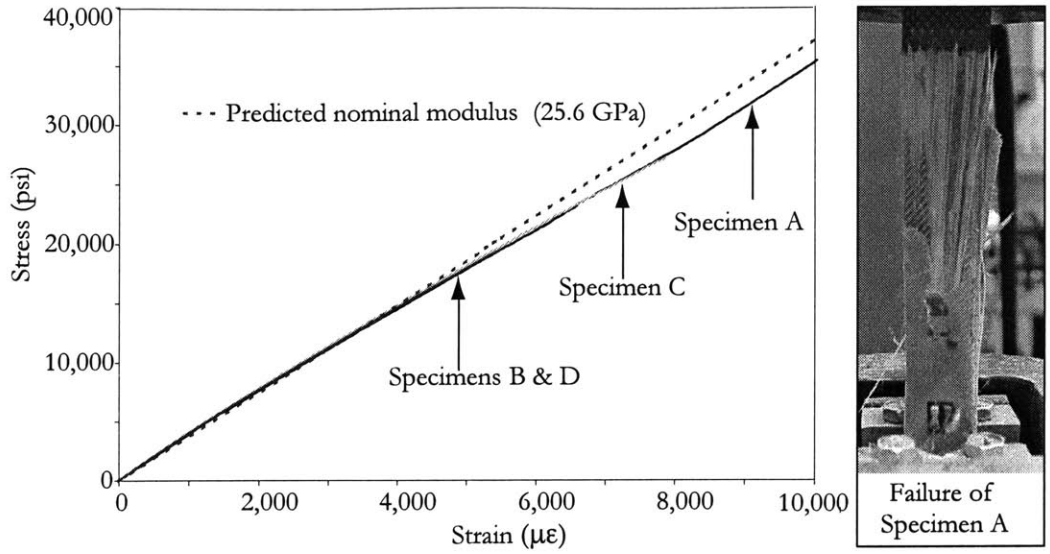

Figure 7-13: Static tensile test results of 0° representative laminate specimens

The mechanical fatigue tests on the 0° representative laminate specimens are conducted at $2000\mu\varepsilon \pm 1650\mu\varepsilon$, the highest fatigue strain level expected in the AMR blade axial direction during the forward flight condition. The Figure 7-14 shows the variation in the modulus observed in the specimens B, C, and D during the fatigue test. It is important to note that the strain data from the specimens B, C, and D are not recorded after 5.1 million cycles, 17,000 cycles, 141,000 cycles, respectively, due to the failure in both strain gages. However, the tests are continued up to 10 million mechanical cycles.

The 0° representative laminate modulus measured during fatigue tests are also closely matches the predicted modulus of 25.6GPa and the modulus of each specimen decreased slightly with the number of mechanical cycles. Approximately ~2.5% reduction in modulus is observed in specimen B at 5 million cycles and both the strain gages failed shortly after this point. All three specimens survived the 10 million cycle test and no evidence of damage is seen at the end of the test.

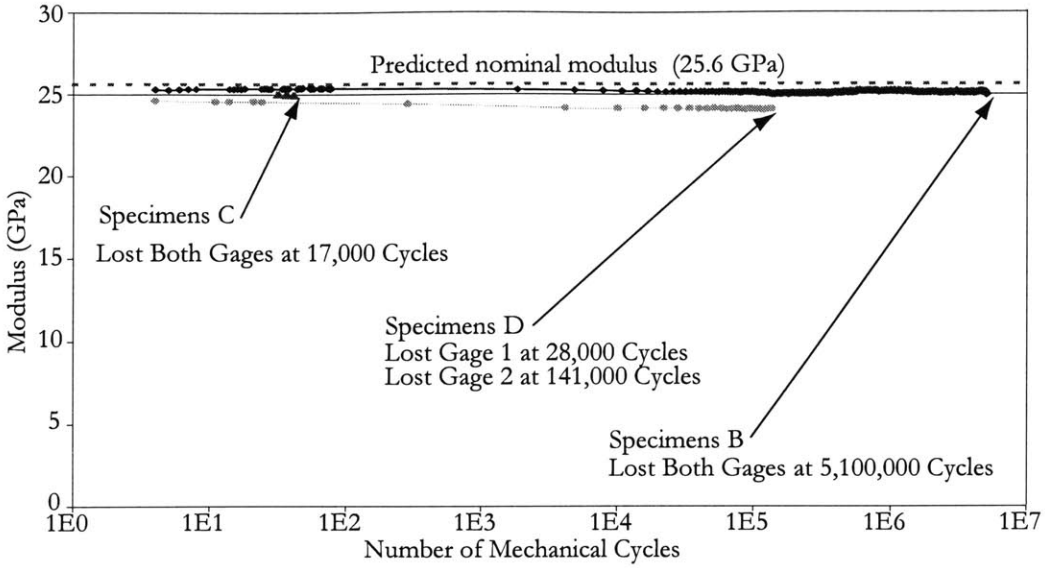

Figure 7-14: Mechanical fatigue test results of 0° representative laminate specimens

7.2.5 Test Results for 45° Representative Laminate Tests

The Figure 7-15 shows the stress-strain results of the static tension tests compared with the predicted nominal modulus for the 45° representative laminate. The specimen G is loaded until failure and the specimens E and F are loaded only up the maximum strain level expected during mechanical fatigue tests.

The predicted initial modulus for the 45° representative laminate is 18.9GPa. The static tension tests conducted using the specimens G, E, and F shows ~10% higher than the expected modulus at strain levels less than $2000\mu\varepsilon$. Furthermore, a highly nonlinear stress-strain behavior is observed during static tension tests. The stress-strain data recorded from all three specimens lie on top of each other, indicating a high certainty in the experimentally determined modulus. The specimen G, which is loaded up to failure, mechanically failed catastrophically at $5500\mu\varepsilon$ under a failure stress of 13ksi. As seen in the Figure 7-13, the failure occurred along an edge of the AFC actuator at 45°to the direction of loading.

Three mechanical fatigue tests are performed on 45° representative laminate specimens at various mechanical fatigue load levels. The Figure 7-14 shows the variation in the modulus observed on each specimen during the fatigue test.

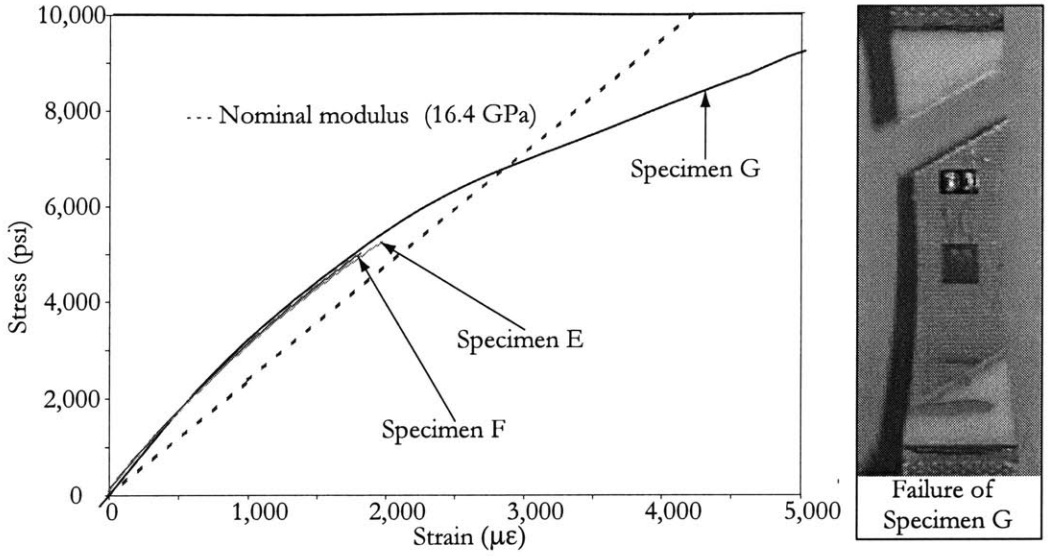

Figure 7-15: Static tenstion test results of 45° representative laminate specimens

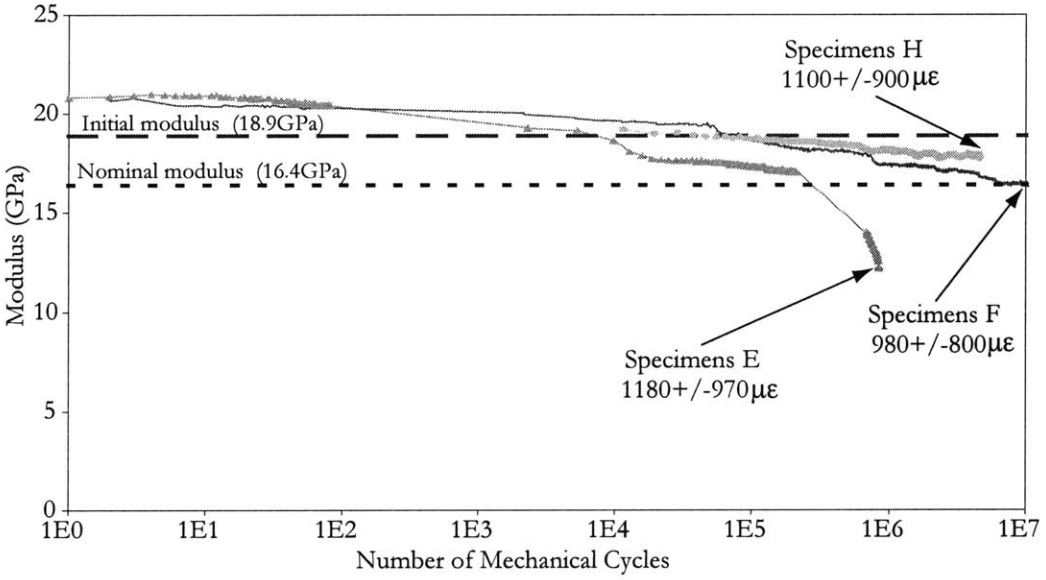

Figure 7-16: Mechanical fatigue test results of 45° representative laminate specimens

The measured modulus for all three specimens are ~21GPa. However, the experimentally determined value is ~10% higher than the predicted initial modulus of 18.9GPa. The specimen E, which is mechanically fatigued under a strain cycle of $1180\mu\varepsilon \pm 970\mu\varepsilon$ catastrophically failed after 0.85 million mechanical cycles. The specimen H, which is fatigued at a lower strain cycle of $1100\mu\varepsilon \pm 900\mu\varepsilon$ also failed after 4.5 million cycles. The specimen F, which is fatigue at $980\mu\varepsilon \pm 800\mu\varepsilon$ completed 10 million cycle test. All three specimens showed gradual deterioration in modulus during the fatigue test. The Figure 7-17 shows the failure mode observed on the 45° representative laminate specimens under mechanical fatigue.

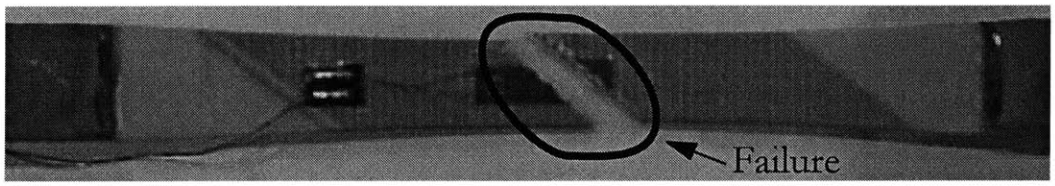

Figure 7-17: Mechanical fatigue failure mode observed on 45° representative laminate specimens

It is observed that the failure in both the specimens E and H occurred at the center of the test section at 45° to the direction of loading. This indicates a failure mode in the direction of the unidirectional S-Glass plies.

7.2.6 Results Discussion

The mechanical fatigue tests are performed on hybrid laminate specimens constructed to represent the composite structure of the AMR blade spar. The fatigue tests conducted on three 0° specimens at $2000\mu\varepsilon \pm 1650\mu\varepsilon$ cycle showed no significant reduction in the modulus up to 10 million cycles.

Three fatigue tests are conducted using the 45° representative laminate specimens resulted in two mechanical failures. The specimen tested at $1180\mu\varepsilon \pm 970\mu\varepsilon$ catastrophically failed after 0.85 million cycles and a similar failure is observed after 4.5 million cycles on the specimen tested at $1100\mu\varepsilon \pm 900\mu\varepsilon$. However, the specimen tested at $980\mu\varepsilon \pm 800\mu\varepsilon$ level completed the 10 million cycle test. A gradual deterioration in the specimen modulus is observed during all three fatigue tests.

A possible explanation for the failure in 45° representative laminate specimens is splitting of unidirectional S-Glass plies in the transverse direction due to the tensile load in the AFC fiber direction. A detailed CLPT analysis conducted at Boeing on the 45° laminate specimen under tension-tension fatigue confirmed that the failure is caused by exceeding the S-Glass allowable endurance strain limits in the transverse direction [Weems, 2000]. However, it is important note that the AFC fiber direction tensile loads on the blade results in compressive or zero load in S-Glass transverse direction. Therefore, the loading on the 45° representative laminate is not indicative of the AFC fiber direction loads in the AMR blade. Thus, mechanical failures observed on 45° representative laminate specimens do not indicate a weakness in the AMR blade spar.

7.3 Summary

The mechanical fatigue tests conducted to simulate the repeated mechanical loading on actuators during the blade operation showed high robustness in the actuator strength and reliability. None of the actuator coupons tested under the nominal fatigue load level of $1000\mu\varepsilon \pm 900\mu\varepsilon$ up to 10 million cycles showed any degradation in performance or reduction in modulus. An actuator coupon was able to retained the stiffness and performance at 50% higher fatigue load level.

The mechanical fatigue tests were also performed on hybrid laminate specimens constructed to represent the composite structure of the blade spar. Three tests conducted on 0° representative laminate specimens at $2000\mu\varepsilon \pm 1650\mu\varepsilon$ up to 10 million cycles showed no significant reduction modulus. The results verified the ability of the spar laminate to withstand the blade axial loads. The fatigue loading on the 45° representative laminate was not indicative of the AFC fiber direction loads in the AMR blade.

The mechanical fatigue tests verified the high robustness qualities of the AFC actuator material system under fatigue conditions. Such qualities are essential to successfully employ the AFC material system as structural actuators in the AMR blade application.

Chapter 8

Summary and Conclusions

The focus of this thesis is to develop a methodology to characterize the Active Fiber Composites (AFC) actuators employed in the Active Material Rotor (AMR) blade application. The AMR blade is a 1/6-scale, Mach-scale advanced CH-47D rotor with AFCs embedded in the spar laminate to generate integral twist actuation to perform vibration reduction. The AFCs are employed in the blade not only as structural actuators but also as structural components. Therefore, the material characterization involves the evaluation of physical, mechanical, electrical and coupled electromechanical properties important to the blade design and operation.

A modified version of the building block methodology used in the design and testing of traditional composite structures is followed in the AFC material characterization process. Simple actuator configurations are tested first and the complexity of the tests are increased to include more complete structure and realistic loading conditions expected in the blade operation. During the characterization process the data is analyzed, fed into the design, and modifications are made to the actuator material system and the blade design to obtain the required properties and behavior in the AMR blade.

8.1 Contributions

This thesis developed a standardized methodology to characterize the AFC actuator system in order to extract the material properties required for the AMR blade development. Only a few characterization efforts with limited scope has been conducted on AFCs previously.

The thesis identified the important material properties for the AMR blade design, analysis of blade performance, and the determination of operational limits. Numerous tests are designed to extract the important mechanical, electrical and coupled properties under simulated blade operating conditions. The following tests are performed in order to completely characterize the AFC actuator material system.

- The stress-strain tests are conducted to extract the elastic modulus and Poisson's ratios as a function of mechanical strain in both the longitudinal and transverse directions.
- The free strain performance tests enabled to understand the variation in the actuator performance due to voltage, frequency, and elastic constraint levels.
- The actuators are tested under tensile loads to determine the actuation degradation and recovery due to tensile loading conditions.
- The electrical fatigue tests are conducted to simulate the repeated actuation in order to evaluate the actuator durability and performance during long term operation.
- The mechanical fatigue tests are performed to simulate the repeated mechanical loading on the actuator in order to qualify the material system as a structural component and to evaluate the robustness of the actuator under high fatigue conditions.

A comprehensive testing methodology is developed for each test to extract the relevant material properties under simulated blade operating conditions. The design of each test included the philosophy for testing, test article design, test matrix, and a detailed step-by-step procedure to perform the test efficiently while minimizing experimental errors.

The complete set of tests conducted on the AFC material system enabled the characterization of the actuator for the AMR blade application. The testing process developed during in this thesis facilitates the characterization of similar actuator material systems for future applications.

8.2 Conclusions

The conclusions are derived from results of the material characterization tests conducted on the 0.01" diameter PZT-5A fiber AFC material system embedded in a dry film matrix. The details of the actuator material system is found in Chapter 2 and the actuators used for characterization tests were manufactured by Continuum Control Corporation[1].

Chapter 3 describes the stress-strain tests conducted to extract the multidirectional elastic modulus and Poisson's ratios. The AFC material system showed a highly nonlinear stress versus strain behavior in the longitudinal direction and the modulus deteriorated rapidly with mechanical strain. The measured modulus for $100\mu\varepsilon$ - $500\mu\varepsilon$ was 39.9GPa and the predicted modulus was 41.0GPa. A nominal longitudinal modulus of 16.9GPa, corresponding $100\mu\varepsilon$ - $3000\mu\varepsilon$, and a transverse modulus of 10.2GPa, corresponding $100\mu\varepsilon$ - $3000\mu\varepsilon$, were used in the blade design. A "knee" in the longitudinal stress-strain locus was observed at $\sim 2500\mu\varepsilon$ indicating an onset of catastrophic damage to the actuator.

Chapter 4 explains the tests performed to measure the actuator induced strain output due to electrical excitation. The average free strain performance of the AFC actuator system was $\sim 300\mu\varepsilon$, $\sim 700\mu\varepsilon$, $\sim 1200\mu\varepsilon$, $\sim 1700\mu\varepsilon$, respectively, for 1000Vpp, 2000Vpp, 3000Vpp and 4000Vpp with 0Vdc at 1Hz. The actuation reduction factors in the longitudinal direction due to 1 E120 and 2 E120 lamination were ~41% and ~57%, respectively. The actuation ratios determined for unlaminated, 1 E120, and 2 E120 laminated actuators were -0.47, -0.13 and -0.10, respectively. The optimum operating voltage cycle select for AMR blade application is 3000Vpp with 0Vdc offset. This voltage cycle provided an adequate actuation performance without repolarizing the AFC which occurs at -1600V.

Chapter 5 outlines the process of determining the AFC performance deterioration and the recovery under static tensile loads. The extend of the total accumulated damage, residual actuation and performance recovery depended on the maximum mechanical load undergone by the actuator. Approximately 90%, 60% and 40% of the original actuation is retained at the maximum load levels of $2000\mu\varepsilon$, $4000\mu\varepsilon$, and $6000\mu\varepsilon$, respectively. Actuators strained up to $2000\mu\varepsilon$, $4000\mu\varepsilon$, and $6000\mu\varepsilon$, respectively, recovered ~100%, ~90% and ~80% of the

[1]Continuum Control Corporation, Billerica, MA, Ph: 978-670-4910.

original performance after unloading. Only a little progressive damage was accumulated due to repeated mechanical loading up to the maximum strain level.

Chapter 6 discusses the electrical fatigue tests conducted to simulated the repeated actuation of AFCs during the blade operation. In free strain condition tests, the actuators are tested up to 20 million electrical cycles and the actuators showed no degradation in performance. The microscopic inspection showed evidence of damage in the form of fatigue burns. However, none of the burns were large enough to cause catastrophic failure. The electrical fatigue tests conducted under tensile load condition up to 10 million electrical cycles showed no significant degradation in performance or large enough fatigue burns to be visible through E-Glass.

Chapter 7 explains the mechanical fatigue tests conducted to simulate the repeated mechanical loading on actuators during the blade operation. Three tests were conducted using E-Glass laminated actuators up to 10 million cycles at the nominal load level of $1000\mu\varepsilon \pm 900\mu\varepsilon$ showed no significant deterioration in the modulus or actuation. An actuator coupon symmetrically laminated with two plies of [0/90] E-Glass retained the stiffness and performance at 50% higher fatigue load levels. The mechanical fatigue tests were also performed on hybrid laminate specimens constructed to represent the composite structure of the blade spar. Three tests conducted on 0° representative laminate specimens at $2000\mu\varepsilon \pm 1650\mu\varepsilon$ up to 10 million cycles showed no significant reduction modulus. The fatigue loading on the 45° representative laminate was not indicative of the AFC fiber direction loads in the AMR blade.

8.3 Recommendations for Future Work

Further work should be performed in order to streamline the material characterization procedures developed in this thesis. The testing methodology developed during this current effort is specifically for the AFC material system. Thus, modifications to testing techniques must be incorporated to generalize the test methodology in order to facilitate the characterization of other similar actuator material systems.

It is important to note that only a preliminary set of material properties for the 0.01" diameter PZT-5A fiber AFC actuator system is presented in this thesis. The number of samples tested under each test condition were limited due to time and cost constrains. Therefore, more

samples must be tested in order to obtain a statistical confidence in the AFC material properties.

The electrical fatigue tests discussed in Chapter 6 are conducted only up to 20 million cycles and microscopic damage in the form of fatigue burns were found on test article. It is recommended to run electrical fatigue tests up to higher cycle levels in order to understand the potential issues due to fatigue burns. The burns may continue to grow larger to cause catastrophic electrical failure in the actuators at higher cycle levels. Improvements to the AFC material system must be considered in future development to address the issue of fatigue burns.

The tests should be perform to extract the shear modulus of the AFC material system. A sensitivity analysis of the active ply mechanical properties on the AMR blade indicated the shear modulus as an important material property required in the blade development. However, the shear modulus was less important than the longitudinal or transverse modulus. Thus, the tests to extract the shear modulus were not conducted due time constraints and unavailability of required actuator configuration. The shear modulus can be extracted by conducting stress-strain tests on actuator specimens with piezoceramic fibers in 45° to the direction of loading [Jones, 1999].

It is also recommended to use smaller diameter piezoceramic fibers in the AFC material system in order to retain the actuator strength at higher mechanical load levels. A "knee" in the longitudinal stress-strain locus was observed, indicating the onset of catastrophic damage to the 0.01" diameter fiber AFC actuators at $\sim 2500\mu\varepsilon$ and $\sim 3500\mu\varepsilon$, for 90% and 75% fiber line fractions, respectively. However, the longitudinal stress-strain tests conducted on 0.005" diameter fiber AFC material system did not indicate such an onset of rapid damage. Therefore, it is beneficial to investigate the use of smaller diameter fibers in future AFC systems. Smaller fibers and higher matrix volume fractions leads to more efficient load transfer capability around fiber cracks in the composite. Furthermore, the use of harder piezoceramic material, such as PZT-4, should be investigated in order to improve the actuator strength. A drawback in PZT-4 is that the induced strain performance is $\sim$50% lower than the currently used PZT-5A. However, the higher stiffness properties in PZT-4 may enable to retain most of the induce stress capability of AFC actuators.

Bibliography

[Amer, 1974] Amer, K. B., Neff, J. R., "Vertical-Plane Pendulum Absorbers for Minimizing Helicopter Vibratory Loads," *Proceedings of Rotorcraft Dynamics Conference*, Moffett Field, CA, NASA Ames Research Center, February, 1974, pp. 219-222.

[Arcidiacono, 1961] Arcidiacono,P.J.,"Theoretical Performance of Helicopters Having Second and Higher Harmonic Feathering Control," *Journal of the American Helicopter Society*, Vol 6, April 1961.

[ASTM, D3039] "Standard Test Method for Tensile Properties of Polymer Matrix Composite Materials," Annual Book of ASTM Standards, Vol. 15.03, ASTM, Philadelphia, PA, pp. 98-108, 1997.

[ASTM, D3479] "Standard Test Method for Tensile-Tension Fatigue of Oriented Fiber Resin Matrix Composites," Annual Book of ASTM Standards, Vol. 15.03, ASTM, Philadelphia, PA, pp. 148-150, 1995.

[Bent, 1997] Bent, A. A., Hagood, N. W., "Active Fiber Composites for Structural Actuation," AMSL #97-1, Massachusetts Institute of Technology, January, 1997.

[Ben-Zeev, 1996] Ben-Zeev, O., Chopra, I., "Development of an Improved Helicopter Rotor Model with Smart Trailing-Edge Flaps for Vibration Suppression," *Journal of Smart Materials and Structures*, 5(1), February 1996.

[Berlincourt, 2000] Berlincourt, D., Krueger, H.H., Near, C., "Important Properties of Morgan Matroc Piezoelectric Ceramics," Technical Publication 226, Morgan Electro Ceramics, Bedford, Ohio, www.morganelectroceramics.com/techpub1.html, 2000.

[Bielawa, 1992] Bielawa, R. L., *Rotary Wing Structural Dynamics and Aeroelasticity*, AIAA Education Series, Ed. Przemieniecki, J.S., 1992.

[Braun, 1984] Braun, D., "Ground and Flight Tests of a Passive Rotor Isolation System for Helicopter Vibration Reduction," *Vertica*, Vol. 8, No. 1, 1984, pp. 1-14.

[Carpernter, 1950] Carpenter P. J., Paulnock S., "Hovering and Low-Speed Performance and Control Characteristics of an Aerodynamic-Servocontrolled Helicopter Rotor System as Determined on the Langley Helicopter Tower," Technical Report TN-2086, NACA, May 1950.

[Cesnik, 1999] Cesnik, C.E., Shin, S., Wilkie, W. K., Wilbur, M. L., Mirick, P. H., "Modeling, Design, and Testing of the NASA/Army/MIT Active Twist Rotor Prototype Blade," *Proceedings of the American Helicopter Society 55th Annual Forum*, Montreal, Canada, 25-27 May, 1999.

[Chen, 1994] Chen, P. C., Chopra, I., "Induced Strain Actuation of Composite Beams and Rotor Blades with Embedded Piezoceramic Elements," *SPIE Proceedings of the Smart Structures and Intelligent Systems Conference*, Vol. 2190, 1994, pp. 123-140.

[Chopra, 1981] Chopra, I., "Dynamic Analysis of Constant-Lift and Free-Tip Rotors," In AIAA Dynamic Specialists Conference, Atlanta, GA, April 1981.

[Derham, 1996] Derham, R.C., Hagood, N.W., "Rotor Design Using Smart Materials to Actively Twist Blades," *Proceedings of the 52nd Annual Forum of the American Helicopter Society*, 1996.

[Desjardins, 1978] Desjardins, R. A., Hooper, W. E., "Helicopter Rotor Vibration Isolation," *Vertica*, Vol. 2, 1978, pp. 145-159.

[Friedmann, 1998] Friedmann, P. P., "Rotary-Wing Aeroelastic Scaling and Its Applications to Adaptive Materials Based Actuation", *Proceedings of the 39th AIAA/ASME/ASCE/AHS/ASC Structures, Structural Dynamics and Materials Conference*, April 20-23, 1998. Long Beach, CA.

[Fulton, 1998] Fulton, M. V., and Ormiston, R. A., "Small-Scale Rotor Experiments with On-Blade Elevons to Reduce Blade Vibratory Loads in Forward Fight," *Proceedings of the American Helicopter Society 54th Annual Forum*, Washington, DC, 1998.

[Garcia, 1994] Garcia, J. C., and Hall, S. R., "Active Helicopter Rotor Control Using Blade-Mounted Actuators" Masters Thesis, Massachusetts Institute of Technology, Department of Mechanical Engineering, February 1994.

[Ghandi, 1998] Ghandi, K., Hagood, N. W., "Non-Linear Modeling and Characterization Techniques for Phase Transitions in Electromechanically Coupled Devices" AMSL #98-1, Massachusetts Institute of Technology, May, 1998.

[Hall, 1996] Hall, S. R., Prechtl, E. F., "Development of a Piezoelectric Servoflap for Helicopter Rotor Control," Journal of Smart Materials and Structures, February 1996.

[Ham, 1987] Ham, N. D., "Helicopter individual-blade-control research at MIT 1977-1985," *Vertica*, Vol. 11, No. 1/2, 1987, pp. 109-122.

[Jacklin, 1994] Jacklin, S. A., Nguyen, K. Q., Blass, A., and Richter, P., "Full-Scale Wind Tunnel Test of a Helicopter Individual Blade Control System," *Proceedings of the 50th Annual Forum of the American Helicopter Society*, Washington, DC, May 11-13, 1994.

[Jaffe, 1971] Jaffe, B., Cook, W. R., Jaffe, H., *Piezoelectric Ceramics*, Academic Press, 1971.

[Janos, 2000] Janos, B. Z., Hagood, N. W., "Smart Materials and Structures: Technological Feasibility and Policy Assessment" Masters thesis in Technology and Policy, AMSL #00-4, Massachusetts Institute of Technology, June 2000.

[Johnson, 1980] Johnson, W., *Helicopter Theory*, Dover Publications, Inc., New York, 1980.

[Jones, 1999] Jones, R. M, *Mechanics of Composite Materials*, Taylor & Francis, 1999.

[Kretz, 1976] Kretz, M., "Research in Multicyclic and Active Control of Rotary Wings," *Vertica*, 1:95-105, 1976.

[Kube, 1989] Kube, R., "New Aspects of Higher Harmonic Control at a Four Bladed Hingeless Model Rotor," *Proceedings of the 15th European Rotorcraft Forum*, Amsterdam, September 12-15, 1989.

[Landgrebe, 1984] Landgrebe, A. J., and Davis, M. W., "Analysis of potential helicopter vibration reduction concepts," *Proceedings of the AHS Decennial Specialists' Meeting on Rotorcraft Dynamics*, 1984.

[Lemnios, 1972] Lemnios, A. Z., Smith, A., F., Nettles, W., E., "The Controllerble Twist Rotor Performance and Blade Dynamics," *Proceedings of the 28th Annual Forum of the American Helicopter Society*, 1972.

[Lemnios, 1976] Lemnios, A. Z., Nettles, W. E., and Howes, H. E., "Full Scale Wind Tunnel Tests of a Controllable Twist Rotor," *Proceedings of the 32th Annual Forum of the American Helicopter Society*, 1976.

[McCloud, 1978] McCloud, J. L., and Weisbrich A. L., "Wind-Tunnel Results of a Full-Scale Multi-Cyclic Controllable Twist Rotor," *Proceedings of the 34th Annual Forum of the American Helicopter Society*, 1978.

[Miller, 1964] Miller R., "Unsteady Air Loads on Helicopter Blades," The Fourth Cierva Memorial Lecture, *Journal of Royal Aeronautical Society*, April 1964.

[Millot, 1992] Millot, T., and Friedman P., "Vibration Reduction in Helicopter Rotors Using Active Control Surface Located on the Blade" AIAA Paper 62-2451-CP, *Proceedings of the 33rd AIAA/ASME/ASCE/AHS/ASC Structures, Structural Dynamics and Materials Conference*, April 13-15, Dlassa, TX.

[Nguyen, 1992] Nguyen, K. and Chopra, I., "Effect of Higher Harmonic Control on Rotor Performance and Control Loads," *Journal of Aircraft*, 29(3), 1992.

[Payne, 1958] Payne, P. R., "Higher Harmonic Rotor Control," Aircraft Engineering, Vol. 30, August, 1958.

[Pizzochero, 2000] Pizzochero, A., Continuum Control Corporation, Billerica, MA, personal correspondence, 2000.

[Pizzochero, 1997] Pizzochero, A., Hagood, N. W., "Residual Actuation and Stiffness Properties of Piezoelectric Composites: Theory and Experiment" Masters Thesis, Massachusetts Institute of Technology, February 1997.

[Prechtl, 2000] Prechtl, E. F., Hall, S. R., "Design and Implementation of a Piezoelectric Servo-Flap Actuation System for Helicopter Rotor Individual Blade Control," AMSL #00-3, Massachusetts Institute of Technology, January, 2000.

[Prechtl, 2000b] Prechtl, E.F., Hall, S.R., "Closed-Loop Vibration Control Experiments on a Rotor with Blade Mounted Actuation," AIAA-1714. *Proceedings of the 41st AIAA/ASME/ASCE/AHS/ASC Structures, Structural Dynamics and Materials Conference*, April 3-6, 2000. Atlanta, GA.

[Rodgers, 1998] Rodgers, J. P., Hagood, N.W., "Development of an Integral Twist Actuated Rotor Blade for Individual Blade Control," PhD Thesis, AMSL #98-6, Massachusetts Institute of Technology, October 1998.

[Rodgers, 1996] Rodgers, J. P., Bent, A. A., Hagood, N. W., "Characterization of Interdigitated Electrode Piezoelectric Fiber Composites Under High Electrical and Mechanical Loading" *Smart Structures and Materials*, San Diego, CA, February 1996.

[Schmidt, 2000a] Schmidt, M. C., Hagood, N. W., "Design and Manufacturing of a Second Generation Integral Twist-Actuated Rotor Blade," *Proceedings of the AIAA-2000-1710, 41st AIAA/ASME/ASCE/AHS/ASC Structures, Structural Dynamics and Materials Conference*, April 3-6, 2000. Atlanta, GA.

[Schmidt, 2000b] Schmidt, M.C., Hagood, N.W., "Development of Integral Actuation Technology for Composite Rotorcraft Structures," Masters Thesis, AMSL #00-6, Massachusetts Institute of Technology, December 2000.

[Shaw, 1985] Shaw, J., Albion, N., Hanker, E. J., and Teal, R. S., "Higher Harmonic Control: Wind Tunnel Demonstration of Fully Effective Vibratory Hub Force Suppression," *Proceedings of the 41st Annual Forum of the American Helicopter Society*, Fort Worth, TX, 1985.

[Shin, 1999] Shin, S. J., Cesnik, C. E. S., "Design, Manufacturing and Testing of an Active Twist Rotor," Masters Thesis, AMSL #99-3, Massachusetts Institute of Technology, June 1999.

[Shin, 2000] Shin S. J., Cesnik, C. E. S., Wilbur, M. L., "Dynamic Response of Active Twist Rotor Blades," *AIAA/ASME/ASCE/AHS/ASC 41st Structures, Structural Dynamics and Materials Conference*, 2000, AIAA Paper No. 2000-1711.

[Shin, 2000b] Shin S. J., Active Materials and Structures Laboratory, Massachusetts Institute of Technology, Cambridge, MA, personal correspondence, 2000.

[Spangler, 1990] Spangler, R. L. and Hall, S. R., "Piezoelectric Actuators for Helicopter Rotor Control," *Proceedings of the 31st Structures, Structural Dynamics and Materials Conference*, Long Beach, CA, April 1990.

[Straub, 1993] Straub F. K., "A Feasibility Study of Using Smart Materials for Rotor Control," *Proceedings of the 49th Annual Forum of the American Helicopter Society*, St. Louis, MO, May 1993.

[Straub, 1996] Straub, F.K., Merkley, D.J., "Design of a Servo-Flap Rotor for Reduced Control Loads," *Smart Materials and Structures*, Vol. 5, No. 1, 1996, pp. 68-75.

[Straub, 2000] Straub, F. K., Kennedy, D. K., Domzalski, D. B., Hassan, A. A., Ngo, H., Anand, V., Birchette, T., "Smart Material Actuated Rotor Technology - SMART." AIAA-2000-1715. *Proceedings of the 41st AIAA/ASME/ASCE/AHS/ASC Structures, Structural Dynamics and Materials Conference*, April 3-6, 2000. Atlanta, GA.

[Strehlow, 1993] Strehlow, H. and Rapp, H., "Smart Materials for Helicopter Rotor Active Control," AGARD, *Smart Structures for Aircraft and Spacecraft*, 16, April 1993.

[Strock, 1999] Strock, H . B., Pascucci, M. R., Parish, M. V., Bent, A. A., Shrout, T. R., "Active PZT Fibers, A Commercial Production Process," *Proceedings of the SPIE*

[Walz, 1994] Walz, C., Chopra, I., "Design and Testing of a Helicopter Rotor Model with Smart Trailing Edge Flaps," *Proceedings of the 35th Structures, Structural Dynamics and Materials Conference, Adaptive Structures Forum*, 1994. AIAA Paper No. 94-1767.

[Weems, 2000] Weems, D., Boeing Helicopters, Philadelphia, PA, personal correspondence, 2000.

[Wilbur, 2000] Wilbur, M. L., Yeager, W. T., Jr., Wilkie, W. K., Cesnik, C. E. S., Shin, S. J., "Hover Testing of NASA/Army/MIT Active Twist Rotor Prototype Blade," *Proceedings of the American Helicopter Society 56th Annual Forum*, Virginia Beach, VA, 2-4 May, 2000.

[Wickramasinghe, 2000] Wickramasinghe, V., Hagood, N.W., "Material Characterization of Active Fiber Composite Actuators for Active Twist Helicopter Rotor Blade Applications", *Proceedings of the AIAA-2000-1499, 41st AIAA/ASME/ASCE/AHS/ASC Structures, Structural Dynamics and Materials Conference*, April 3-6, 2000. Atlanta, GA.

Appendix A

E-Glass Stress-Strain Tests

The stress-strain tests are conducted on pure E-Glass in order to accomplish multiple objectives. The primary objective is to familiarize with the stress-strain testing procedure that would be used to conducted similar testing on the AFC material system. An adequate familiarization in the procedure is necessary due to the limited number of AFC test articles available for testing.

Furthermore, many AFC characterization tests are conducted on actuators laminated with E-Glass because the AFCs are designed to be used in hybrid laminates. The AFC properties are extracted from E-Glass laminated actuators by removing the contribution of E-Glass analytically. Therefore an accurate knowledge of the E-Glass stress-strain behavior in both the longitudinal and transverse directions are essentials at corresponding mechanical strain levels.

The stress-strain tests are conducted based on the ASTM testing standard for tensile properties of polymer matrix composite materials [ASTM, D3039]. This standard provides guidelines for test article design, test procedure, apparatus, and calculations. These guidelines are incorporated into the stress-strain tests and they are discussed in detail in Chapter 3.

A.1 Test Articles

The E-Glass modulus tests are conducted on laminates constructed with Hexcel E120-155 style prepreg cloth[1]. The nominal thickness of a single E-Glass ply is 0.0045". The test specimens are made with dimensions similar to AFC longitudinal modulus specimens as shown in Figure A-

[1]Hexcel E120-155 prepreg cloth, Pleasanton, CA, Ph: 925-847-9500.

1. The specimen are made by laminating 2 or 4 plies of E-Glass together using the lamination process is discussed Section 2.5.1. The bidirectional strain gages are used to acquire the longitudinal and transverse strain data from both sides of the specimen. The details of the bidirectional strain gage and the gage application procedure is described in Section 2.5.3. The tests are conducted on symmetric E-Glass lay-ups oriented at [0°/90°] and [-45°/45°] direction to the loading. The nominal thicknesses for specimens constructed with 2 and 4 plies of E-Glass are 0.009" and 0.018", respectively.

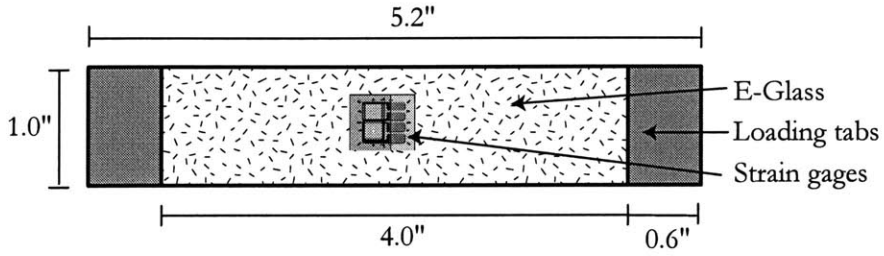

Figure A-1: E-Glass stress-strain test specimen dimensions

A.2 Test Matrix

Three specimens are tested under each configuration. The complete test matrix is shown in Table A.1

Specimen ID	Lay-up	# of Plies
E1,E2,E3	$[0°/90°]_S$	2
E4,E5,E6	$[0°/90°]_{2S}$	4
E11,E12,E13	$[-45°/45°]_S$	2
E14,E15,E16	$[-45°/45°]_{2S}$	4

Table A.1: Test matrix for E-Glass tensile tests

A.3 Test Setup and Test Procedure

The stress-strain test setup is discussed in Section 3.1.3 and the step-by-step testing procedure is explained in Section 3.1.4.

A.4 Test Results for [0°/90°] E-Glass Laminates

Figure A-2 shows a typical stress versus strain behavior for $[0/90]_S$ and $[0/90]_{2S}$ E-Glass test specimens. As seen, the stress-strain behavior of pure [0/90] E-Glass is relatively linear.

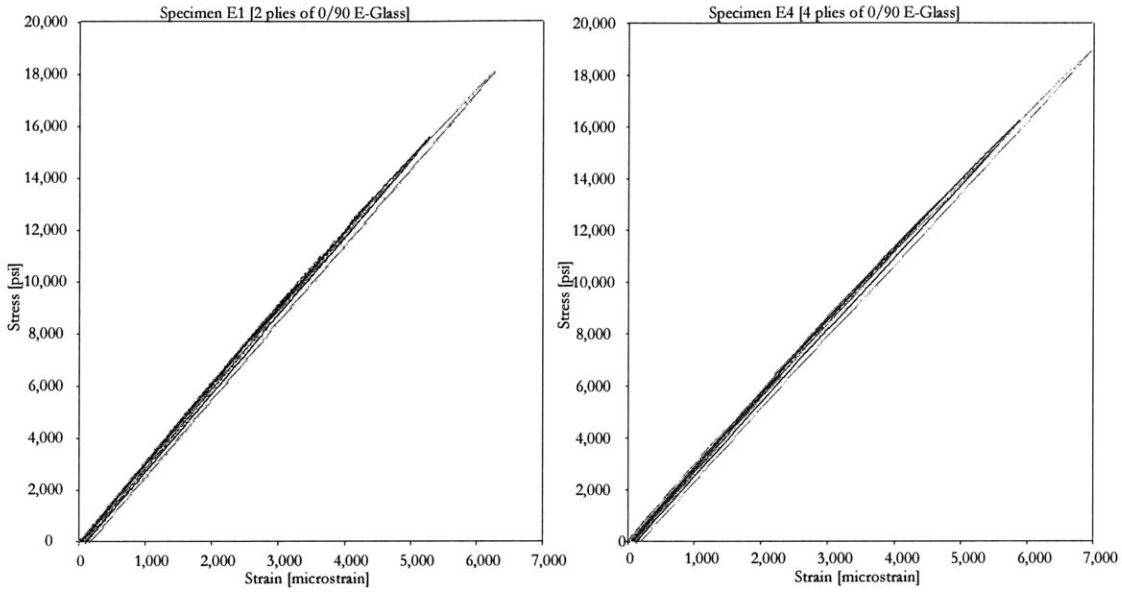

Figure A-2: Stress-strain plots of $[0°/90°]_S$ and $[0°/90°]_{2S}$ E-Glass specimens

The chord modulus and Poisson's ratios calculated from [0/90] E-Glass stress-strain tests are shown in Table A.2. The chord modulus is defined in Section 3.1.5.

A.5 Results for [-45°/45°] E-Glass Laminates

Similar stress-strain tests are conducted on [-45/45] E-Glass specimens. Figure A-3 shows a typical stress versus strain behavior for $[-45/45]_S$ and $[-45/45]_{2S}$ E-Glass test specimens. As expected, the stress-strain behavior of [-45/45] E-Glass is more non-linear and hysteretic than [0/90] E-Glass specimens.

The chord modulus and Poisson's ratios calculated from [-45/45] E-Glass stress-strain tests are shown in Table A.3. The chord modulus is defined in Section 3.1.5.

	$[0/90]_S$ Specimen Data				$[0/90]_{2S}$ Specimen Data			
Specimen ID	**E1**	**E2**	**E3**	**Avg**	**E4**	**E5**	**E6**	**Avg**
Gage length (in)	3.96	3.99	3.98	**3.97**	4.04	4.01	3.98	**4.01**
Specimen width (in)	1.03	1.03	1.00	**1.02**	0.98	0.99	0.99	**0.99**
Actual thickness (mils)	8.01	7.95	8.03	**7.99**	15.3	15.3	15.2	**15.3**
Nominal thickness (mils)	9.0	9.0	9.0	**9.0**	18.0	18.0	18.0	**18.0**
Strain Ranges	$[0/90]_S$ **Modulus (GPa)**				$[0/90]_{2S}$ **Modulus (GPa)**			
100$\mu\varepsilon$ - 500$\mu\varepsilon$	22.1	20.3	23.2	**21.9**	21.1	21.1	19.7	**20.6**
100$\mu\varepsilon$ - 1000$\mu\varepsilon$	21.5	20.4	21.7	**21.0**	20.4	20.6	19.0	**20.5**
100$\mu\varepsilon$ - 2000$\mu\varepsilon$	21.4	20.6	21.6	**21.0**	20.1	20.1	18.8	**20.1**
100$\mu\varepsilon$ - 3000$\mu\varepsilon$	20.9	20.5	21.2	**20.7**	19.9	19.9	18.7	**19.9**
100$\mu\varepsilon$ - 4000$\mu\varepsilon$	20.7	20.2	20.9	**20.5**	19.5	19.5	18.4	**19.5**
100$\mu\varepsilon$ - 5000$\mu\varepsilon$	20.5	20.0	20.7	**20.3**	19.3	19.1	18.1	**19.2**
100$\mu\varepsilon$ - 6000$\mu\varepsilon$	20.1	19.8	20.2	**19.9**	18.9	18.8	17.8	**18.9**
Strain Ranges	$[0/90]_S$ **Poisson's Ratio**				$[0/90]_{2S}$ **Poisson's Ratio**			
100$\mu\varepsilon$ - 500$\mu\varepsilon$	0.106	0.132	0.069	**0.102**	0.099	0.136	0.113	**0.116**
100$\mu\varepsilon$ - 1000$\mu\varepsilon$	0.099	0.117	0.096	**0.104**	0.130	0.132	0.108	**0.123**
100$\mu\varepsilon$ - 2000$\mu\varepsilon$	0.110	0.112	0.101	**0.107**	0.118	0.122	0.105	**0.115**
100$\mu\varepsilon$ - 3000$\mu\varepsilon$	0.105	0.113	0.101	**0.106**	0.116	0.116	0.103	**0.111**
100$\mu\varepsilon$ - 4000$\mu\varepsilon$	0.105	0.111	0.103	**0.106**	0.109	0.115	0.098	**0.108**
100$\mu\varepsilon$ - 5000$\mu\varepsilon$	0.100	0.109	0.101	**0.104**	0.106	0.111	0.094	**0.104**
100$\mu\varepsilon$ - 6000$\mu\varepsilon$	0.099	0.107	0.097	**0.101**	0.103	0.109	0.092	**0.101**

Table A.2: Chord modulus and Poisson's ratios for [0/90] E-Glass

A.6 Summary

The experimental modulus data for pure E-Glass closely matches the theoretical modulus. The nominal E-Glass modulus quoted by the manufacturer is 21.7GPa for [0/90] fabric. The average modulus determined experimentally for the 100$\mu\varepsilon$ - 500$\mu\varepsilon$ strain range are 21.9GPa and 20.6GPa using $[0/90]_S$ and $[0/90]_{2S}$ specimens, respectively. Similarly, the nominal E-Glass modulus for [-45/45] configuration is 11.4GPa. The average modulus determined experimentally for the 100$\mu\varepsilon$ - 500$\mu\varepsilon$ strain range are 11.8GPa and 11.2GPa using $[-45/45]_S$ and $[-45/45]_{2S}$ specimens, respectively.

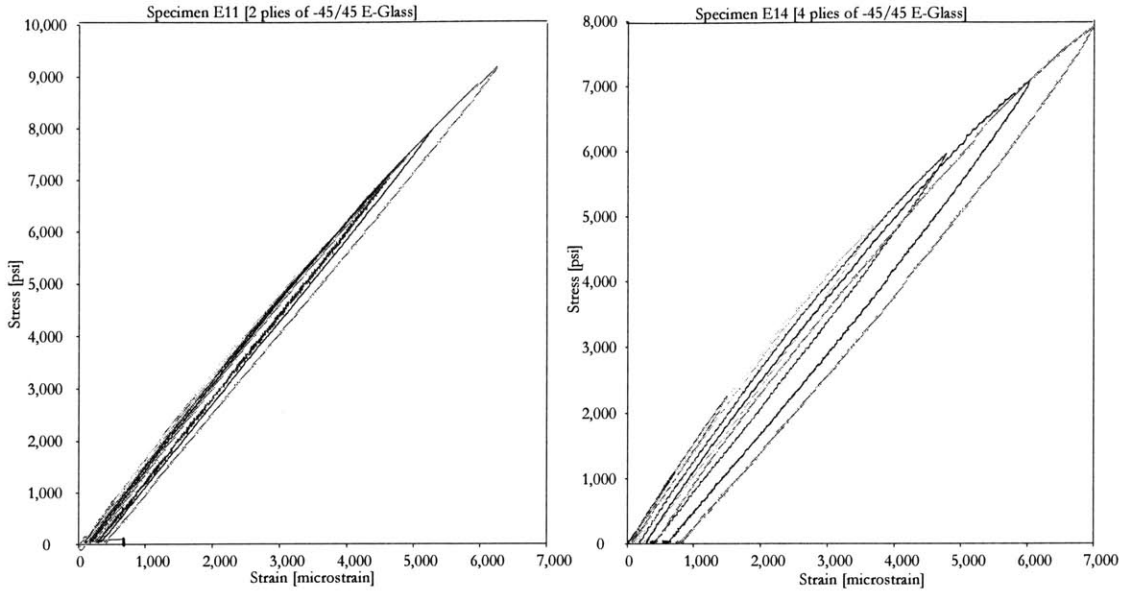

Figure A-3: Stress-strain plots of $[-45°/45°]_S$ and $[-45°/45°]_{2S}$ E-Glass specimens

	$[-45/45]_S$ Specimen Data				$[-45/45]_{2S}$ Specimen Data			
Specimen ID	**E11**	**E12**	**E13**	**Avg**	**E14**	**E15**	**E16**	**Avg**
Gage length (in)	4.00	4.01	4.00	**4.00**	3.98	3.99	3.98	**3.99**
Specimen width (in)	0.99	0.97	0.98	**0.98**	0.98	0.96	0.99	**0.98**
Actual thickness (mils)	7.90	8.18	8.07	**8.05**	15.5	14.8	15.1	**15.1**
Nominal thickness (mils)	9.0	9.0	9.0	**9.0**	18.0	18.0	18.0	**18.0**
Strain Ranges	$[-45/45]_S$ **Modulus (GPa)**				$[-45/45]_{2S}$ **Modulus (GPa)**			
100$\mu\varepsilon$ - 500$\mu\varepsilon$	12.1	11.6	11.9	**11.8**	10.9	11.4	11.3	**11.2**
100$\mu\varepsilon$ - 1000$\mu\varepsilon$	11.6	11.7	12.0	**11.6**	10.4	11.0	11.0	**10.7**
100$\mu\varepsilon$ - 2000$\mu\varepsilon$	11.5	10.8	11.1	**11.2**	10.0	10.0	10.4	**10.0**
100$\mu\varepsilon$ - 3000$\mu\varepsilon$	11.2	10.4	10.7	**10.8**	9.4	9.7	9.8	**9.5**
100$\mu\varepsilon$ - 4000$\mu\varepsilon$	10.8	10.2	10.2	**10.5**	8.9	9.0	9.3	**8.9**
100$\mu\varepsilon$ - 5000$\mu\varepsilon$	10.6	9.7	9.7	**10.1**	8.4	8.5	8.8	**8.4**
100$\mu\varepsilon$ - 6000$\mu\varepsilon$	10.2	9.3	9.3	**9.7**	8.1	7.6	8.3	**7.8**
Strain Ranges	$[-45/45]_S$ **Poisson's Ratio**				$[-45/45]_{2S}$ **Poisson's Ratio**			
100$\mu\varepsilon$ - 500$\mu\varepsilon$	0.397	0.463	0.440	**0.433**	0.449	0.470	0.434	**0.451**
100$\mu\varepsilon$ - 1000$\mu\varepsilon$	0.415	0.499	0.465	**0.460**	0.434	0.470	0.451	**0.451**
100$\mu\varepsilon$ - 2000$\mu\varepsilon$	0.436	0.517	0.485	**0.479**	0.449	0.487	0.474	**0.470**
100$\mu\varepsilon$ - 3000$\mu\varepsilon$	0.447	0.526	0.503	**0.492**	0.476	0.519	0.495	**0.497**
100$\mu\varepsilon$ - 4000$\mu\varepsilon$	0.455	0.533	0.517	**0.501**	0.495	0.520	0.512	**0.509**
100$\mu\varepsilon$ - 5000$\mu\varepsilon$	0.465	0.538	0.533	**0.512**	0.510	0.530	0.528	**0.523**
100$\mu\varepsilon$ - 6000$\mu\varepsilon$	0.474	0.545	0.543	**0.521**	0.519	0.542	0.539	**0.534**

Table A.3: Chord modulus and Poisson's ratios for [-45/45] E-Glass

Appendix B

Additional Stress-Strain Plots

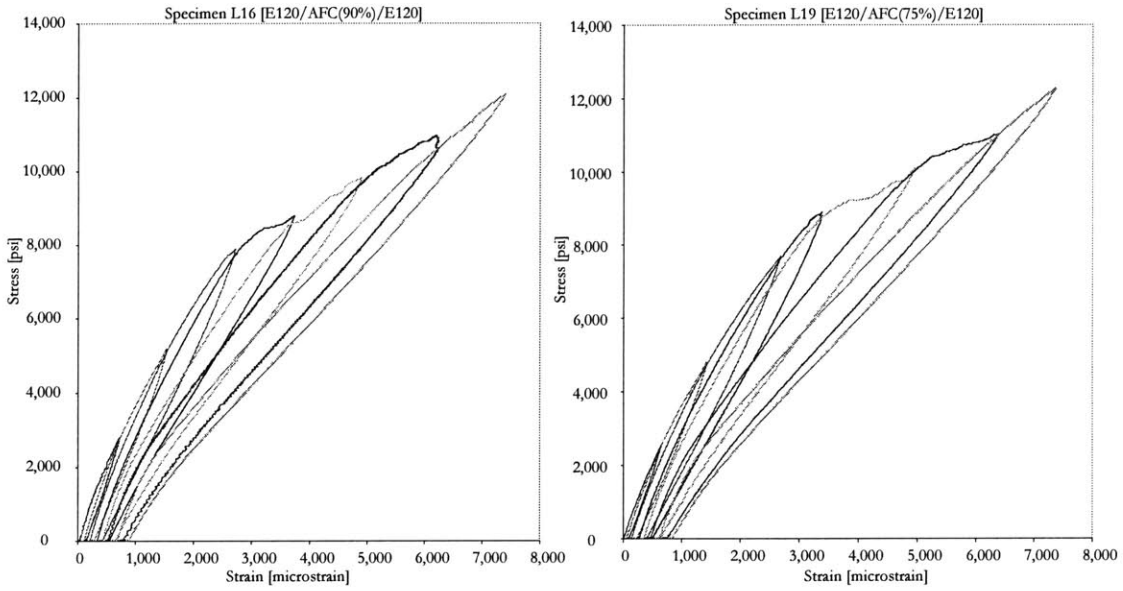

Figure B-1: Longitudinal stress-strain behavior of 0.01" diameter fiber AFCs symmetrically laminated with one ply of [0/90] E-Glass on either side (90% and 75% fiber line fractions)

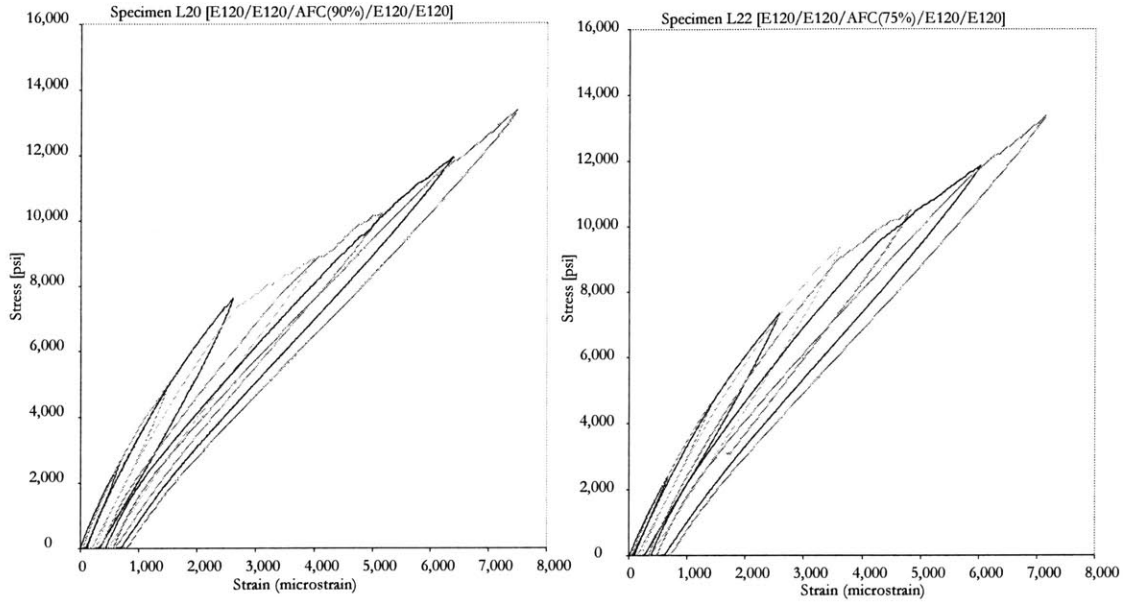

Figure B-2: Longitudinal stress-strain behavior of 0.01" diameter fiber AFCs symmetrically laminated with two plies of [0/90] E-Glass on either side (90% and 75% fiber line fractions)

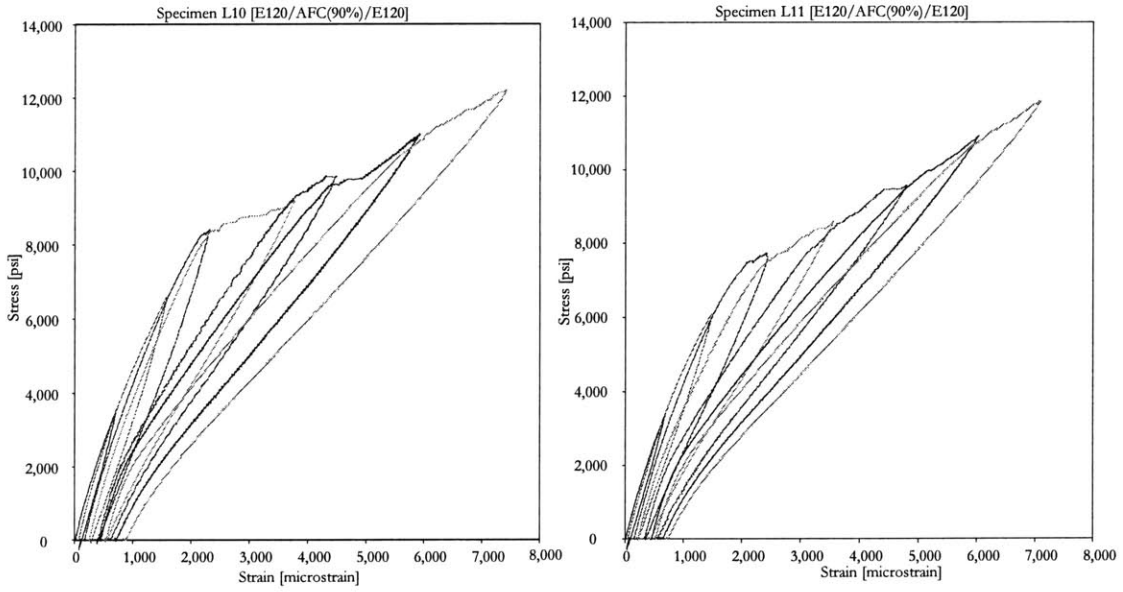

Figure B-3: Longitudinal stress-strain behavior of 0.01" diameter fiber AFCs symmetrically laminated with one ply of [0/90] E-Glass on either side (90% fiber line fraction)

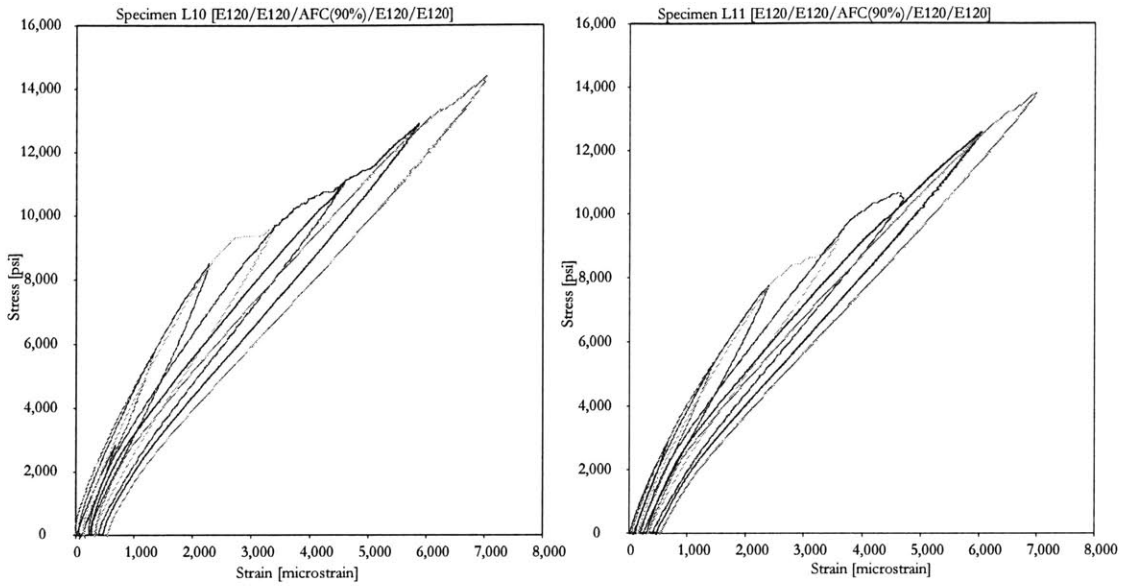

Figure B-4: Longitudinal stress-strain behavior of 0.01" diameter fiber AFCs symmetrically laminated with two plies of [0/90] E-Glass on either side (90% fiber line fraction)

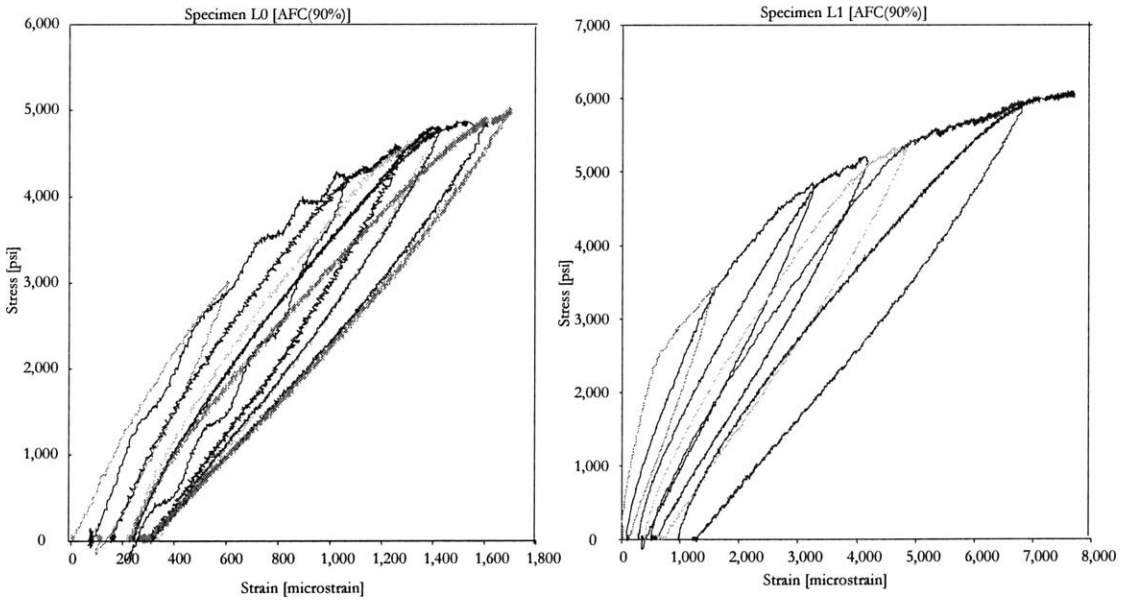

Figure B-5: Longitudinal stress-strain behavior of 0.01" diameter fiber unlaminated AFCs (90% fiber line fraction)

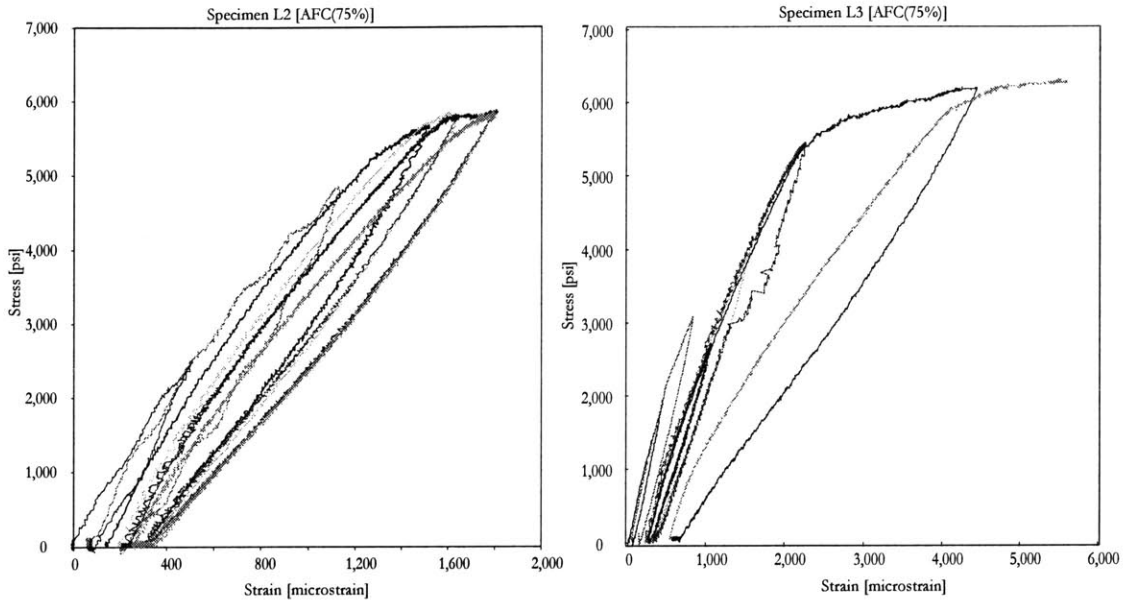

Figure B-6: Longitudinal stress-strain behavior of 0.01" diameter fiber unlaminated AFCs (75% fiber line fraction)

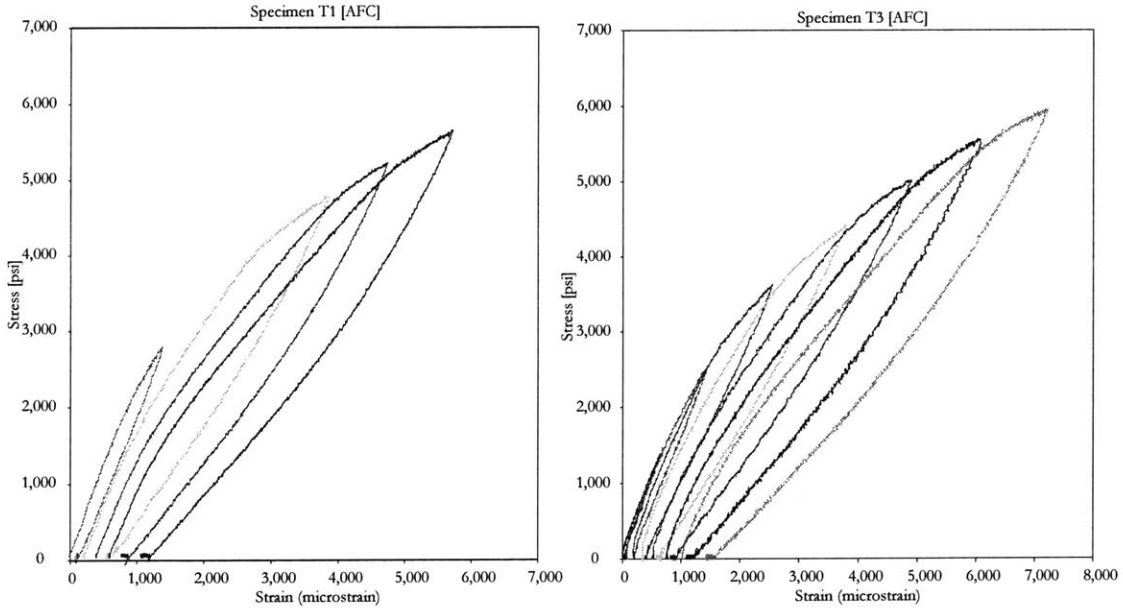

Figure B-7: Transverse stress-strain behavior of 0.01" diameter fiber unlaminated AFCs (90% fiber line fraction)

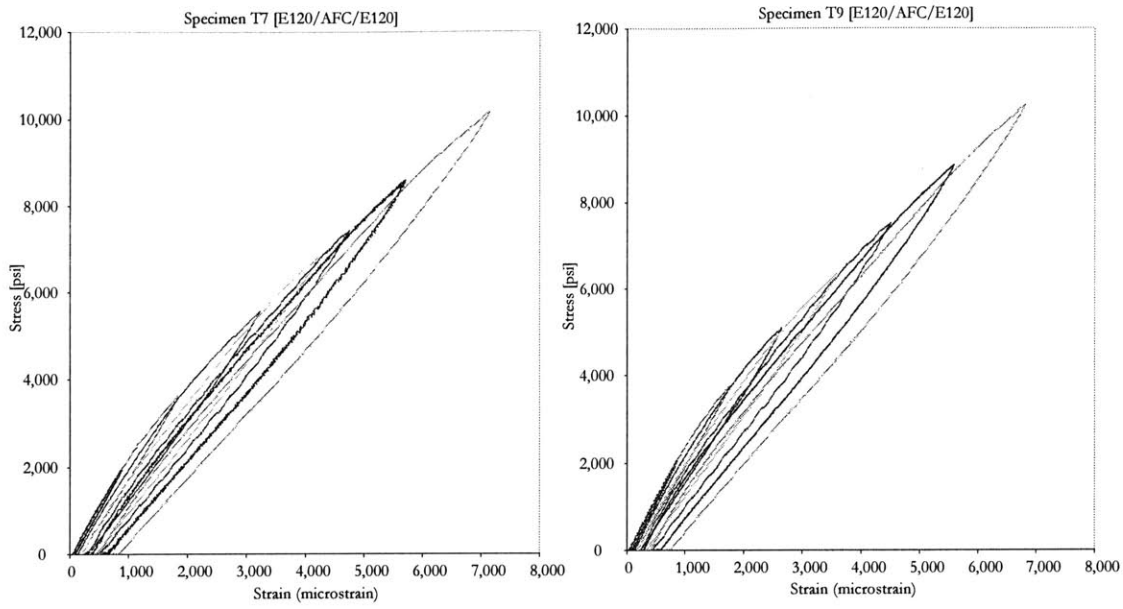

Figure B-8: Transverse stress-strain behavior of 0.01" diameter fiber AFCs symmetrically laminated with one ply of [0/90] E-Glass (90% fiber line fraction)

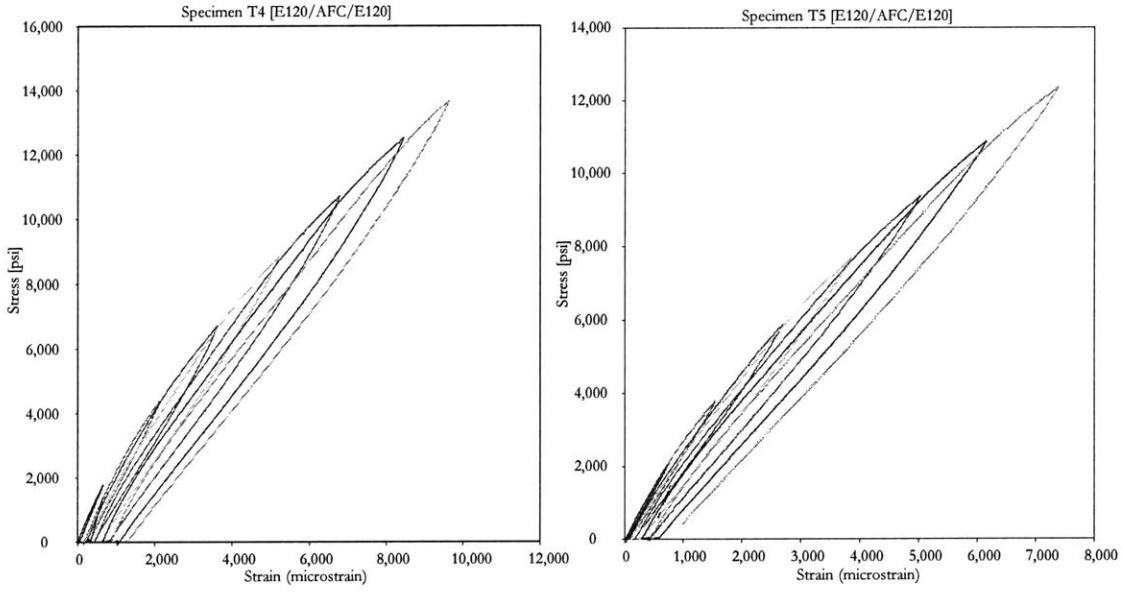

Figure B-9: Transverse stress-strain behavior of 0.01" diameter fiber AFCs symmetrically laminated with one ply of [0/90] E-Glass (90% fiber line fraction)

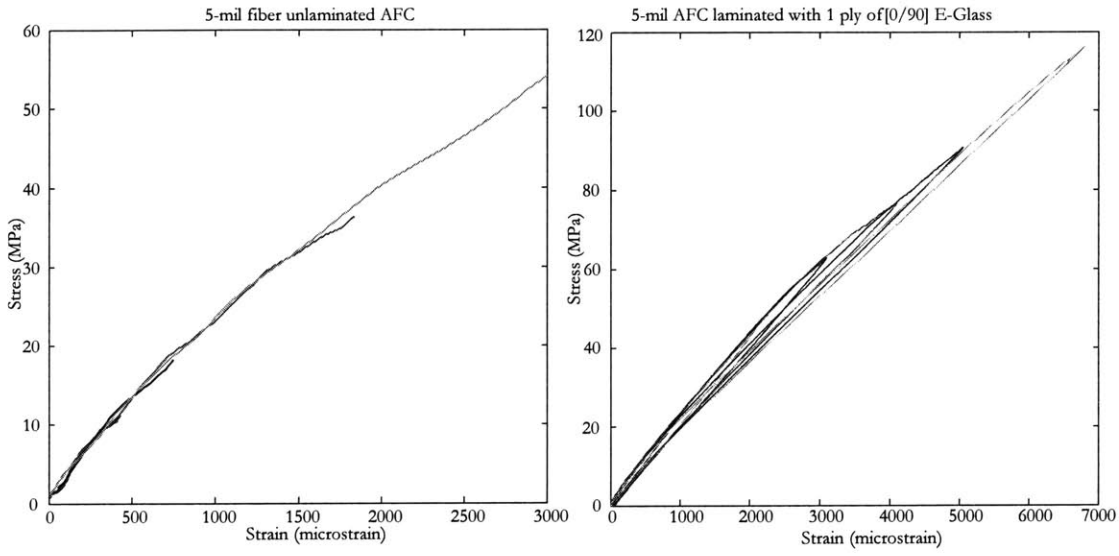

Figure B-10: Longitudinal stress-strain behavior of 0.005" diameter fiber AFCs (unlaminated and symmetrically laminated with one of [0/90] E-Glass (80% fiber line fraction)

Appendix C

Additional Results of Performance Under Tensile Load Tests

This Appendix provides additional results of actuators performance tests conducted under tensile loads. The test is described in Chapter 5 and the complete test matrix is shown in Table 5.1. Following figures show the performance of additional actuators tested up to the maximum strain limits of $2000\mu\varepsilon$, $4000\mu\varepsilon$, and $6000\mu\varepsilon$.

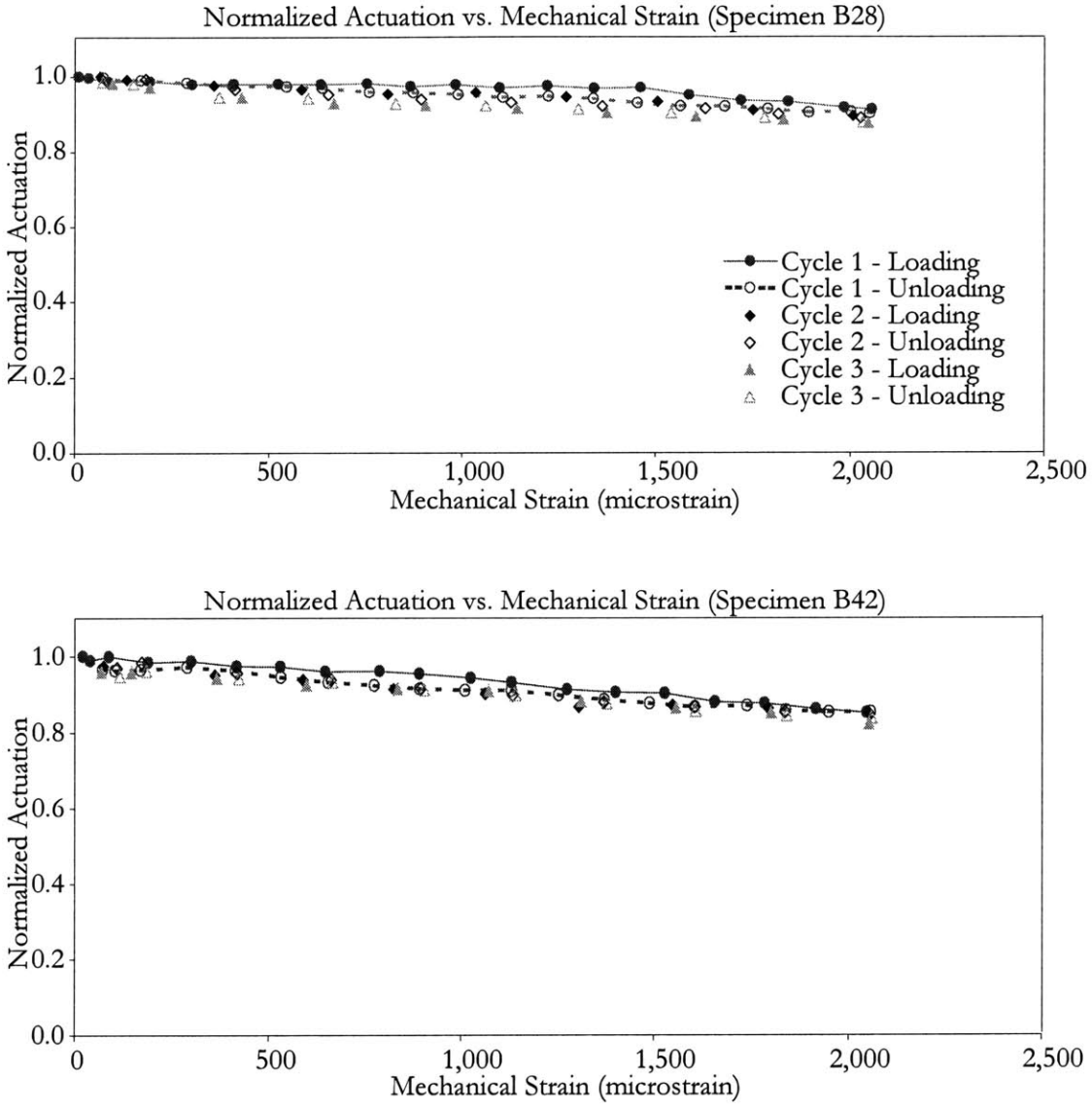

Figure C-1: Actuation performance under tensile load (Maximum Strain $= 2000\mu\varepsilon$)

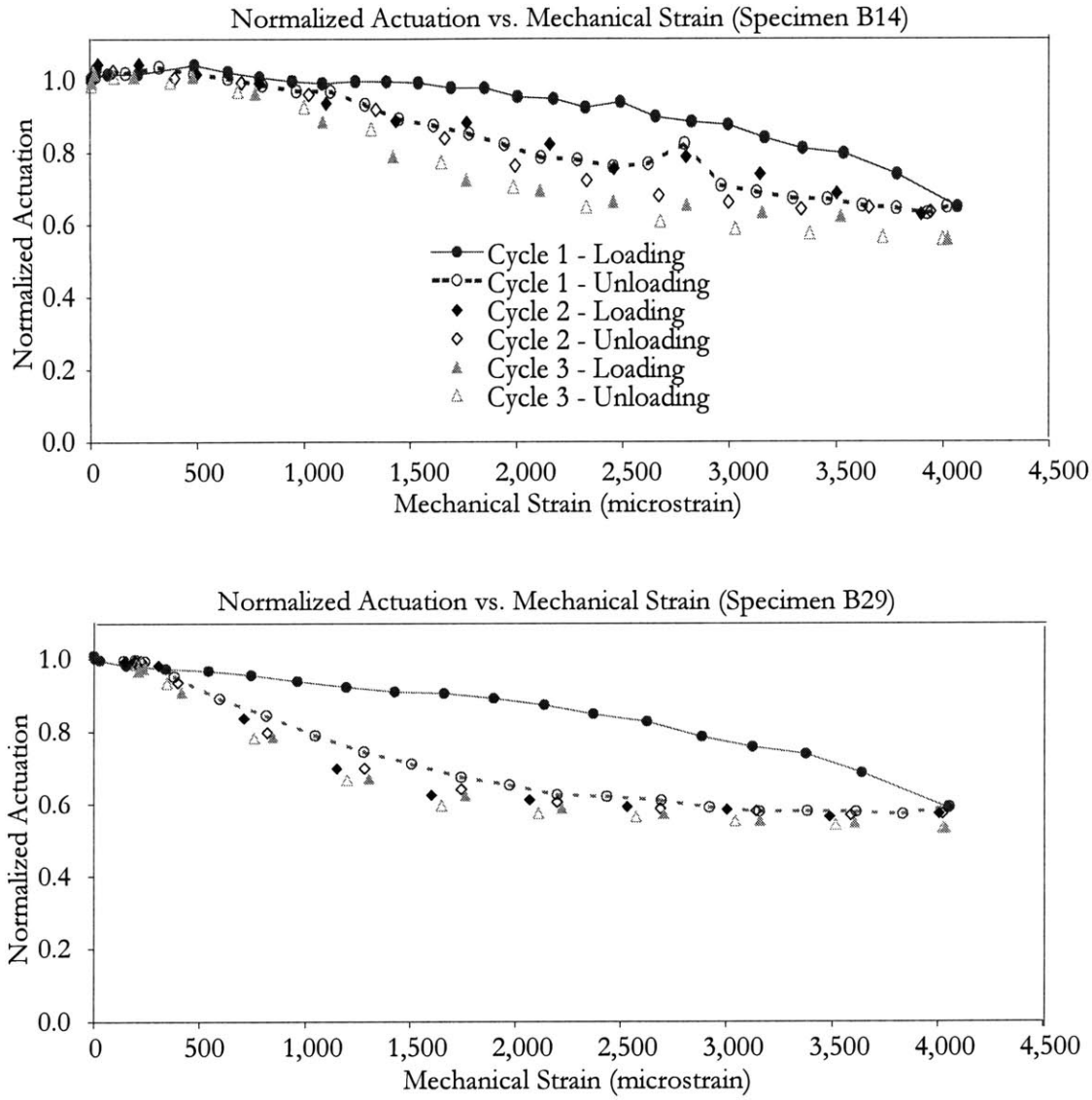

Figure C-2: Actuation performance under tensile load (Maximum Strain $= 4000\mu\varepsilon$)

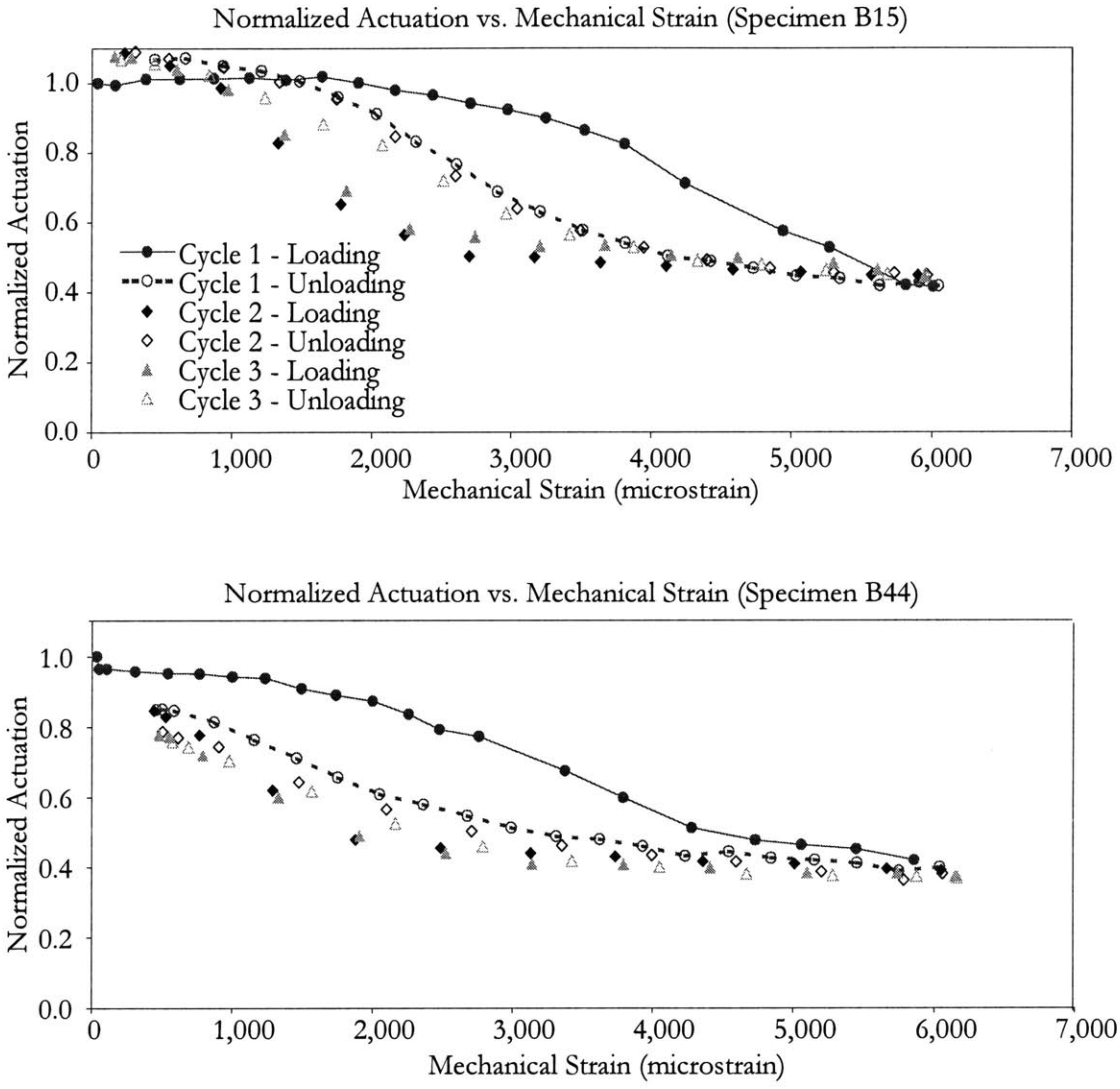

Figure C-3: Actuation performance under tensile load (Maximum Strain $= 6000\mu\varepsilon$)